Upper-Air Data Collected on Ice Station Weddell

Kerry J. Claffey, Edgar L Andreas and Aleksandr P. Makshtas August 1994

Abstract

From February to June 1992, as Ice Station Weddell (ISW) drifted through the uncharted western Weddell Sea, we launched radiosondes, typically twice a day, to study the structure of the lower atmosphere. Here, we describe the ISW radiosounding program, report on the availability of the data, and offer preliminary analyses of some of the atmospheric features we observed. For 10 days in late May and early June, as the Russian icebreaker *Akademik Fedorov* approached ISW from the northeast to help remove the ice camp, we made simultaneous soundings four times a day from ISW and from the *Fedorov*. We, therefore, also describe here the radiosounding system on the *Fedorov*, report on the availability of these data, and present preliminary comparisons of the simultaneous ISW and *Fedorov* soundings. Our soundings showed that temperature inversions were very common in this part of the Weddell Sea in fall and winter. Over 95% of the ISW soundings and 100% of the *Fedorov* soundings showed low-level temperature inversions. Of these, over 40% of the ISW soundings and over 67% of the *Fedorov* soundings were surface-based. A low-level jet in the wind speed profile was also common. We found such a jet in almost 80% of the ISW soundings for which we had wind information. The jet core was usually between 25 and 175 m above the surface, and speeds in the core were commonly between 4 and 10 m/s.

For conversion of SI metric units to U.S./British customary units of measurement consult *Standard Practice for Use of the International System of Units (SI)*, ASTM Standard E380-89a, published by the American Society for Testing and Materials, 1916 Race St., Philadelphia, Pa. 19103.

Special Report 94-25

US Army Corps of Engineers
Cold Regions Research & Engineering Laboratory

Upper-Air Data Collected on Ice Station Weddell

Kerry J. Claffey, Edgar L Andreas and Aleksandr P. Makshtas

August 1994

Prepared for
OFFICE OF POLAR PROGRAMS
NATIONAL SCIENCE FOUNDATION

PREFACE

This report was prepared by Kerry J. Claffey and Dr. Edgar L Andreas, Research Physical Scientist and Physicist, respectively, Snow and Ice Branch, Research Division, U.S. Army Cold Regions Research and Engineering Laboratory (CRREL), and by Dr. Aleksandr P. Makshtas, head of the Laboratory of Air–Sea Interaction, Arctic and Antarctic Research Institute (AARI), St. Petersburg, Russia. The authors thank Valery Timachev of AARI, who was responsible for making the radiosoundings on the *Akademik Fedorov*; Stephen F. Ackley and Dr. Charles C. Ryerson of CRREL, who provided helpful technical reviews of this report; and the Office of Polar Programs of the U.S. National Science Foundation, which supported this research through grant OPP-9024544.

CONTENTS

ILLUSTRATIONS

Figure

Figure

TABLES

Table

Upper-Air Data Collected on Ice Station Weddell

KERRY J. CLAFFEY, EDGAR L ANDREAS AND ALEKSANDR P. MAKSHTAS

INTRODUCTION

In early February 1992, Ice Station Weddell 1 (ISW) was deployed in the perennially ice-covered western Weddell Sea near (51°W, 71°S) by the Russian icebreaker *Akademik Fedorov*. ISW drifted roughly 600 km northward with 32 American and Russian inhabitants until the *Fedorov* and the *Nathaniel B. Palmer* picked it up in early June near (53°W, 66°S). Not only was ISW the first station ever deployed on drifting Antarctic sea ice, its occupants were the first human visitors to this remote corner of the Weddell Sea since Ernest Shackleton and the crew of the *Endurance* were beset and drifted through the area in 1915 (*Antarctic Journal of the United States* 1992, ISW Group 1993).

Here we report on the upper-air data collected on ISW and on the *Fedorov* during the recovery phase of the expedition. The upper-air program was part of wide-ranging meteorological studies carried out on ISW (Andreas et al. 1992, ISW Group 1993). We have reported on some of our other observations elsewhere (Andreas and Claffey 1992) and will prepare a companion data report on our surface-based meteorological program in the near future.

The broad objective of the meteorological program on ISW was to study air–sea–ice interaction in the heretofore unknown western Weddell. Our surface-based program focused on the turbulent exchange of momentum, heat, and moisture between the air and the sea ice and on the radiative forcing of the heat fluxes. For these surface observations to be useful in a larger context, however—i.e., to be useful in large-scale sea ice modeling, in weather forecasting models, and in general circulation models—we need to tie our surface observations to synoptic-scale conditions. Our radiosoundings through the atmospheric boundary layer (ABL) will, we hope, provide this link.

For example, in predicting surface-level winds and the resulting turbulent transfers of momentum and heat and, consequently, sea ice growth and drift, models usually start with the geostrophic wind (derived from surface pressure charts) (e.g., Hibler 1979). This geostrophic wind is taken as the wind vector at the top of the ABL, and a boundary layer model is used to extrapolate this wind down to the surface (e.g., Brown 1981, Brown and Liu 1982). If the ABL over the Weddell Sea behaves as it does elsewhere over the globe, the extrapolation is fairly straightforward. If not, we must devise an ABL model that is accurate over the Weddell Sea.

We have some inkling that the ABL in the Weddell Sea may be more complex than it is elsewhere. The sea ice of the Weddell Sea is a transition zone between the cold atmosphere over the Antarctic continent and the relatively warm atmosphere over the open ocean. The ABL over the Weddell Sea is thus quite sensitive to wind direction (Andreas 1985). When the wind blows from the north, off the open ocean, the ABL can be relatively warm and moist and only weakly stratified; when the wind blows from the south, off the continent, the ABL will be very cold, dry and quite stable (Andreas 1983).

Other influences may act in the western Weddell, as well. Schwerdtfeger (1984) described the low-level barrier winds that blow northward on the eastern side of the Antarctic Peninsula, guided by the high relief of the mountains there. According to Parish's (1983) model, this mountain barrier can produce a low-level atmospheric jet whose effect can extend up to 300 km east from the mountains and, thus, into the Weddell sea. ISW was usually beyond this limit, but observations of the barrier winds—except near mountains—are rare, so we cannot be sure of their extent.

As we will show later in this report (also, see Andreas et al. 1993), the ABL above our camp was usually quite

stably stratified; and in roughly three-fourths of our soundings, we observed a low-level jet. The presence of a low-level jet will confound any of the normal routines for extrapolating geostrophic wind down to the surface and, in fact, is evidence that the surface is frictionally decoupled from the upper air by the strong stability in the ABL.

With this report, we document our ISW upper-air sounding program and provide a description of the data available. We anticipate that in the near future these data will help us sort out some of these complexities of air–sea–ice coupling in the western Weddell Sea and, thus, lead to improved predictions for this climatologically important region.

SOUNDING STRATEGY

Our initial radiosounding plan was very optimistic. It called for making two upper-air soundings a day, at 0000 and 1200 GMT, relying on a tethered balloon and sounding instrumentation package for most of these soundings. We would use a free-flying balloon and expendable instrumentation package only during unfavorable weather conditions such as high surface winds or surface turbulence that made the tethered balloon impossible to control during its launch and flight. We initially brought to the ice station five tethered balloons with three instrumentation packages to go with them. We also brought 50 of the free-flying, expendable instrumentation packages, known as Airsondes.

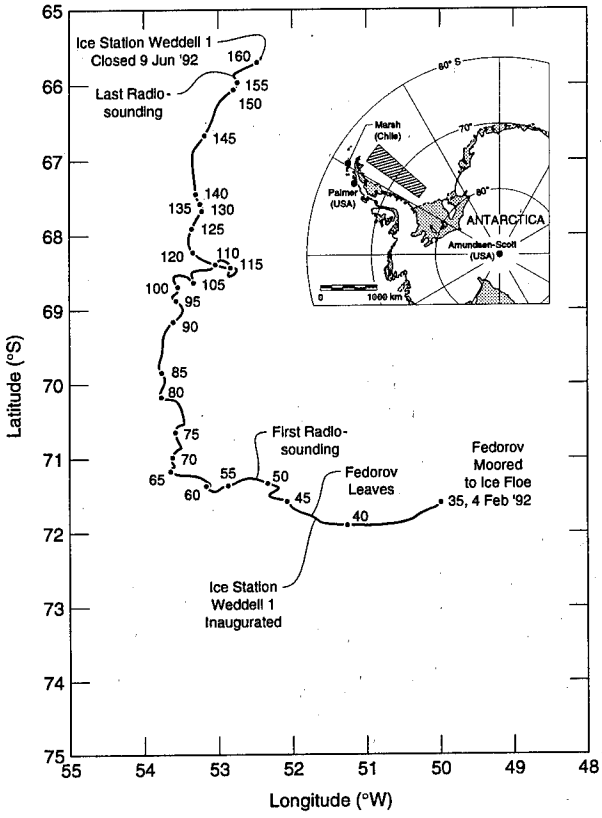

Figure 1. The drift track of Ice Station Weddell, showing station highlights and the duration of our radiosounding program. The numbers indicate the Julian day in 1992.

Setting up the ice station took longer than most of us thought it would. It was 17 days from the time that the *Fedorov* found a floe suitable for the camp until we made the first radiosounding (Fig. 1). Six out of the first seven soundings had to be done with the free-flying Airsondes because of high surface winds. With the initial weather conditions at the camp and what then seemed like a limited number of free-flying Airsondes, we decided to fly Airsondes, if needed, only for the 1200 GMT sounding and to forego the 0000 GMT sounding if conditions prevented the tethered balloon from flying. This decision proved to be the right one: At the end of our deployment we had very few of the Airsondes left.

The tethered balloon and sounding package, called the Tethersonde, had some unique problems. Two of the balloons, one with an instrument package attached, became separated from the tethering winch and were lost by mid-March. There were also two major cold-related problems with the tethered balloons. The balloon material was very brittle in the cold and constantly developed small holes; the balloons would thus lose helium. Most of these small holes developed in the tail fins, where the material was under a lot of stress. Although we attempted to patch these holes, with time the balloon would become unrepairable. By late April, the remaining three Tethersonde balloons had to be retired; thus, between April 21 and May 1, there were no balloons available to fly the Tethersonde instrumentation packages. During this period, we used only Airsondes. Replacement Tethersonde balloons arrived on May 2 and were immediately put into service.

The second cold-related problem was with the internal structure of the balloon, which was made of rubber surgical tubing. The tubing was supposed to stretch and let the rising balloon expand as the atmospheric pressure decreased. As the balloon was pulled back to earth, the tubing was supposed to contract, thus keeping the walls of the Tethersonde balloon taut. In the cold at ISW, however, the rubber tubing would lose its elasticity. It would stretch as the balloon went up but would not retract as the balloon came back down. Between the stretching of this internal structure and the loss of helium through the holes, the balloon would begin to lose its shape; we would, thus, often lose control of it on the descent. Our plan initially was to fly the Tethersonde to just over 1000 m; but because of these problems, we generally let the Tethersonde rise until the measured

wind speed was 13–15 m/s, typically around a height of 500 to 600 m, and then brought it back down. Even with this rule, we had some exciting balloon landings.

Despite these balloon problems, the radiosounding program was very successful. One hundred sixty-four flights yielded good data, with 129 of these flights being with Tethersondes. Thus, we averaged more then one successful Tethersonde sounding per day.

One of the very successful parts of the program was the coordinated soundings that were done with the *Fedorov* as it approached the camp for pickup. As the *Fedorov* neared the ice camp, we made simultaneous soundings at the camp and from the *Fedorov* every 6 hours, at 0000, 0600 ,1200, and 1800 GMT. A total of 32 soundings were performed at the camp in conjunction with 40 soundings from the *Fedorov* during a 10-day period.

DESCRIPTION OF THE SONDES

The radiosounding system used on the ice camp was made by AIR (Atmospheric Instrumentation Research, Inc.) of Boulder, Colorado. This system consisted of a combined ground receiver station and data processor, called the Advanced Atmospheric Data Acquisition System (ADAS), and Airsonde and Tethersonde instrumentation packages carried aloft by helium-filled balloons.

Tethersonde

The Tethersonde was raised underneath a helium-filled, blimp-like, 3.25-cubic meter balloon tethered to an electric winch (Fig. 2). The winch controlled the rate of ascent of the Tethersonde at 1 to 2 m/s. The Tethersonde has a 10-s sampling interval, giving us a vertical resolution of between 10 and 20 m. Typically, we would raise the sonde to 500 to 600 m; however, during a few soundings, we flew the Tethersonde up to just over 1000 m.

The Tethersonde instrumentation package (Fig. 3) provided us with pressure, temperature, dew point, wind speed and direction. Two different types of Tethersonde packages were used: one used a wet-bulb thermistor to determine humidity, and the other used a carbon hygristor. In all other aspects, the two types of Tethersondes were the same. The temperature and humidity sensors were located in an air duct and were ventilated by a fan. Temperature was provided by a bead thermistor. In the wet-bulb model, a bead thermistor covered with a cotton wick supplied with distilled water from a reservoir provided the wet-bulb temperature. In the hygristor model, the resistance across a carbon

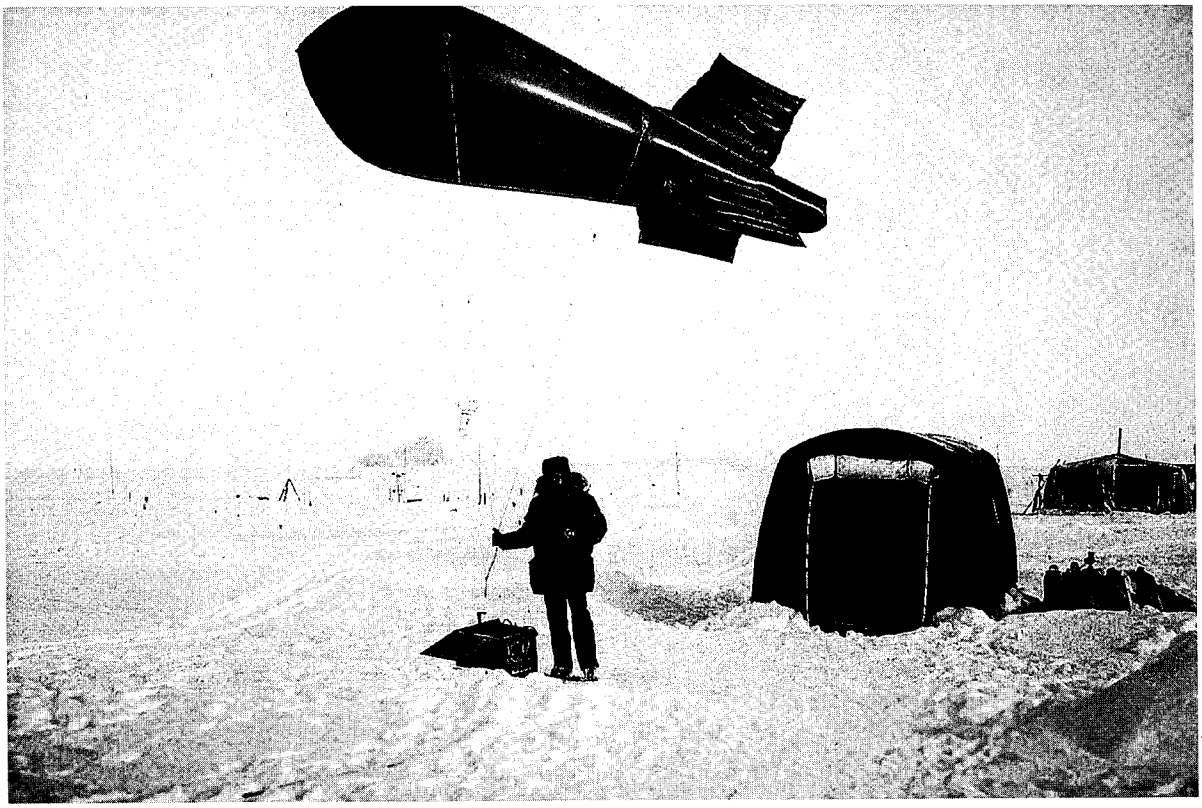

Figure 2. The Tethersonde just before launch. The instrumentation package is barely visible just above the iceberg in the background.

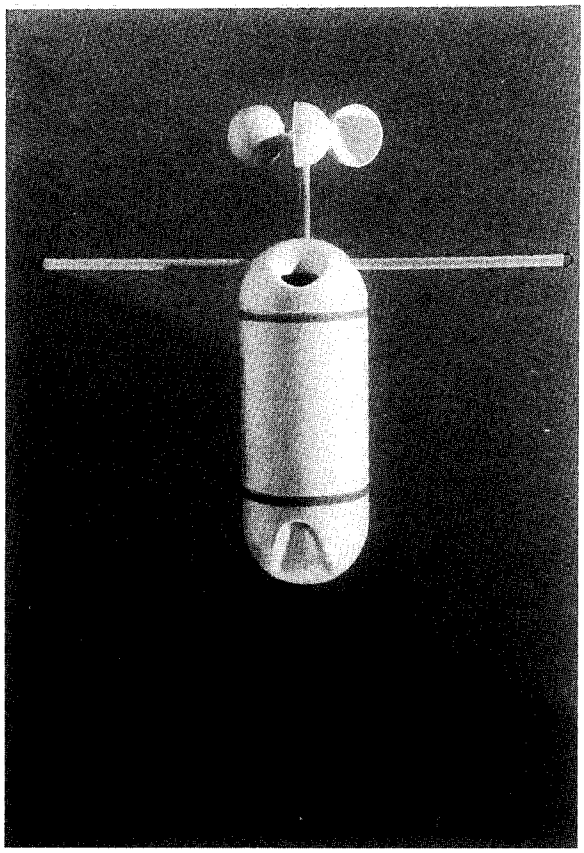

Figure 3. Closeup of the Tethersonde. A small fan inside the unit pulls air through the upper orifice past the temperature and humidity sensors. The package fastens to the balloon harness with clips at each end of the horizontal dowel.

hygristor was measured and the relative humidity was calculated based on this resistance. In both models, the dew point is calculated from these measurements by the microprocessor in the ADAS ground station. Air pressure was measured by a temperature-compensated aneroid sensor. From the pressure, temperature, and humidity data, the ADAS ground station calculated the height of the instrument. All calculations made by the ADAS ground station are further described in the ADAS section.

Wind speed was measured by a three-cup anemometer located on the top of the package. The Tethersonde balloon was shaped to point into the wind during the flight; thus, the Tethersonde's internal compass provided the wind direction. Because of this measurement scheme, the wind direction reported in the ISW data files is the direction from which the wind is blowing. The magnetic declination is not accounted for in the archived data; however, the table in Appendix A gives these declinations. The Tethersonde instrumentation package was recovered after every flight and used over again.

Airsonde

The Airsonde package (Fig. 4) also measures pressure, temperature, and humidity, but it does not measure wind speed or direction. Airsondes were carried by free-flying, 1-m-diameter, 100-g helium balloons that typically rose at a rate of 5 m/s. Because the Airsonde instrumentation package has a sampling interval of 5 s, the vertical resolution of the Airsonde was 20–25 m. Airsondes typically flew to altitudes between 6,000 and 10,000 m before the radio signal was lost. Unlike the Tethersonde instrumentation package, the Airsonde package was used once and not recovered after the flight. Airsondes were used in weather conditions (high wind) when flying or controlling the tethered balloon was impossible or when the Tethersonde balloon or instrument package was grounded for repairs.

The temperature-compensated aneroid sensor, the dry-bulb bead thermistor, and wet-bulb bead thermistor are the same as those used in the Tethersonde package. The thermistors are located in radiation shields on either side of the Airsonde, one thermistor in each shield. As the Airsonde rises, it spins, causing air to flow past these

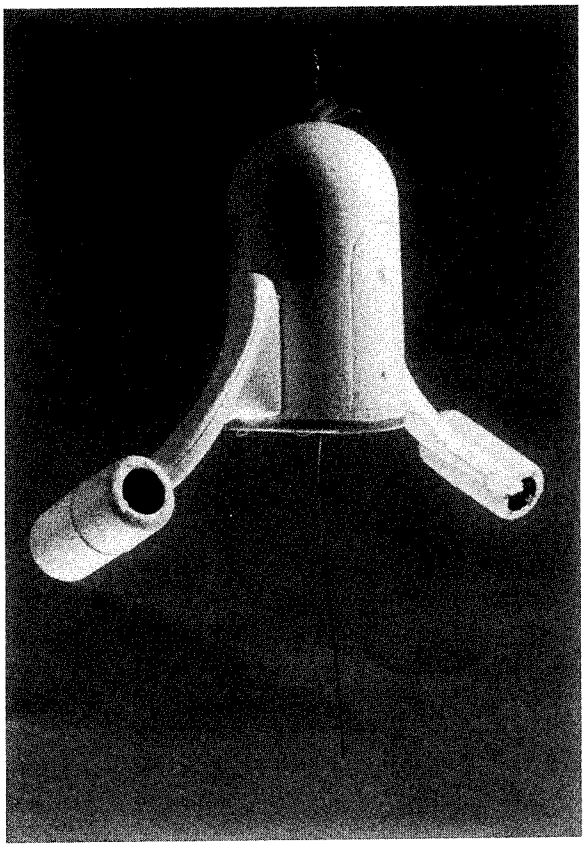

Figure 4. Closeup of the Airsonde. The wings make the sonde spin as it rises and, thus, force air past the dry- and wet-bulb thermistors—one in each radiation shield at the ends of the wings.

thermistors. Similar to the Tethersonde, the wet-bulb bead thermistor is covered with a cotton wick that is moistened with distilled water before the flight. The dew point is calculated by the ADAS ground station based on the wet-bulb temperature. The height of the Airsonde is also calculated by the ADAS based on the pressure, temperature, and humidity measurements.

Sensor Accuracy

To check that the sondes were operating properly, we compared their measured wind speed, direction and temperature with our nearby surface-based instruments as we held each sonde at the surface ready for launching. There were seldom significant discrepancies. When there were, however, we either switched sondes or restarted the data acquisition program.

The pressure sensors in the sondes were factory calibrated. Entering this calibration information was a step in starting the data acquisition program. Another step was initializing the pre-launch sonde pressure with the station pressure. In other words, if a sonde's absolute pressure calibration had drifted, it made no difference; we ensured that its absolute pressure was correct by tying its output to the station pressure. This step gives us confidence that the measured radiosonde pressures are accurate, because, in general, an instrument's gain is more stable then its DC offset.

Measuring humidity at temperatures below freezing is a challenge. Andreas and Richter (1982) have already discussed some of the problems with radiosonde humidity measurements. Wet-bulb thermistors, in particular, are poor sensors for subfreezing humidity measurements; but such humidity sensors are the only ones available for Airsondes. All of our radiosonde flights began in surface-level temperatures below freezing. Thus, to make sure that the wet-bulb wick was frozen when we launched the sonde—that is, that an in-flight phase change would not lead to spurious humidity measurements—we hung the sonde outside after we moistened its wick to give the wick time to freeze.

The hygristor elements, which most of our Tethersondes had, seemed to yield more reasonable humidity values then the wet-bulb thermistors. We have somewhat more confidence in the humidity from these sondes. We had a supply of spare hygristor elements and, thus, replaced hygristors after three or four Tethersonde ascents or whenever the humidity data seemed questionable.

ADVANCED ATMOSPHERIC DATA ACQUISITION SYSTEM

The ADAS ground station receiver was set at 403.5 MHz, the frequency at which the sondes broadcast. The ADAS received the data taken by the sensors on each of the packages, processed them, and output both measured and calculated values. The ADAS provided us with a printout of the data and also stored the data on magnetic (audio) tape.

ADAS calculations

Table 1 shows the variables output by the ADAS to the radiosounding data files. Both the Tethersonde and Airsonde instrumentation packages measure three main variables: air pressure, dry-bulb temperature, and wet-bulb temperature or the resistance of the carbon hygristor in the Tethersondes that contain this sensor. The Tethersonde also measures wind speed and direction. The other variables that we recorded, dew point, relative humidity, potential temperature, and height are calculated by the ADAS from the measured variables.

Humidity variables

To calculate the humidity variables, the fundamental humidity variables, vapor pressure, e, and saturation vapor pressure e_{sat}, must be found. The ADAS uses equations similar to Murray's (1967) to find the saturation vapor pressure in millibars:

$$e_{sat} = 6.1078 \exp\left[\frac{aT}{T+b}\right] \qquad (1)$$

where T is the dry-bulb temperature in °C and

over ice:	over water:
$a = 21.457$	$a = 17.265$
$b = 261.24$	$b = 237.29$

Table 1. Variables available in the radiosounding data files from Ice Station Weddell and from the *Akademik Fedorov*.

	ISW		
Variable	*Airsonde*	*Tethersonde*	Fedorov
Pressure	M	M	M
Height	C	C	C
Wind speed		M	M
Wind direction		M	M
Temperature (dry-bulb)	M	M	M
Wet-bulb temperature	M1	M1	
(or Hygristor resistance*)		M1	
Dew point	C	C	C
Relative humidity	C	C	M
Potential temperature	C	C	

* Resistance of the carbon hygristor is measured in the Tethersonde with this sensor.

M — measured by the radiosonde and output to the data files.

M1 — measured by the radiosonde package but used only in calculating other variables, not reported in the data files.

C — calculated by the ground station from measurements made by the radiosonde and output to the data file.

In the sondes containing the wet-bulb thermistor, the ADAS uses the wet-bulb temperature, T_w, and the air pressure, P, to calculate vapor pressure from the psychrometer equation (List 1984, p. 365):

$$e = e_{sat} - P(T - T_w)\,(0.000660 + 7.59 \times 10^{-7}\, T_w), \quad (2)$$

where P is in millibars, and T and T_w are in °C.

The dew point, T_d in °C, is then determined by

$$T_d = \frac{237.29 \ln\left(\frac{e}{6.1078}\right)}{17.265 - \ln\left(\frac{e}{6.1078}\right)} \qquad \text{if } T_w \geq 0 \quad (3a)$$

$$T_d = \frac{261.24 \ln\left(\frac{e}{6.1078}\right)}{21.457 - \ln\left(\frac{e}{6.1078}\right)} \qquad \text{if } T_w < 0. \quad (3b)$$

Relative humidity in percent is

$$RH = \frac{e}{e_{sat}} \times 100. \quad (4)$$

To determine the dew point, T_d, from the carbon hygristor for the Tethersondes containing this sensor, the ADAS calculates the relative humidity (in percent) from the measured resistance of the hygristor and the measured temperature:

$$RH = A - \frac{69}{\sum_{k=0}^{4} D_k [f(R_s)]^k}, \quad (5)$$

where A and D_0 to D_4 are constants, and

$$f(R_s) = f(T) \ln\left(\frac{R_s}{R_{33}}\right), \quad (6)$$

where $f(T)$ = temperature coefficient of the sensor
R_s = measured resistance of the hygristor
R_{33} = hygristor calibration value provided by the factory.

The calibration value (R_{33}) is equal to the resistance of the carbon hygristor at 25°C when the relative humidity is 33%. The hygristor calibration factor is entered into the ADAS during the start up of the data acquisition program. Once RH is determined, the ADAS calculates the dew point using the measured temperature and eq 1–4.

Temperature variables

Potential temperature, θ in kelvins, with respect to a reference of 1000 mb is found by the ADAS using (Fleagle and Businger 1980, p. 51)

$$\theta = (T + 273.15)\left(\frac{1000}{P}\right)^{R/c_p M_a} \quad (7)$$

where R = universal gas constant, 8.31441 J mol^{-1} K^{-1},
c_p = specific heat of air at constant pressure, 1.005×10^3 J kg^{-1} K^{-1}
M_a = molecular weight of dry air, 28.9644×10^{-3} kg/mol.

The virtual temperature, T_v (in °C), which is used in calculating the geopotential height, is determined by the ADAS using

$$T_v = T + \frac{w}{6}, \quad (8)$$

where w is the mixing ratio in g/kg,

$$w = \frac{622\, e}{P - e}, \quad (9)$$

where P is the measured air pressure (mb) and e is the vapor pressure (mb) from eq 2.

Height

The heights calculated by the ADAS are the geopotential heights obtained by integrating the hydrostatic equation:

$$H_i = H_{i-1} + \Delta H \quad (10)$$

where H_i = current height (m)
H_{i-1} = height (m) at the last reading
ΔH = change in height (m).

Here

$$\Delta H = \left(\frac{R}{2gM_a}\right) T_v \left[\ln\left(\frac{P_{i-1}}{P_i}\right)\right], \quad (11)$$

where P_i = current pressure
P_{i-1} = pressure at the last reading
g = acceleration of gravity, 9.81 m/s^2

and T_v must be in kelvins here.

FEDOROV SOUNDING SYSTEM

The sounding system on the *Akademik Fedorov* is the MicroCORA, made by Vaisala of Helsinki, Finland. Andreas and Richter (1982) evaluated an earlier version of the MicroCORA that we used in the Antarctic; modern Vaisala sounding systems are built on the same basic philosophy and with several of the same sensors in the sonde.

The *Fedorov* launched Vaisala's RS-80 radiosondes. Typically the radiosondes would rise to between 8,000 and 9,000 m before losing contact with the ground station. These are expendable sondes that measure pressure, temperature, humidity, wind speed, and wind di-

rection. The RS-80 measures pressure with an aneroid capacitor, temperature with a capacitance bead, and relative humidity with Vaisala's popular Humicap, a thin-film capacitor (Table 1).

The MicroCORA uses the Omega navigational aid signals to track the radiosonde and finds wind speed and direction from these navaid fixes. Although the MicroCORA balloon ascends at about 5 m/s, approximately the same rate as the Airsonde balloons, the sonde transmits data only once every 10 s, half the rate at which the Airsonde transmits. The MicroCORA also needs sequential Omega fixes on the radiosonde for computing wind speed and direction; therefore, it has a vertical resolution of, nominally, 100 m for wind speed and direction—roughly five to ten times coarser than our Tethersondes. We do not mean to imply here that this coarse resolution is a fault of the MicroCORA. Its purpose is to measure average atmospheric properties accurately high into the atmosphere, and it does this well. The Tethersonde, on the other hand, is designed specifically for boundary layer profiling; thus, it has better resolution then the MicroCORA, but it also has a limited height range. The wind direction reported in the MicroCORA data files is also the direction from which the wind was blowing. The directions reported in these files, however, are with respect to true north; no declination correction is necessary.

DATA COLLECTED

Despite the harsh polar marine environment of the western Weddell Sea and the limited daylight toward the end of our deployment, we operated continuously for almost four months. Our ISW radiosounding program was thus very successful. Between February 21 and June 4 1992, 164 soundings were made that provided good data (Table 2). One hundred twenty-nine of the soundings were made with the Tethersonde instrument package, giving us wind speed and direction measurements for those flights. Between May 26 and June 4, soundings were made at the camp at 6-hour intervals to coincide with radiosonde launches from the *Akademik Fedorov* (Table 3) as it approached camp. Figure 5 shows the positions of the *Fedorov* and ISW during these coordinated soundings. When the simultaneous soundings began, the *Fedorov* was roughly 750 km northeast of ISW. During this 10-day period, 32 radiosonde launches were made at ISW, and 40 launches were made from the *Fedorov*.

Appendix C shows plots to 1000 m of all of the radiosoundings made on Ice Station Weddell. Appendix D shows plots to 1000 m of all the radiosoundings made on the *Akademik Fedorov* during our coordinated program. Both data sets, and the file with the daily declinations (App. A) are available on disks from the authors or from the CRREL Library.

Table 2. Inventory of the radiosoundings made on Ice Station Weddell, 1992. For each of these, there is a corresponding file in the data archive and a plot in Appendix C.

	ID	Date	JD	Time (GMT) Nominal	Time (GMT) Actual	Lat. (deg.)	Long. (deg.)	Sonde	Max. height (m)
1	IS022100	21 Feb	52	00	00:18:46	–71.33	–52.42	AS	8,189
2	IS022112	21 Feb	52	12	12:15:56	–71.30	–52.47	Th	980
3	IS022200	22 Feb	53	00	00:17:56	–71.27	–52.53	AS	11,324
4	IS022300	23 Feb	54	00	00:06:49	–71.29	–52.63	AS	7,117
5	IS022312	23 Feb	54	12	12:06:53	–71.31	–52.71	AS	9,902
6	IS022412	24 Feb	55	12	12:09:34	–71.36	–52.87	AS	8,066
7	IS022512	25 Feb	56	12	12:12:33	–71.41	–53.02	AS	8,931
8	IS022600	26 Feb	57	00	01:50:43	–71.43	–53.09	Th	173
9	IS022612	26 Feb	57	12	12:36:41	–71.41	–53.09	Th	818
10	IS022700	27 Feb	58	00	23:56:36	–71.41	–53.14	Th	1,008
11	IS022712	27 Feb	58	12	12:13:01	–71.40	–53.10	Th	1,327
12	IS022800	28 Feb	59	00	00:11:10	–71.41	–53.13	Th	1,098
13	IS022812	28 Feb	59	12	12:26:58	–71.39	–53.12	Th	1,328
14	IS022900	29 Feb	60	00	00:05:59	–71.39	–53.20	Th	1,350
15	IS022912	29 Feb	60	12	12:12:17	–71.37	–53.18	Th	1,185
16	IS030100	1 Mar	61	00	00:04:26	–71.38	–53.20	Th	509
17	IS030112	1 Mar	61	12	12:20:55	–71.36	–53.12	Th	1,013
18	IS030200	2 Mar	62	00	00:00:17	–71.36	–53.16	Th	901
19	IS030212	2 Mar	62	12	12 :11:48	–71.35	–53.14	Th	576
20	IS030312	3 Mar	63	12	12:11:49	–71.37	–53.07	Th	422
21	IS030400	4 Mar	64	00	00:12:30	–71.34	–53.19	AS	7,632
22	IS030412	4 Mar	64	12	12:12:43	–71.27	–53.19	AS	8,189
23	IS030512	5 Mar	65	12	12:15:45	–71.16	–53.61	Th	952
24	IS030600	6 Mar	66	00	00:39:53	–71.12	–53.66	Th	540
25	IS030612	6 Mar	66	12	12:13:33	–71.10	–53.66	Th	1,046
26	IS030700	7 Mar	67	00	23:54:00	–71.09	–53.64	Th	982
27	IS030712	7 Mar	67	12	13:01:51	–71.09	–53.61	Th	673
28	IS030800	8 Mar	68	00	00:23:02	–71.08	–53.61	Th	651
29	IS030812	8 Mar	68	12	12:14:16	–71.09	–53.57	Th	746
30	IS030900	9 Mar	69	00	23:57:32	–71.08	–53.57	Tw	568

Table 2 (cont'd). Inventory of the radiosoundings made on Ice Station Weddell, 1992. For each of these, there is a corresponding file in the data archive and a plot in Appendix C.

	ID	Date	JD	Time (GMT) Nominal	Time (GMT) Actual	Lat. (deg.)	Long. (deg.)	Sonde	Max. height (m)
31	IS030912	9 Mar	69	12	12:10:36	–71.04	–53.64	Th	759
32	IS031000	10 Mar	70	00	23:55:41	–71.02	–53.62	Th	361
33	IS031012	10 Mar	70	12	12:19:12	–70.99	–53.61	Th	739
34	IS031100	11 Mar	71	00	00:01:33	–70.99	–53.66	Th	771
35	IS031112	11 Mar	71	12	12:18:38	–70.95	–53.60	Th	368
36	IS031212	12 Mar	72	12	12:32:27	–70.86	–53.57	Tw	255
37	IS031312	13 Mar	73	12	12:22:33	–70.83	–53.49	Tw	334
38	IS031412	14 Mar	74	12	12:09:45	–70.72	–53.58	AS	5,041
39	IS031512	15 Mar	75	12	12:56:25	–70.66	–53.54	Tw	260
40	IS031612	16 Mar	76	12	12:18:45	–70.57	–53.54	AS	4,492
41	IS031712	17 Mar	77	12	12:10:22	–70.50	–53.44	Th	549
42	IS031800	18 Mar	78	00	23:55:14	–70.48	–53.45	Th	410
43	IS031812	18 Mar	78	12	12:01:18	–70.48	–53.54	Th	526
44	IS031912	19 Mar	79	12	13:08:04	–70.28	–53.62	AS	5,068
45	IS032012	20 Mar	80	12	12:14:12	–70.17	–53.75	AS	7,225
46	IS032100	21 Mar	81	00	23:48:27	–70.12	–53.78	Th	627
47	IS032112	21 Mar	81	12	12:01:50	–70.11	–53.74	Th	543
48	IS032200	22 Mar	82	00	23:54:33	–70.09	–53.72	Th	386
49	IS032212	22 Mar	82	12	12:17:27	–70.04	–53.73	AS	6,895
50	IS032312	23 Mar	83	12	12:09:39	–69.94	–53.69	Th	363
51	IS032400	24 Mar	84	00	23:58:34	–69.91	–53.73	Th	1,042
52	IS032412	24 Mar	84	12	12:15:13	–69.89	–53.70	Th	634
53	IS032500	25 Mar	85	00	23:50:22	–69.87	–53.77	Th	552
54	IS032512	25 Mar	85	12	12:19:14	–69.83	–53.76	Th	589
55	IS032600	26 Mar	86	00	23:51:52	–69.80	–53.81	Th	450
56	IS032612	26 Mar	86	12	12:28:49	–69.73	–53.77	AS	3,159
57	IS032712	27 Mar	87	12	13:00:16	–69.55	–53.74	AS	6,254
58	IS032812	28 Mar	88	12	12:11:39	–69.37	–53.74	Th	157
59	IS032912	29 Mar	89	12	12:28:00	–69.24	–53.70	Th	419
60	IS033012	30 Mar	90	12	12:16:49	–69.12	–53.51	AS	1,552
61	IS033112	31 Mar	91	12	12:32:15	–69.01	–53.48	Th	530
62	IS0331SP	31 Mar	91	13	13:18:03	–69.01	–53.48	Th	92
63	IS040100	1 Apr	92	00	00:03:18	–68.99	–53.48	Th	569
64	IS040112	1 Apr	92	12	12:24:26	–68.97	–53.49	Th	538
65	IS040212	2 Apr	93	12	12:38:45	–68.95	–53.48	Th	399
66	IS040312	3 Apr	94	12	12:59:49	–68.87	–53.54	Th	518
67	IS040412	4 Apr	95	12	12:29:47	–68.86	–53.55	Th	544
68	IS040500	5 Apr	96	00	00:11:14	–68.85	–53.56	Th	520
69	IS040512	5 Apr	96	12	12:13:14	–68.85	–53.55	Th	255
70	IS040612	6 Apr	97	12	12:00:05	–68.86	–53.50	Th	461
71	IS040712	7 Apr	98	12	12:15:36	–68.82	–53.61	AS	7,239
72	IS040900	9 Apr	100	00	00:06:37	–68.70	–53.56	Th	451
73	IS040912	9 Apr	100	12	12:47:29	–68.70	–53.52	Th	465
74	IS041112	11 Apr	102	12	12:29:29	–68.54	–53.59	Th	465
75	IS041200	12 Apr	103	00	00:14:19	–68.52	–53.58	Th	351
76	IS041312	13 Apr	104	12	12:11:05	–68.54	–53.39	AS	8,977
77	IS041512	15 Apr	106	12	12:18:23	–68.57	–53.33	AS	8,902
78	IS041612	16 Apr	107	12	12:45:51	–68.49	–53.36	Th	360
79	IS041712	17 Apr	108	12	12:18:18	–68.45	–53.28	AS	6,322
80	IS041812	18 Apr	109	12	13:42:46	–68.43	–53.07	Th	107
81	IS041912	19 Apr	110	12	12:49:43	–68.38	–53.05	Th	272
82	IS042000	20 Apr	111	00	00:29:28	–68.35	–53.07	Th	320
83	IS042012	20 Apr	111	12	12:25:52	–68.35	–53.01	Th	314
84	IS042100	21 Apr	112	00	00:24:02	–68.34	–53.00	Th	216
85	IS042112	21 Apr	112	12	13:10:40	–68.32	–52.99	Th	311
86	IS042212	22 Apr	113	12	13:33:32	–68.32	–52.93	AS	8,280
87	IS042312	23 Apr	114	12	12:25:24	–68.37	–52.85	AS	10,051
88	IS042412	24 Apr	114	12	12:35:15	–68.46	–52.81	AS	8,911
89	IS042512	25 Apr	116	12	12:59:09	–68.51	–52.86	AS	1,700
90	IS042612	26 Apr	117	12	12:58:34	–68.44	–52.72	AS	2,785
91	IS042712	27 Apr	118	12	12:49:28	–68.45	–52.89	AS	8,551
92	IS042912	29 Apr	120	12	12:35:17	–68.21	–53.34	AS	10,094
93	IS043012	30 Apr	121	12	12:32:28	–68.09	–53.42	AS	6,465
94	IS050112	1 May	122	12	12:27:44	–68.02	–53.37	AS	8,895
95	IS050200	2 May	123	00	23:57:47	–67.99	–53.37	Th	654
96	IS050212	2 May	123	12	12:32:15	–67.98	–53.38	Th	671
97	IS050300	3 May	124	00	23:56:15	–67.96	–53.37	Th	655
98	IS050312	3 May	124	12	12:23:11	–67.95	–53.38	Th	747
99	IS050400	4 May	125	00	00:06:03	–67.93	–53.38	Th	474
100	IS050412	4 May	125	12	12:26:47	–67.92	–53.36	Th	699
101	IS050500	5 May	126	00	00:12:21	–67.89	–53.37	Th	376
102	IS050512	5 May	126	12	12:17:44	–67.84	–53.35	Th	594
103	IS050600	6 May	127	00	00:10:46	–67.80	–53.34	Th	615

Table 2 (cont'd).

	ID	Date	JD	Time (GMT) Nominal	Time (GMT) Actual	Lat. (deg.)	Long. (deg.)	Sonde	Max. height (m)
104	IS050612	6 May	127	12	12:27:16	–67.78	–53.29	Th	645
105	IS050700	7 May	128	00	00:08:24	–67.77	–53.27	Th	207
106	IS050712	7 May	128	12	12:26:48	–67.77	–53.21	Th	614
107	IS050812	8 May	129	12	12:42:18	–67.69	–53.28	Th	419
108	IS050900	9 May	130	00	00:17:29	–67.67	–53.28	Th	384
109	IS050912	9 May	130	12	12:23:22	–67.68	–53.20	Th	614
110	IS051012	10 May	131	12	12:38:52	–67.68	–53.26	Th	618
111	IS051100	11 May	132	00	00:09:51	–67.67	–53.27	Th	683
112	IS051112	11 May	132	12	13:01:17	–67.65	–53.24	Th	630
113	IS051200	12 May	133	00	00:00:07	–67.64	–53.23	Th	529
114	IS051212	12 May	133	12	12:25:18	–67.65	–53.22	Th	616
115	IS051300	13 May	134	00	00:10:18	–67.64	–53.19	Th	624
116	IS051312	13 May	134	12	12:31:44	–67.62	–53.20	Th	655
117	IS051400	14 May	135	00	00:06:35	–67.62	–53.23	Th	515
118	IS051412	14 May	135	12	12:18:25	–67.62	–53.28	Th	619
119	IS051500	15 May	136	00	00:26:51	–67.63	–53.34	Th	523
120	IS051512	15 May	136	12	12:35:03	–67.64	–53.37	Th	588
121	IS051600	16 May	137	00	00:04:01	–67.59	–53.31	Th	327
122	IS051612	16 May	137	12	13:54:11	–67.56	–53.28	AS	7,544
123	IS051700	17 May	138	00	00:02:35	–67.52	–53.28	Th	625
124	IS051712	17 May	138	12	12:15:07	–67.50	–53.28	Th	620
125	IS051800	18 May	139	00	00:07:30	–67.48	–53.31	Th	619
126	IS051812	18 May	139	12	12:33:45	–67.47	–53.31	Th	620
127	IS051900	19 May	140	00	00:01:39	–67.45	–53.33	Th	532
128	IS051912	19 May	140	12	12:19:50	–67.45	–53.32	Th	616
129	IS052000	20 May	141	00	00:26:26	–67.44	–53.34	Th	693
130	IS052012	20 May	141	12	12:28:31	–67.41	–53.32	AS	6,516
131	IS052112	21 May	142	12	12:34:23	–67.28	–53.30	AS	8,285
132	IS052212	22 May	143	12	13:02:31	–67.15	–53.32	AS	5,442
133	IS052612	26 May	147	12	12:56:24	–66.31	–53.01	AS	7,002
134	IS052618	26 May	147	18	18:17:46	–66.29	–53.00	Th	364
135	IS052700	27 May	148	00	00:30:30	–66.26	–52.98	AS	7,033
136	IS052712	27 May	148	12	12:38:33	–66.20	–52.91	Th	410
137	IS052718	27 May	148	18	18:46:15	–66.18	–52.88	Th	348
138	IS052800	28 May	149	00	00:09:33	–66.16	–52.86	Th	671
139	IS052806	28 May	149	06	06:12:36	–66.14	–52.86	Th	675
140	IS052812	28 May	149	12	12:27:03	–66.12	–52.85	Th	609
141	IS052818	28 May	149	18	18:20:41	–66.13	–52.84	Th	485
142	IS052900	29 May	150	00	00:07:59	–66.08	–52.83	Th	492
143	IS052906	29 May	150	06	06:09:15	–66.07	–52.82	Th	620
144	IS052912	29 May	150	12	12:31:56	–66.06	–52.80	Th	617
145	IS052918	29 May	150	18	18:20:25	–66.05	–52.80	Th	624
146	IS053000	30 May	151	00	00:16:34	–66.04	–52.80	Th	617
147	IS053006	30 May	151	06	06:21:08	–66.04	–52.80	Th	627
148	IS053018	30 May	151	18	18:31:31	–66.04	–52.81	Th	640
149	IS053100	31 May	152	00	00:05:16	–66.03	–52.81	Th	646
150	IS053106	31 May	152	06	06:27:08	–66.03	–52.82	Th	644
151	IS053112	31 May	152	12	12:18:57	–66.02	–52.81	Th	628
152	IS053118	31 May	152	18	18:05:04	–66.02	–52.80	Th	611
153	IS060100	1 June	153	00	00:29:13	–66.01	–52.84	Th	579
154	IS060106	1 June	153	06	06:38:58	–66.01	–52.85	Th	631
155	IS060112	1 June	153	12	12:56:15	–66.00	–52.83	Th	518
156	IS060118	1 June	153	18	18:07:29	–66.00	–52.84	Th	638
157	IS060200	2 June	154	00	00:17:13	–66.00	–52.84	Th	655
158	IS060206	2 June	154	06	06:23:02	–66.01	–52.82	Th	646
159	IS060212	2 June	154	12	12:53:18	–66.00	–52.80	Th	440
160	IS060218	2 June	154	18	18:22:26	–65.99	–52.77	Th	444
161	IS060300	3 June	155	00	00:19:15	–65.98	–52.77	Th	626
162	IS060306	3 June	155	06	06:31:05	–65.97	–52.76	Th	590
163	IS060312	3 June	155	12	12:33:04	–65.95	–52.75	Th	426
164	IS060400	4 June	156	00	00:12:08	–65.92	–52.77	AS	6,057

Definitions:

ID Name of the data file.

JD Julian day.

Time The time when the sonde began its ascent.

Sonde AS is an Airsonde; measures height, temperature, humidity (with a wet–bulb thermistor).
Th is a Tethersonde with hygristor; measures wind speed, direction, height, temperature, humidity (with a hygristor).
Tw is a Tethersonde with wet–bulb; measures wind speed, direction, height, temperature, humidity (with a wet–bulb thermistor).

Max. height Maximum height that the sonde reached.

Table 3. Inventory of the radiosoundings made on *Akademik Fedorov* during the coordinated sounding program, 1992. For each of these, there is a corresponding file in the data archive and a plot in Appendix D

	ID	Date	JD	Time (GMT)	Lat. (deg.)	Long. (deg.)	Max. height (m)
1	ZOND020	26 May	147	06	–61.20	–43.20	8,270
2	ZOND021	26 May	147	12	–61.70	–43.50	8,251
3	ZOND022	26 May	147	18	–62.70	–43.90	8,213
4	ZOND023	27 May	148	00	–63.20	–44.00	8,200
5	ZOND024	27 May	148	06	–63.50	–44.10	8,207
6	ZOND025	27 May	148	12	–63.70	–43.80	8,211
7	ZOND026	27 May	148	18	–64.00	–44.00	8,232
8	ZOND027	28 May	149	00	–64.40	–44.50	8,237
9	ZOND028	28 May	149	06	–64.40	–45.30	8,258
10	ZOND029	28 May	149	12	–64.40	–45.60	8,263
11	ZOND030	28 May	149	18	–64.60	–46.20	8,294
12	ZOND031	29 May	150	00	–64.70	–46.70	8,327
13	ZOND032	29 May	150	06	–64.70	–47.30	8,345
14	ZOND033	29 May	150	12	–64.80	–47.50	8,320
15	ZOND034	29 May	150	18	–65.20	–48.60	8,334
16	ZOND035	30 May	151	00	–65.50	–49.70	8,363
17	ZOND036	30 May	151	06	–65.60	–50.90	8,372
18	ZOND037	30 May	151	12	–65.60	–50.90	8,371
19	ZOND038	30 May	151	18	–65.60	–50.90	8,371
20	ZOND039	31 May	152	00	–65.60	–50.90	8,368
21	ZOND040	31 May	152	06	–65.60	–50.90	8,428
22	ZOND041	31 May	152	12	–65.60	–50.90	8,466
23	ZOND042	31 May	152	18	–65.60	–51.20	8,509
24	ZOND043	1 June	153	00	–65.70	–51.30	8,549
25	ZOND044	1 June	153	06	–65.60	–51.30	8,534
26	ZOND045	1 June	153	12	–65.60	–51.30	8,521
27	ZOND046	1 June	153	18	–65.60	–51.20	8,523
28	ZOND047	2 June	154	00	–65.80	–51.50	8,519
29	ZOND048	2 June	154	06	–65.80	–51.50	8,575
30	ZOND049	2 June	154	12	–65.80	–51.60	8,614
31	ZOND050	2 June	154	18	–65.80	–51.60	8,584
32	ZOND051	3 June	155	00	–65.80	–51.70	8,587
33	ZOND052	3 June	155	06	–65.80	–51.80	8,611
34	ZOND053	3 June	155	12	–65.90	–52.00	8,624
35	ZOND054	3 June	155	18	–65.80	–52.20	8,640
36	ZOND055	4 June	156	00	–65.80	–52.20	8,676
37	ZOND056	4 June	156	06	–65.80	–52.50	8,647
38	ZOND057	4 June	156	12	–65.80	–52.50	8,638
39	ZOND058	4 June	156	18	–65.90	–52.70	8,701
40	ZOND059	5 June	157	00	–65.90	–52.80	8,736

Definitions:

ID Name of the data file.
JD Julian day.
Time Nominal time when the sonde began its ascent.
Max. height Maximum height that the sonde reached.

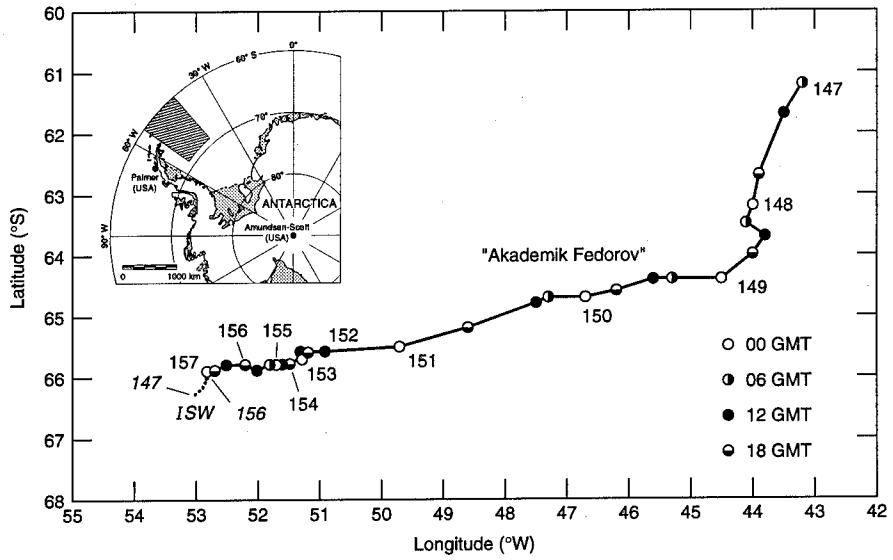

Figure 5. Positions of Ice Station Weddell and Akademik Fedorov *during our simultaneous radiosoundings from 26 May through 4 June 1992. The numbers indicate the Julian day in 1992; the various circles indicate the* Fedorov's *location for the indicated sounding.*

RESULTS

Figures 6 and 7 show sample plots for an ISW Tethersonde sounding and a MicroCORA radiosonde sounding from the *Fedorov*, respectively. Both of these flights were made on June 3 at 00 GMT, when the *Fedorov* was approximately 53 km northeast of ISW. The Tethersonde balloon was raised to a height 629 m. The radiosonde from the *Fedorov* flew to a height of 8,587 m; however, we plotted only the lower 1000 m of the sounding. The plot from ISW shows a lot of structure, including a low-level jet with a core at 79 m; the *Fedorov* plot does not show this jet, nor does it show much of the other structure that can be seen in the ISW sounding. We attribute this difference in the two profiles to the coarse vertical resolution of the MicroCORA described above. The other MicroCORA profiles from

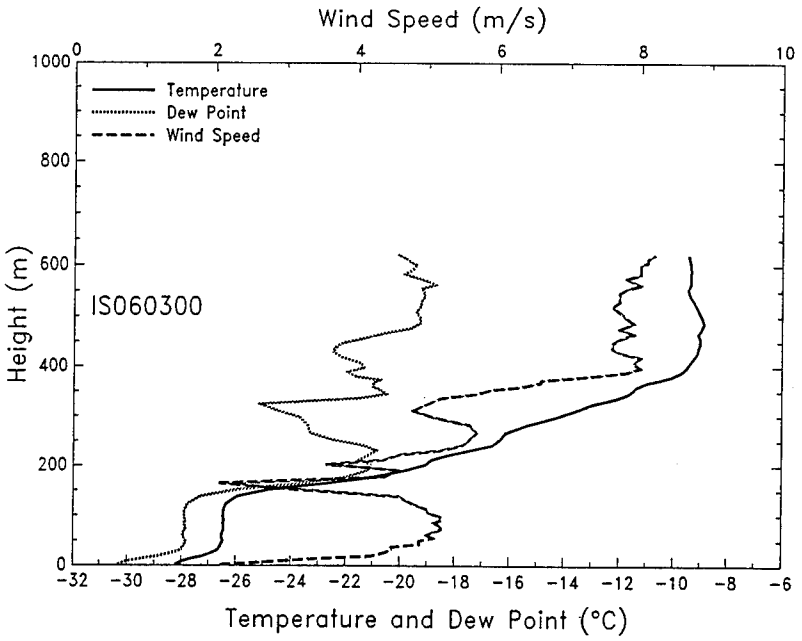

Figure 6. Typical plot of a Tethersonde sounding from ISW. This sounding was made on 3 June 1992, at 0000 GMT.

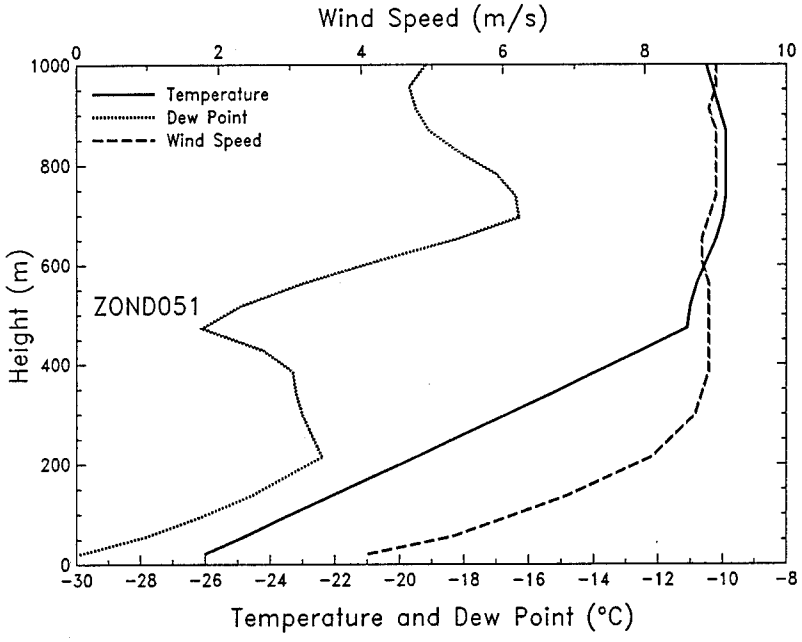

Figure 7. Typical plot of the lower 1000 m of a sounding made from the Fedorov. *This sounding was made at the same time as the sounding in Figure 6.*

the *Fedorov* show the same coarseness when compared with the profiles measured at ISW. Thus, we can only make very general comparisons between soundings from the *Fedorov* and from ISW.

Low-level inversion

Figure 8 shows how we define parameters of the low-level temperature inversion. Following Kahl (1990), we scanned up each temperature profile. If the temperature at a level increased, we called the level immediately below it the base of the inversion. Continuing up the profile, if the temperature at a subsequent level decreased, we called the level immediately below it the top of the inversion. We did, however, ignore thin layers (100 m thick or less) with negative lapses rates that were imbedded within a deeper inversion layer.

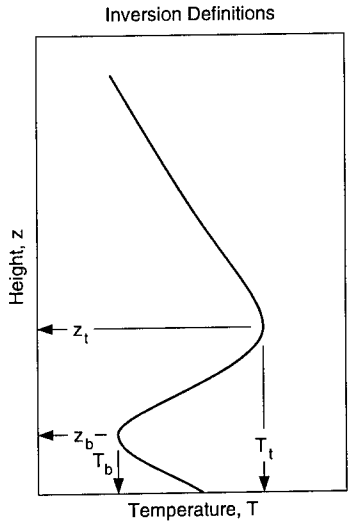

Figure 8. Sketch that defines the parameters of the low-level temperature inversion. z_b is the height of the base of the inversion; T_b is the temperature there. z_t is the height at the top of the inversion; T_t is the temperature there. (See Kahl 1990.)

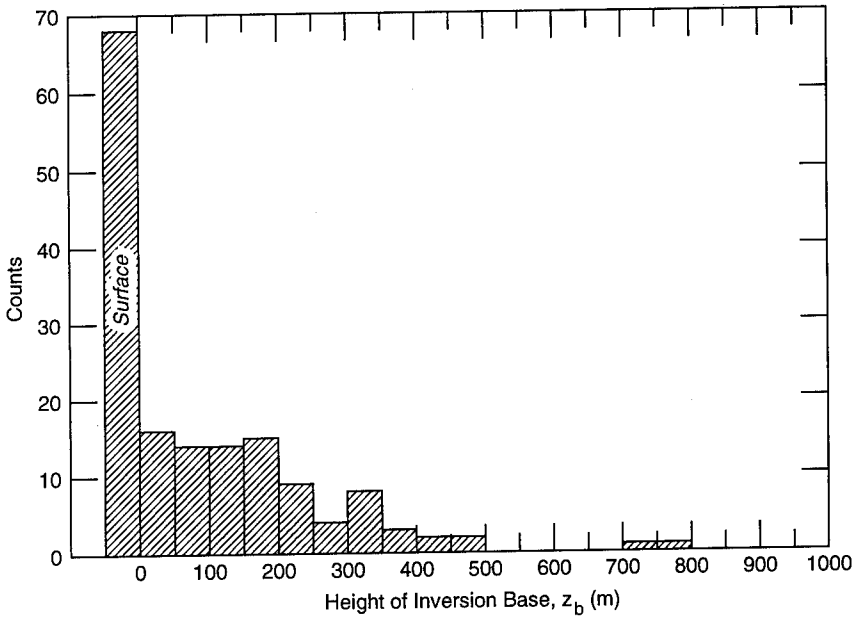

Figure 9. Heights of the base of the inversions (z_b) observed on Ice Station Weddell.

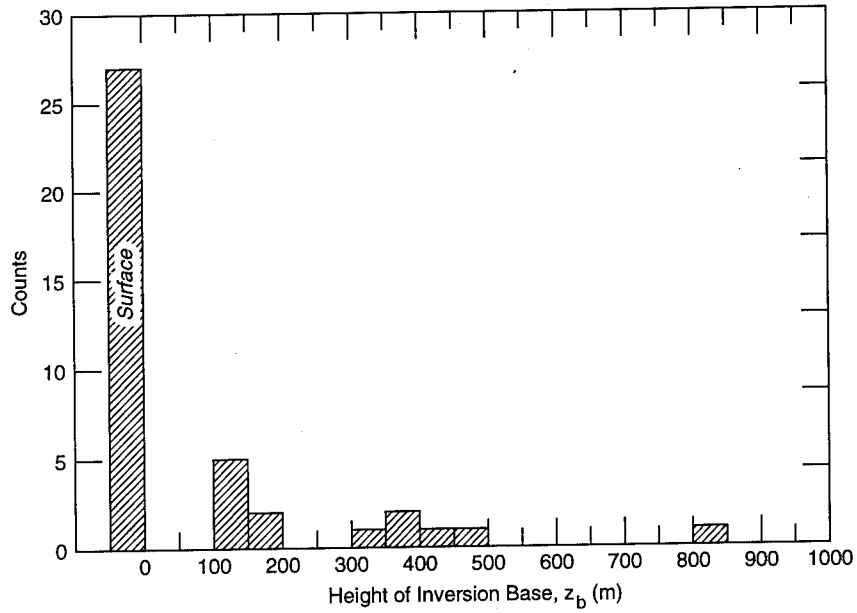

Figure 10. Same as Figure 9, except this is for the inversions observed from the Fedorov.

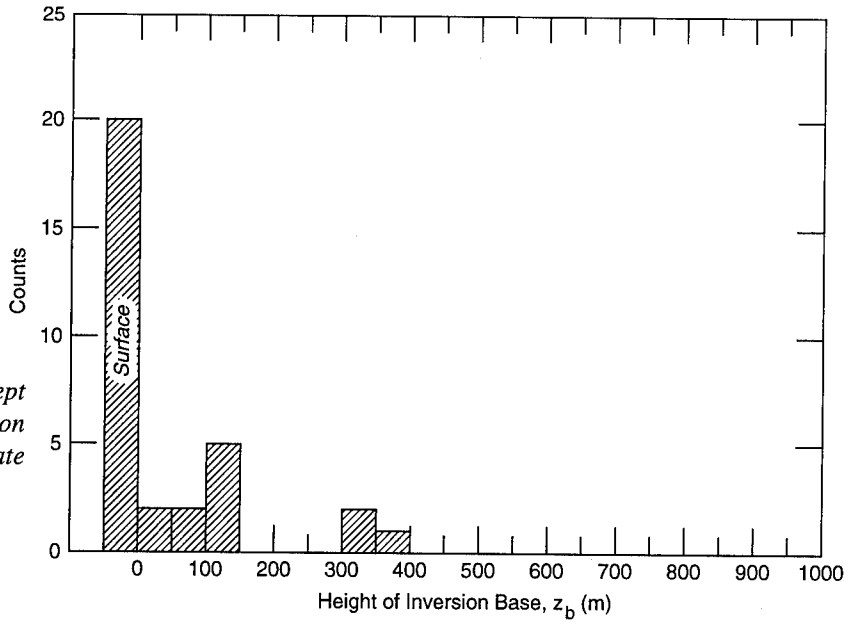

Figure 11. Same as Figure 9, except this is for the inversions observed on ISW during the joint program, late May to early June.

Of the 164 available ISW radiosoundings, 158 (over 95%) showed the presence of a low-level inversion, 4 showed no inversion, and 2 flights were too short to show evidence either way. Inversions with bases below 1000 m were seen in all of the soundings made on the F*edorov* and on the ice camp during our joint sounding program. These frequencies for the occurrence of inversions are similar to those reported by Serreze et al. (1992) for soundings from Soviet Arctic drifting stations in the fall and winter. Tables in Appendix B list inversion parameters for the ISW and F*edorov* soundings.

Figures 9 and 10 show histograms of the base heights of the inversions observed on ISW and *Fedorov*, respectively. As can be seen, 68, or just over 40%, of the ISW inversions were surface-based, and 27 out of 40, or 67.5%, of the *Fedorov* inversions were surface-based. We should note here that we began our ISW sounding program in late February and, thus, sampled many air masses that were quite warm and therefore fairly well mixed in the lower layers. The *Fedorov*, however, made all of its soundings in late May and early June—deep winter—when the stable boundary layer was well developed. To compare the *Fedorov* data with the ISW data, we need to look at the subset of ISW soundings made during the period of the joint study, late May and early June. There were a total of 32 soundings made at the ice camp during this period. Twenty out of the 32, or 62.5%, of the ISW joint soundings had inversions that were surfaced-based (Fig. 11). This percentage agrees well with surfaced-based inversions that were measured from the *Fedorov*, 67.5%. These high percentages of surface-based inversions agree with the observations that Kahl (1990) and Serreze et al. (1992) reported for fall and winter radiosoundings over the Arctic Ocean.

Figures 12 and 13 show histograms of the inversion depth ($z_t - z_b$, see Fig. 8) for the joint ISW and *Fedorov* soundings, respectively, and Figure 14 shows the histogram for the inversion depth of all of the ISW soundings. Both Figures 12 and 14 show that the inversions measured by the ISW radiosondes are fairly thin; most were thinner than 550 m. The *Fedorov* soundings, on the other hand, suggest thicker inversion layers; for these, the median depth is about 500 m. These thicker inversions are more in line with what Kahl (1990) and Serreze et al. (1992) reported over the Arctic Ocean in winter. We, nevertheless, believe that the thinner ISW inversion layers better represent the structure of the lower atmosphere over sea ice in the fall and winter. Our ISW radiosondes simply had better vertical resolution than the *Fedorov* radiosondes and the radiosondes that produced the archived data that Kahl and Serreze et al. used; the picture they yield must therefore be more accurate.

Figures 15 and 16 show histograms of the temperatures at the base of the inversions in the joint ISW and the *Fedorov* soundings, respectively. That these figures are quite similar is encouraging. First, the similarity means that the temperature sensors on the ISW and *Fedorov* radiosondes were well calibrated; their measurements at the lowest levels, where the coarse resolution of the MicroCORA has not smoothed the profile much yet, agree well. Second, this good agreement suggests that the ABL over the western Weddell Sea was fairly uniform, since the ISW and *Fedorov* soundings were often separated by hundreds of kilometers. Figure 17 shows the histogram of the temperatures of the base of the inversions for all of the ISW soundings. Notice that this plot shows some relatively warm inversion bases that we do not see later in the winter (i.e., in Fig. 15 and 16).

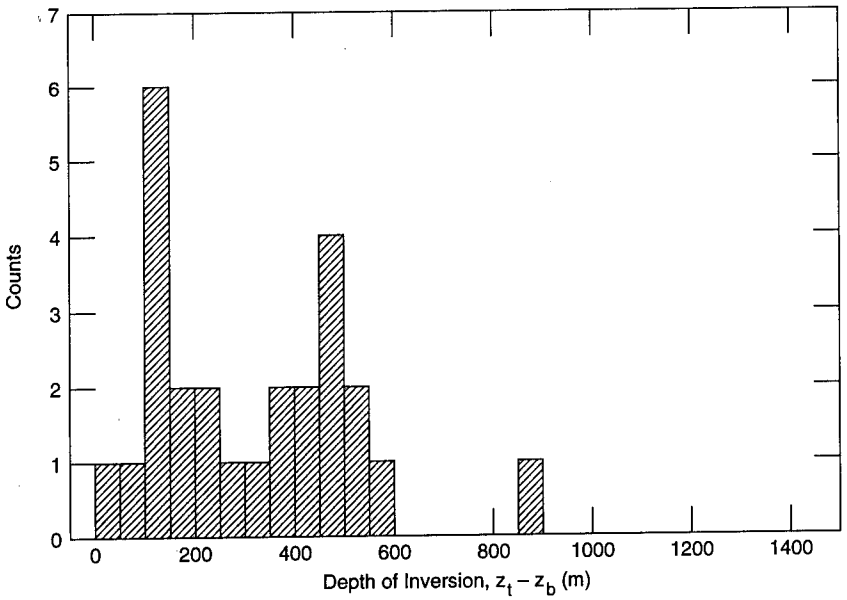

Figure 12. Histogram of the depths (i.e., z_t–z_b) of the inversions observed on Ice Station Weddell during the joint program, late May to early June.

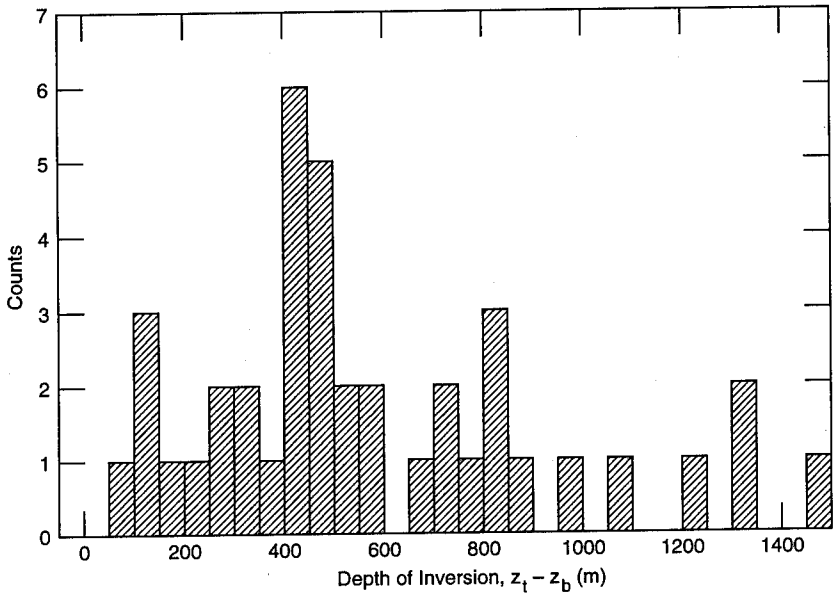

Figure 13. Same as Figure 12, except these are inversion depths observed from the Fedorov.

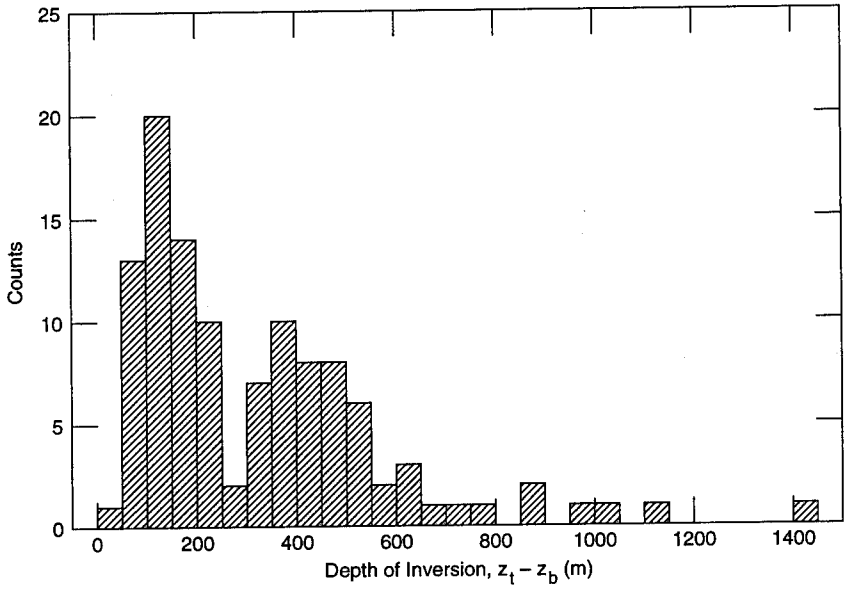

Figure 14. Same as Figure 12, except these are all of the inversion depths observed on Ice Station Weddell.

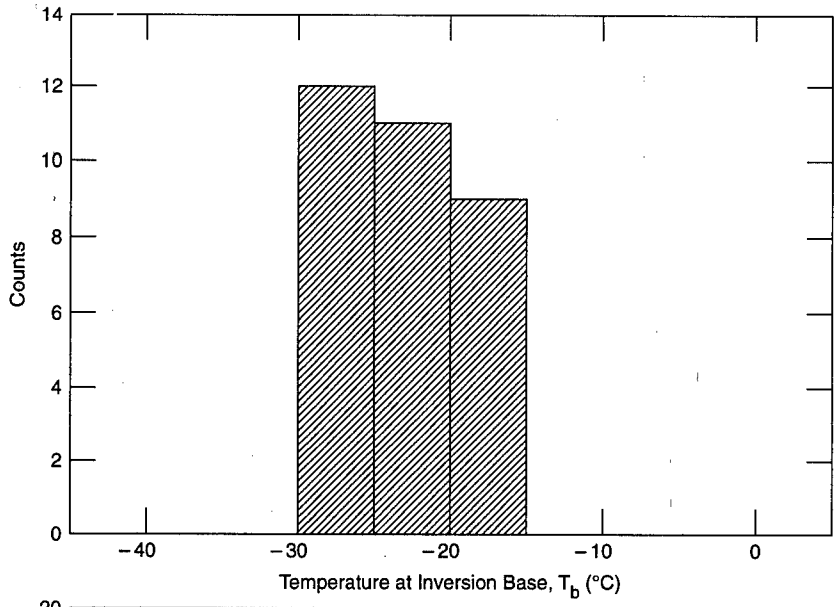

Figure 15. Histogram of the temperatures at the base of the inversions observed on Ice Station Weddell during the joint program, late May to early June.

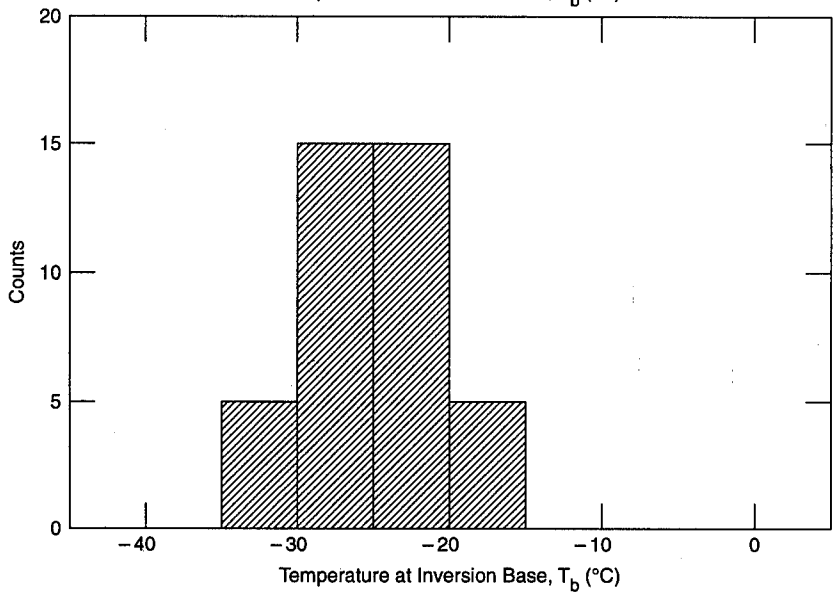

Figure 16. Same as Figure 15, except these are base temperatures observed from the Fedorov.

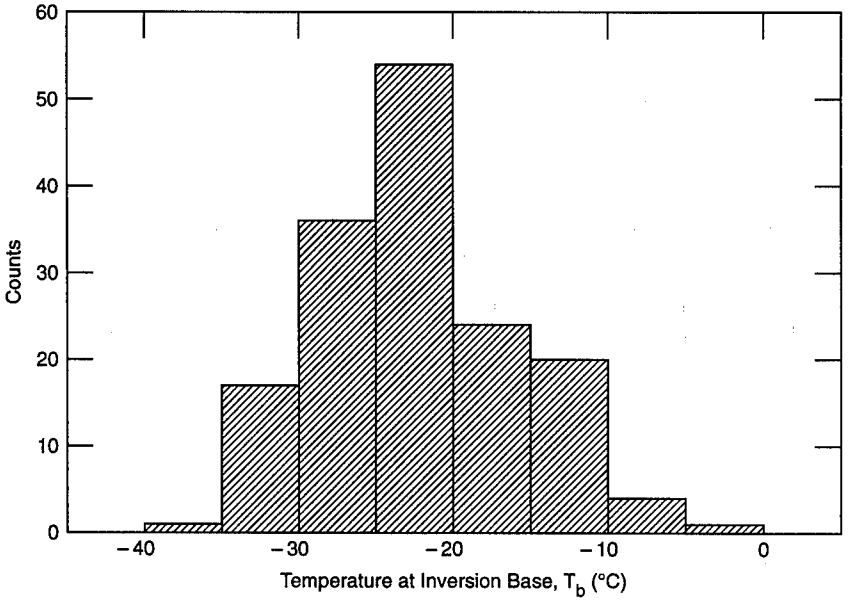

Figure 17. Same as Figure 15, except these are base temperatures for all of the inversions observed on Ice Station Weddell.

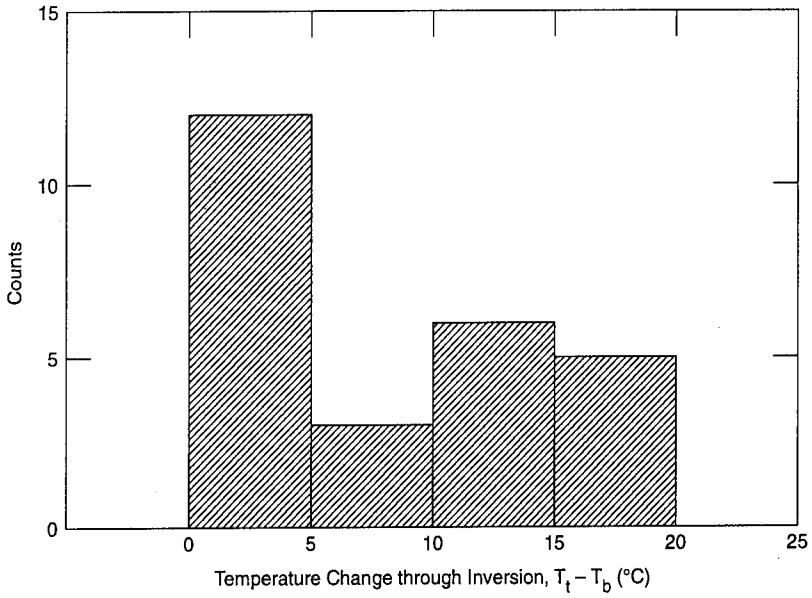

Figure 18. Histogram of the temperature change, T_t–T_b, through the inversions observed on Ice Station Weddell during the joint program, late May to early June.

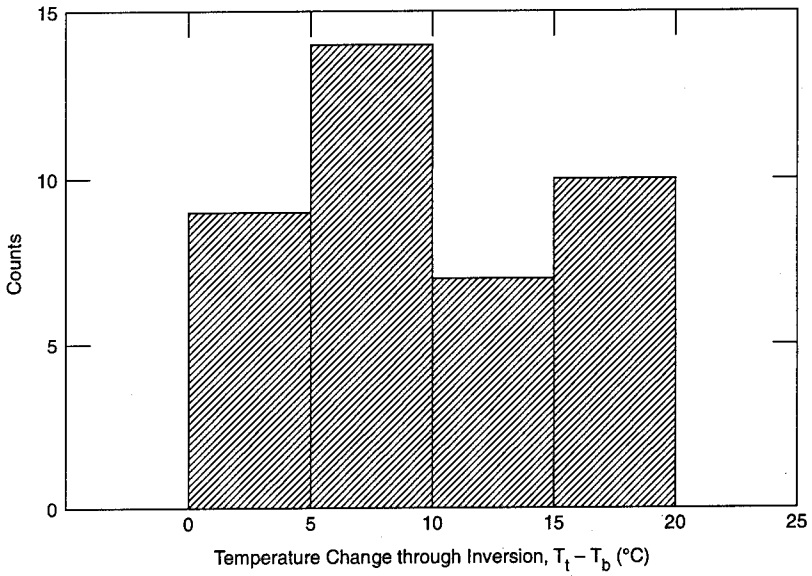

Figure 19. Same as Figure 18, except these temperature changes were observed from the Fedorov.

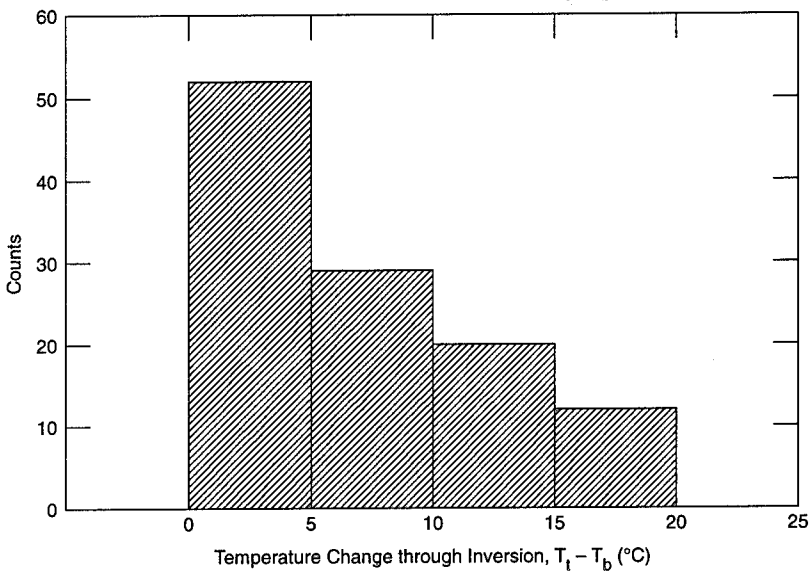

Figure 20. Same as Figure 18, except these are the temperature changes for all of the inversions observed on Ice Station Weddell.

Figures 18 and 19 show histograms of the temperature change though the inversion layers for the joint program, and Figure 20 shows the same for all of the ISW soundings. That is, these are histograms of $T_t - T_b$. The three histograms show many similarities. The temperature increase through the inversion layer was never more than 20°C, and most increases were 0–10°C at both platforms. These results are again roughly what Kahl (1990) and Serreze et al. (1992) reported as temperature differences across Arctic inversions in the fall and winter.

Low-Level Jet

Equally interesting was the low-level atmospheric jet found in many of the soundings made on the ice camp. Remember, the Tethersonde instrumentation package alone supplied us with wind speed and direction profiles at ISW. Therefore, to describe the jet, we had available only the 103 Tethersonde soundings that unambiguously showed whether or not a jet was present. Although the MicroCORA on the *Fedorov* also supplied wind data, a low-level jet was evident in only one of the *Fedorov* soundings during our coordinated sounding program. During that same period, 23 of the 29 ISW Tethersonde soundings showed a jet. We believe that this discrepancy is due to the coarse vertical resolution of the MicroCORA, as discussed above, and not because low-level jets were not present over the *Fedorov*. Therefore, we will discuss only the jets measured at the ice camp.

We used a definition similar to Stull's (1988, p. 521) to identify a low-level jet. If the wind speed profile showed a local maximum that was 2 m/s higher than speeds both above and below it, we called the feature a jet. Notice, with this definition, the jet must be elevated—it cannot occur at the surface. Figure 21 defines the jet parameters that we measured. Figure 6 shows a typical ISW sounding with a jet of 5.2 m/s centered at a height of 79 m. Tables in Appendix B list jet parameters for the ISW and F*edorov* radiosoundings.

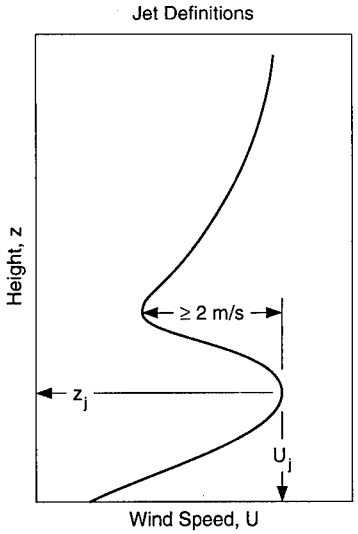

Figure 21. Sketch that defines the parameters of the low-level jet. Stull's (1988, p. 521) criterion defines a jet: The speed in the jet core must be at least 2 m/s greater than speeds both above and below the core. z_j is the height of the jet core; U_j is the wind speed in the core.

Eighty-two (79.6%) of the ISW Tethersonde profiles showed a low-level jet. Figure 22 shows that all of these jets occurred below 500 m with two-thirds occurring between 25 and 175 m. Speeds at the core of the jet ranged from 3.0 to 13.6 m/s, with a majority of the speeds being between 4 and 10 m/s (Fig. 23).

Figure 24 shows that the low-level jet is truly a boundary-layer phenomenon. In only seven of the 82 profiles with jets was the core of the jet above the top of

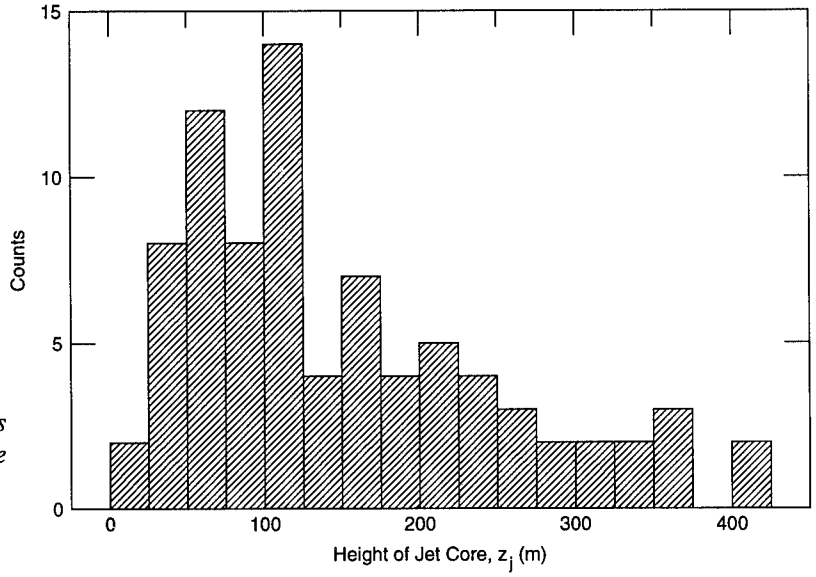

Figure 22. Histogram of the core heights of the low-level jets observed on Ice Station Weddell.

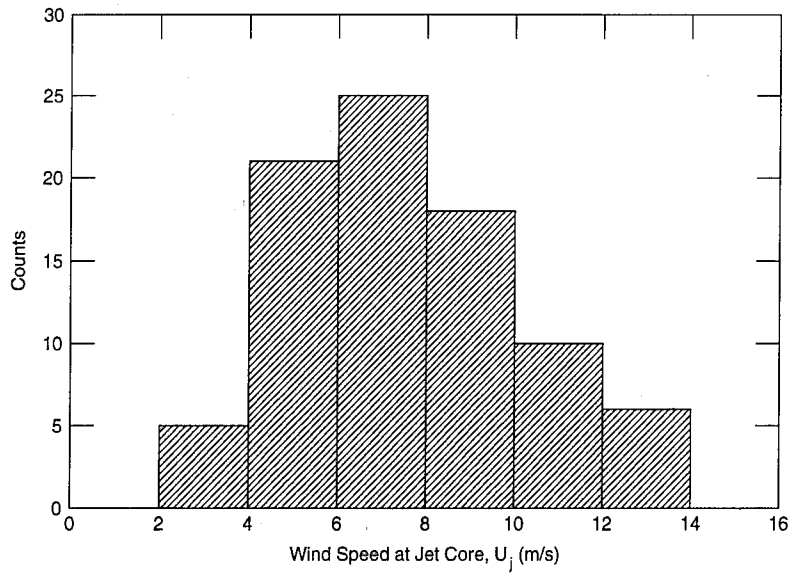

Figure 23. Histogram of the speeds at the core of the low-level jets observed on Ice Station Weddell.

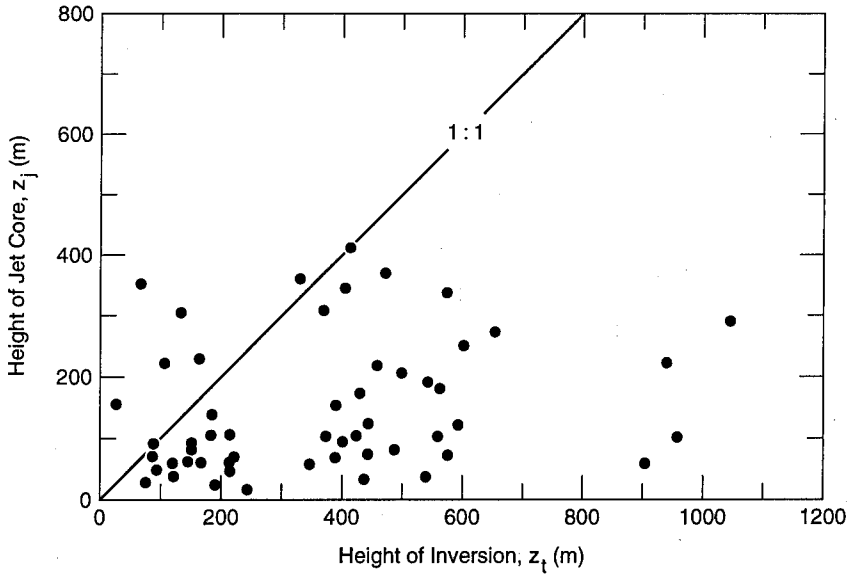

Figure 24. A comparison of the height of the jet core, z_j, and the height of the top of the inversion layer, z_t. The 1:1 line shows where the two heights are equal.

the inversion layer, which is often taken as the nominal height of the ABL.

Figure 25 shows the distribution of wind vectors in the jet cores. Compare this distribution with the surface wind vectors, also measured by the Tethersonde (Fig. 26). Some turning in the wind is evident between the surface and the core of the jet. But if geostrophy is what sets the basic flow in this region, comparing Figures 25 and 26 seems to suggest that the jet has nearly the same direction as the geostrophic wind. It does seem to be supergeostrophic though.

The distribution of jet directions in Figure 25 is a clue to the dynamics governing the ISW jets. Stull (1988, p. 521) listed several causes for low-level jets. Of these, the following four seem most plausible for our situation: 1) undamped inertial oscillations that occur when the lower layer of the atmosphere becomes frictionally decoupled from the surface because of the strong stability there (e.g., Blackadar 1957); 2) baroclinic effects resulting from the temperature gradient between the open ocean and the pack ice; 3) effects of the barrier wind that flows northward at low levels, guided by the mountains of the Antarctic Peninsula (Schwerdtfeger 1984); 4) isallobaric winds that must flow into a deepening low pressure center or out of a rising high because the lower atmosphere can only be quasi-geostrophic (Gill 1982 p. 311 ff.).

From Figure 25, we see that the jet winds tend to blow north and northeastward or south and southwestward. Thus, it seems unlikely that inertial oscillations are the primary cause of the jets. Inertial oscillations would add vectorially to the geostrophic wind and, thus, lead to a supergeostrophic wind only about a quarter of the time—not 80% of the time, as we observed.

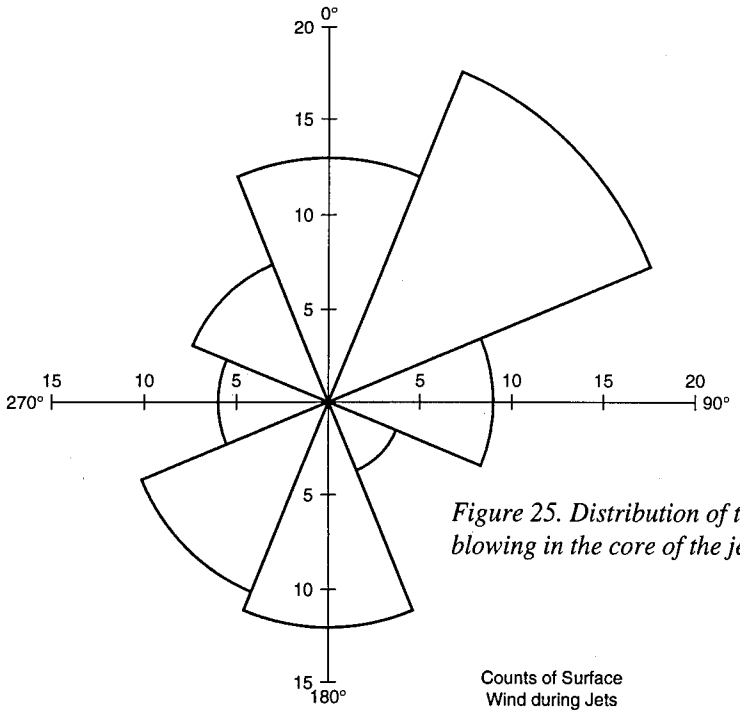

Figure 25. Distribution of the directions toward which the wind was blowing in the core of the jets observed on Ice Station Weddell.

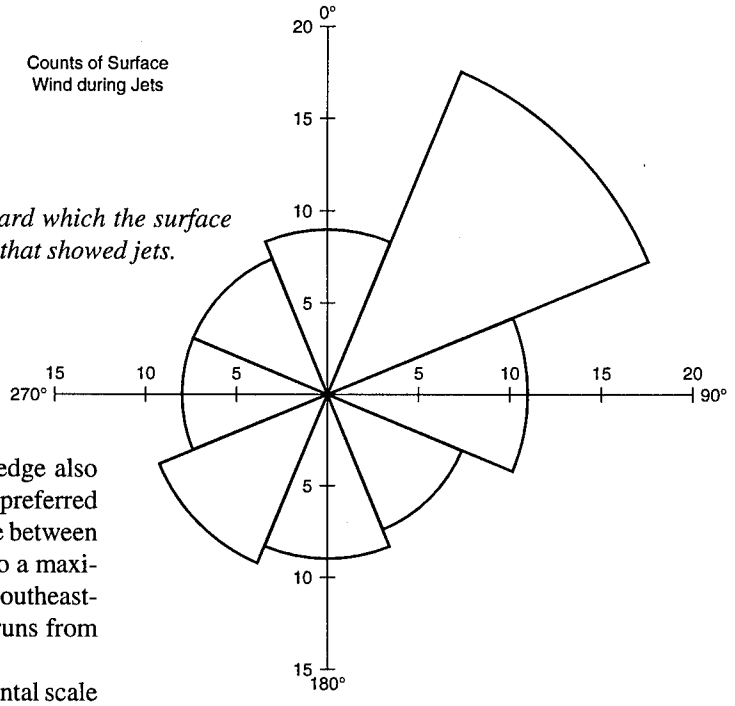

Figure 26. Distribution of the directions toward which the surface wind was blowing in all Tethersonde profiles that showed jets.

The baroclinicity associated with the ice edge also seems an unlikely cause for the jets because the preferred direction is wrong. The temperature difference between the open ocean and the pack ice would lead to a maximum in the wind speed profile that is directed southeasterly in this region since the closest ice edge runs from northwest to southeast.

Again the direction is wrong and the horizontal scale is not right for the jets to be associated with the barrier wind. In this region, the barrier wind would tend to produce a jet directed north-northwest, parallel to the nearest mountains of the Antarctic Peninsula. Parish (1983) also showed that the barrier wind extends only about 200–300 km eastward from the mountains; ISW was always beyond this limit. Admittedly, Parish's are model results that have not been confirmed experimentally. Parish* suggested though that, even if the jet is not a direct consequence of the barrier winds, another kind of topographic guidance may explain the jets directed north and northeastward. There are mountains along the Antarctic Peninsula at latitudes far south of ISW's. With the stable stratification in the boundary layer and the consequent frictional decoupling from the surface, a barrier wind associated with these mountains could initiate a low-level jet that would propagate far northward even after it has lost contact with the mountains. We will, thus, continue to keep our eyes open for the effect of barrier winds in these and in our other ISW data.

If the pressure gradient increases with time, the isallobaric wind is directed down the pressure gradient. That

* T.R. Parish, University of Wyoming, personal communication, 1993.

is, the isallobaric wind acts to fill a deepening low or to evacuate a rising high. As such, the isallobaric wind is generally almost at right angles to the geostrophic wind. Therefore, if the distributions in Figures 25 and 26 primarily reflect the geostrophic wind, the isallobaric wind cannot explain the low-level jet—we would expect more turning. But surface level pressure charts show that during our deployment on ISW, low and high pressure centers tended to follow the ice edge from low latitudes into the Weddell Sea. Thus, the jets do seem to be preferentially directed toward the north and northeast, into evolving and migrating low pressure centers. Likewise, when a high tracked southeastward to our north, the isallobaric wind would contribute a component directed south and southeastward, away from the high. This is the second dominant jet direction we observed. To accept this explanation for the cause of the jets would mean we could not interpret Figures 25 and 26 as indications of the geostrophic wind.

But maybe we do not need to invoke any of these specific causes at all. Yamada (1976, or see Garratt 1992, p. 68 ff.) showed that the components of the mean wind vector in a stably stratified boundary layer obey similarity relations when properly scaled and that a low-level jet is the dominant feature of the stable boundary layer. In the near future, we will try to fit our temperature and wind velocity profiles with these empirical similarity relations. If this existing theory describes our data, our quandary over identifying the cause of the jet may be moot.

LITERATURE CITED

Andreas, E.L (1983) Reports of the U.S.–U.S.S.R. Weddell Polynya Expedition, October–November 1981, Volume 6: Upper-air data. USA Cold Regions Research and Engineering Laboratory, Special Report 83-13.

Andreas, E.L (1985) Heat and moisture advection over Antarctic sea ice. *Monthly Weather Review*, 113: 736–746.

Andreas, E.L and K.J. Claffey (1992) The air–ice drag coefficient in the Weddell Sea deduced from profile measurements. In preprint volume, *Tenth Symposium on Turbulence and Diffusion, 29 September–2 October 1992, Portland, Oregon*. Boston: American Meteorological Society, J109–J112.

Andreas, E.L and W.A. Richter (1982) An evaluation of Vaisala's MicroCORA Automatic Sounding System. USA Cold Regions Research and Engineering Laboratory, CRREL Report 82-28.

Andreas, E.L, K.J. Claffey, A.P. Makshtas and B.V. Ivanov (1992) Atmospheric sciences on Ice Station Weddell. *Antarctic Journal of the United States*, **27**(5): 115–117.

Andreas, E.L, K.J. Claffey and A.P. Makshtas (1993) Low-level atmospheric jets and inversion on Ice Station Weddell. *Antarctic Journal of the United States*, in press.

Antarctic Journal of the United States (1992) U.S. and Russian scientists complete historic Weddell Sea investigation. *Antarctic Journal of the United States*, **27**(4): 8–11.

Blackadar, A.K. (1957) Boundary layer wind maxima and their significance for the growth of nocturnal inversions. *Bulletin of the American Meteorological Society*, **38**: 283-290.

Brown, R.A. (1981) Modeling the geostrophic drag coefficient for AIDJEX. *Journal of Geophysical Research*, **86**: 1989–1994.

Brown, R.A. and W.T. Liu (1982) An operational large-scale marine planetary boundary layer model. *Journal of Applied Meteorology*, **21**: 261–269.

Fleagle, R.G. and J.A. Businger (1980) *An Introduction to Atmospheric Physics*. New York: Academic Press.

Garratt, J.R. (1992) *The Atmospheric Boundary Layer*. Cambridge: Cambridge University Press.

Gill, A.E. (1982) *Atmosphere–Ocean Dynamics*. New York: Academic Press.

Hibler, W. D. III (1979) A dynamic thermodynamic sea ice model. *Journal of Physical Oceanography*, **9**: 815–846.

ISW Group (1993) Weddell Sea exploration from ice station. *Eos, Transactions of the American Geophysical Union*, **74**: 121–126.

Kahl, J.D. (1990) Characteristics of the low-level temperature inversion along the Alaskan Arctic coast. *International Journal of Climatology*, **10**: 537–548.

List, R.J. (1984) *Smithsonian Meteorological Tables*. Sixth Edition. Washington, D.C.: Smithsonian Institution Press.

Murray, F.W. (1967) On the computation of saturation vapor pressure. *Journal of Applied Meteorology*, **1**: 203–204.

Parish, T.R. (1983) The influence of the Antarctic Peninsula on the wind fields over the western Weddell Sea. *Journal of Geophysical Research*, **88**: 2684–2692.

Schwerdtfeger, W. (1984) *Weather and Climate of the Antarctic*. Amsterdam: Elsevier.

Serreze, M.C., J.D. Kahl and R.C. Schnell (1992) Low-level temperature inversions of the Eurasian Arctic and comparisons with Soviet drifting station data. *Journal of Climate*, **5**: 615–629.

Stull, R.B. (1988) *An Introduction to Boundary-Layer Meteorology*. Dordrecht: Kluwer.

Yamada, T. (1976) On the similarity functions A, B and C of the planetary boundary layer. *Journal of the Atmospheric Sciences*, **33**: 781–793.

APPENDIX A: MAGNETIC DECLINATION

These are the magnetic declinations at Ice Station Weddell. We read them off Jet Navigation Chart JNC 120 (obtained from the Defense Mapping Agency) by locating the noon GMT position of the ice station. All angles are degrees east of north. Thus, to correct the ISW Tethersonde's measured compass readings to true north,

Angle, true = Angle, measured + Declination.

In the table that follows, the first column is the date in 1992, the second column is the corresponding Julian day, and the third column is the declination in degrees.

Date	*Julian day*	*Declination (deg.)*	*Date*	*Julian day*	*Declination (deg.)*	*Date*	*Julian day*	*Declination (deg.)*
11 Feb	42	13.	22 Mar	82	13.	1 May	122	12.
12 Feb	43	13.	23 Mar	83	13.	2 May	123	12.
13 Feb	44	13.	24 Mar	84	13.	3 May	124	12.
14 Feb	45	13.	25 Mar	85	13.	4 May	125	12.
15 Feb	46	13.	26 Mar	86	13.	5 May	126	11.
16 Feb	47	13.	27 Mar	87	13.	6 May	127	11.
17 Feb	48	13.	28 Mar	88	13.	7 May	128	11.
18 Feb	49	13.	29 Mar	89	12.	8 May	129	11.
19 Feb	50	13.	30 Mar	90	12.	9 May	130	11.
20 Feb	51	13.	31 Mar	91	12.	10 May	131	11.
21 Feb	52	13.	1 Apr	92	12.	11 May	132	11.
22 Feb	53	13.	2 Apr	93	12.	12 May	133	11.
23 Feb	54	13.	3 Apr	94	12.	13 May	134	11.
24 Feb	55	13.	4 Apr	95	12.	14 May	135	11.
25 Feb	56	13.	5 Apr	96	12.	15 May	136	11.
26 Feb	57	13.	6 Apr	97	12.	16 May	137	11.
27 Feb	58	13.	7 Apr	98	12.	17 May	138	11.
28 Feb	59	13.	8 Apr	99	12.	18 May	139	11.
29 Feb	60	13.	9 Apr	100	12.	19 May	140	11.
1 Mar	61	13.	10 Apr	101	12.	20 May	141	11.
2 Mar	62	13.	11 Apr	102	12.	21 May	142	11.
3 Mar	63	13.	12 Apr	103	12.	22 May	143	11.
4 Mar	64	13.	13 Apr	104	12.	23 May	144	11.
5 Mar	65	14.	14 Apr	105	12.	24 May	145	11.
6 Mar	66	14.	15 Apr	106	12.	25 May	146	10.
7 Mar	67	14.	16 Apr	107	12.	26 May	147	10.
8 Mar	68	14.	17 Apr	108	12.	27 May	148	10.
9 Mar	69	14.	18 Apr	109	12.	28 May	149	10.
10 Mar	70	14.	19 Apr	110	12.	29 May	150	10.
11 Mar	71	13.	20 Apr	111	12.	30 May	151	10.
12 Mar	72	13.	21 Apr	112	12.	31 May	152	10.
13 Mar	73	13.	22 Apr	113	12.	1 June	153	10.
14 Mar	74	13.	23 Apr	114	12.	2 June	154	10.
15 Mar	75	13.	24 Apr	115	12.	3 June	155	10.
16 Mar	76	13.	25 Apr	116	12.	4 June	156	10.
17 Mar	77	13.	26 Apr	117	11.	5 June	157	10.
18 Mar	78	13.	27 Apr	118	12.	6 June	158	10.
19 Mar	79	13.	28 Apr	119	12.	7 June	159	10.
20 Mar	80	13.	29 Apr	120	12.	8 June	160	10.
21 Mar	81	13.	30 Apr	121	12.	9 June	161	10.

APPENDIX B: JET AND INVERSION STATISTICS

The tables in this appendix list the parameters of the low–level inversions and jets observed on ISW and on the *Fedorov*. Figure 8 defines the inversion parameters listed in the tables; Figure 21 defines the jet parameters.

Table B1. Parameters of the low–level jets and inversions observed on Ice Station Weddell.

	Sounding	*Inversion?*	z_b *(m)*	z_t *(m)*	T_b *(°C)*	T_t *(°C)*	*Jet?*	z_j *(m)*	U_j *(m/s)*	*Direction at core (deg.)*
1	IS022100	Yes	263	319	–10.26	–10.03	NA			
2	IS022112	Yes	498	574	–11.06	–9.71	Yes	337	8.4	141
3	IS022200	Yes	146	228	–5.35	–4.72	NA			
4	IS022300	No					NA			
5	IS022312	No					NA			
6	IS022412	No					NA			
7	IS022512	No					NA			
8	IS022600	Unk					Unk			
9	IS022612	Yes	294	486	–10.48	–6.58	No			
10	IS022700	Yes	141	262	–9.80	–6.84	No			
11	IS022712	Yes	339	458	–11.90	–8.46	Yes	217	5.4	7
12	IS022800	Yes	347	472	–11.75	–9.92	Unk			
13	IS022812	Yes	180	297	–12.47	–11.64	NA			
14	IS022900	Yes	176	268	–12.29	–11.86	No			
15	IS022912	Yes	171	244	–12.93	–11.73	Yes	16	5.8	55
16	IS030100	Yes	171	331	–14.41	–13.23	Yes	360	9.5	342
17	IS030112	Yes	0	149	–14.59	–14.03	No			
18	IS030200	Yes	788	901	–20.08	–12.32	Yes	57	3.0	121
19	IS030212	Yes	461	574	–15.23	–11.56	No			
20	IS030312	Unk					Yes	214	12.1	312
21	IS030400	Yes	447	894	–15.25	–4.92	NA			
22	IS030412	Yes	350	1777	–20.47	–8.42	NA			
23	IS030512	Yes	145	941	–27.01	–13.76	Yes	224	9.3	138
24	IS030600	Yes	224	Unk	–23.27	Unk	Yes	125	10.1	177
25	IS030612	Yes	0	1046	–24.87	–10.63	Yes	289	6.8	196
26	IS030700	Yes	80	959	–18.81	–10.78	Yes	102	7.3	347
27	IS030712	Yes	309	Unk	–16.89	Unk	Yes	149	6.0	261
28	IS030800	Yes	0	Unk	–21.21	Unk	Yes	54	6.4	292
29	IS030812	Yes	172	654	–18.87	–6.56	Yes	274	10.3	321
30	IS030900	Yes	98	252	–14.41	–10.01	Unk			
31	IS030912	Yes	213	405	–23.38	–18.01	Yes	346	12.2	206
32	IS031000	Yes	0	Unk	–19.36	Unk	Yes	97	8.1	355
33	IS031012	Yes	143	Unk	–21.08	Unk	Yes	185	5.9	123
34	IS031100	Yes	0	Unk	–23.89	Unk	Yes	284	5.6	95
35	IS031112	Yes	0	316	–21.12	–17.68	Unk			
36	IS031212	Yes	0	103	–18.40	–14.68	Unk			
37	IS031312	Yes	0	305	–20.83	–7.90	Unk			
38	IS031412	Yes	0	459	–26.00	–12.13	NA			
39	IS031512	Yes	161	Unk	–20.21	Unk	Unk			
40	IS031612	Yes	199	410	–25.05	–21.20	NA			
41	IS031712	Yes	0	91	–23.12	–18.96	Yes	48	7.5	228
42	IS031800	Yes	0	217	–26.08	–19.20	Unk			
43	IS031812	Yes	0	238	–26.63	–18.49	Unk			
44	IS031912	Yes	285	449	–18.44	–13.72	NA			
45	IS032012	Yes	234	626	–17.04	–11.36	NA			
46	IS032100	Yes	0	215	–22.03	–12.28	Yes	45	5.6	272
47	IS032112	Yes	0	164	–21.92	–10.78	Yes	227	9.0	121
48	IS032200	Yes	0	150	–16.61	–7.87	Yes	91	12.6	260
49	IS032212	Yes	397	1523	–29.34	–17.29	NA			
50	IS032312	Yes	0	212	–26.06	–23.42	Yes	106	12.3	206
51	IS032400	Yes	0	67	–25.32	–23.67	Yes	352	5.6	205
52	IS032412	Yes	102	569	–23.45	–18.95	No			
53	IS032500	Yes	190	411	–22.16	–20.04	Yes	411	4.0	146
54	IS032512	Yes	0	150	–24.99	–24.59	Yes	81	7.3	180
55	IS032600	Yes	0	87	–26.56	–26.20	Yes	92	9.7	197
56	IS032612	Yes	406	525	–17.44	–16.26	NA			

Table B1 (cont'd). Parameters of the low–level jets and inversions observed on Ice Station Weddell.

	Sounding	*Inversion?*	z_b *(m)*	z_t *(m)*	T_b *(°C)*	T_t *(°C)*	*Jet?*	z_j *(m)*	U_j *(m/s)*	*Direction at core (deg.)*
57	IS032712	Yes	332	679	–23.95	–15.89	NA			
58	IS032812	Unk				Unk				
59	IS032912	Yes	309	Unk	–25.05	Unk	Unk			
60	IS033012	Yes	215	365	–25.35	–21.47	NA			
61	IS033112	Yes	0	392	–24.27	–14.04	Yes	150	7.5	209
62	IS0331SP	Yes	0	Unk	–24.45	Unk	Unk			
63	IS040100	Yes	0	442	–23.13	–16.29	Yes	72	6.7	217
64	IS040112	Yes	0	208	–27.79	–16.95	Unk			
65	IS040212	Yes	34	Unk	–28.47	Unk	Yes	231	8.6	203
66	IS040312	Yes	50	Unk	–21.84	Unk	No			
67	IS040412	Yes	15	74	–19.47	–17.98	Yes	30	3.6	103
68	IS040500	Yes	0	488	–20.64	–15.03	No			
69	IS040512	Yes	44	Unk	–17.82	Unk	Unk			
70	IS040612	Yes	0	Unk	–24.49	Unk	Unk			
71	IS040712	Yes	0	697	–24.21	–6.63	NA			
72	IS040900	Yes	0	Unk	–24.96	Unk	Yes	43	5.8	241
73	IS040912	Yes	0	Unk	–25.29	Unk	Unk			
74	IS041112	Yes	0	389	–27.65	–22.19	Yes	68	4.9	189
75	IS041200	Yes	0	Unk	–12.65	Unk	Yes	104	8.1	299
76	IS041312	Yes	165	669	–12.79	–8.14	NA			
77	IS041512	Yes	246	853	–11.70	–5.05	NA			
78	IS041612	Yes	299	Unk	–26.61	Unk	Unk			
79	IS041712	Yes	65	490	–22.37	–6.32	NA			
80	IS041812	Yes	0	Unk	–12.07	Unk	Yes	82	13.0	234
81	IS041912	Yes	0	212	–10.56	–0.56	Yes	68	11.9	202
82	IS042000	Yes	0	190	–16.98	1.47	Yes	25	7.0	24
83	IS042012	Yes	0	Unk	–14.48	Unk	Yes	101	11.5	290
84	IS042100	Yes	0	Unk	–19.91	Unk	Yes	160	13.6	179
85	IS042112	Yes	0	Unk	–22.93	Unk	Unk			
86	IS042212	Yes	39	423	–19.35	–0.41	NA			
87	IS042312	Yes	235	782	–4.89	3.60	NA			
88	IS042412	Yes	247	856	–6.14	–1.23	NA			
89	IS042512	Yes	116	292	–9.25	–4.70	NA			
90	IS042612	Yes	62	592	–16.42	–6.24	NA			
91	IS042712	Yes	168	880	–13.01	–4.45	NA			
92	IS042912	Yes	707	891	–16.72	–16.31	NA			
93	IS043012	Yes	0	403	–26.70	–21.08	NA			
94	IS050112	Yes	176	579	–30.90	–16.44	NA			
95	IS050200	Yes	93	231	–20.67	–13.30	No			
96	IS050212	Yes	89	177	–19.37	–15.67	No			
97	IS050300	Yes	112	448	–18.72	–15.22	No			
98	IS050312	Yes	77	259	–17.69	–14.47	No			
99	IS050400	Yes	48	240	–16.87	–14.79	No			
100	IS050412	Yes	0	121	–23.98	–15.64	Yes	39	6.8	340
101	IS050500	Yes	225	Unk	–27.32	Unk	Unk			
102	IS050512	Yes	377	Unk	–28.58	Unk	No			
103	IS050600	Yes	0	87	–26.11	–23.81	Yes	71	7.6	204
104	IS050612	Yes	47	426	–23.25	–20.12	Yes	105	7.4	344
105	IS050700	Yes	0	Unk	–26.96	Unk	Unk			
106	IS050712	Yes	147	Unk	–22.80	Unk	Yes	254	6.6	328
107	IS050812	Yes	12	Unk	–34.31	Unk	Unk			
108	IS050900	Yes	0	Unk	–37.02	Unk	Yes	47	8.6	358
109	IS050912	Yes	195	499	–20.66	–12.19	Yes	207	4.4	272
110	IS051012	Yes	162	Unk	–16.99	Unk	Yes	162	5.1	14
111	IS051100	Yes	40	Unk	–23.83	Unk	No			
112	IS051112	Yes	37	Unk	–23.79	Unk	No			
113	IS051200	Yes	80	444	–20.24	–0.58	Yes	121	9.1	356
114	IS051212	Yes	89	429	–10.65	0.60	Yes	171	10.0	244
115	IS051300	Yes	0	363	–20.74	–3.05	Yes	303	6.9	224
116	IS051312	Yes	0	Unk	–24.48	Unk	Yes	143	5.4	48
117	IS051400	Yes	0	Unk	–22.72	Unk	Yes	425	9.5	23
118	IS051412	Yes	0	557	–17.27	–7.45	Yes	103	9.1	51
119	IS051500	Yes	209	471	–11.09	–5.55	Yes	367	8.6	38

Table B1 (cont'd).

	Sounding	Inversion?	z_b (m)	z_t (m)	T_b (°C)	T_t (°C)	Jet?	z_j (m)	U_j (m/s)	Direction at core (deg.)
120	IS051512	Yes	53	Unk	–21.09	Unk	Yes	194	9.2	235
121	IS051600	Yes	0	Unk	–25.86	Unk	Yes	123	11.5	201
122	IS051612	Yes	17	1010	–32.58	–13.51	NA			
123	IS051700	Yes	62	Unk	–28.90	Unk	Yes	156	5.3	181
124	IS051712	Yes	44	Unk	–27.14	Unk	Yes	231	5.1	39
125	IS051800	Yes	21	Unk	–24.27	Unk	Yes	86	5.0	130
126	IS051812	Yes	0	502	–23.23	–13.44	No			
127	IS051900	Yes	51	Unk	–23.34	Unk	Yes	113	7.5	29
128	IS051912	Yes	176	563	–21.98	–16.11	No			
129	IS052000	Yes	31	122	–21.31	–20.29	Yes	56	4.3	171
130	IS052012	Yes	171	337	–25.26	–22.81	NA			
131	IS052112	Yes	0	449	–30.90	–23.12	NA			
132	IS052212	Yes	122	770	–33.73	–26.55	NA			
133	IS052612	Yes	0	207	–34.46	–30.85	NA			
134	IS052618	Yes	101	214	–29.85	–28.19	Unk			
135	IS052700	Yes	332	749	–31.77	–23.41	NA			
136	IS052712	Yes	82	184	–30.76	–26.81	Yes	134	9.5	232
137	IS052718	Yes	142	Unk	–26.45	Unk	Yes	160	6.5	256
138	IS052800	Yes	134	Unk	–23.45	Unk	Yes	156	5.5	258
139	IS052806	Yes	108	592	–22.90	–14.76	Yes	121	5.0	233
140	IS052812	Yes	94	217	–22.68	–18.97	Yes	116	9.1	194
141	IS052818	Yes	0	400	–23.50	–18.67	Yes	93	10.4	198
142	IS052900	Yes	0	107	–26.73	–25.18	Yes	220	9.5	224
143	IS052906	Yes	139	598	–27.27	–15.93	Yes	249	6.2	212
144	IS052912	Yes	0	27	–26.98	–26.04	Yes	156	3.1	235
145	IS052918	Yes	0	559	–28.86	–16.19	Yes	178	3.7	277
146	IS053000	Yes	0	542	–31.03	–15.94	Yes	190	5.7	27
147	IS053006	Yes	0	537	–32.48	–17.50	Yes	39	6.5	21
148	IS053018	Yes	0	133	–26.28	–21.42	Yes	305	6.4	34
149	IS053100	Yes	395	Unk	–23.95	Unk	Yes	72	4.8	85
150	IS053106	Yes	31	112	–24.98	–21.67	No			
151	IS053112	Yes	28	145	–24.35	–20.91	Yes	60	7.5	142
152	IS053118	Yes	0	182	–23.39	–21.60	Yes	104	7.7	96
153	IS060100	Yes	314	573	–24.30	–21.99	Yes	71	6.9	79
154	IS060106	Yes	0	372	–29.79	–20.87	Yes	102	6.6	107
155	IS060112	Yes	0	227	–30.98	–19.72	No			
156	IS060118	Yes	0	166	–31.35	–19.37	Yes	57	7.0	25
157	IS060200	Yes	0	437	–34.00	–18.67	Yes	33	6.6	359
158	IS060206	Yes	0	345	–32.68	–17.21	Yes	56	8.0	346
159	IS060212	Yes	0	Unk	–31.99	Unk	Unk			
160	IS060218	Yes	0	Unk	–29.14	Unk	Yes	275	10.6	243
161	IS060300	Yes	0	487	–28.22	–8.87	Yes	79	5.2	165
162	IS060306	Yes	0	451	–31.75	–13.66	No			
163	IS060312	Yes	0	Unk	–30.37	Unk	Unk			
164	IS060400	Yes	0	878	–25.82	–13.11	NA			

Explanations:

Inversion? We use Kahl's (1990) definition of an inversion. If there was no inversion in the lowest 1000 m, we enter 'No' in this column. If the sounding was short and there was no evidence of a temperature increase in it, we enter 'Unk' for Unknown.

Jet? We identify a jet as a feature in the wind speed profile for which the speed is at least 2 m/s higher than speeds both above above and below. In other words, a jet cannot occur at the surface. If the sounding was from an Airsonde, no winds were measured and we, thus, have no way of knowing whether there was a jet. For these ascents, we enter "NA" in the column for Not Applicable. If the sounding was a short one with a Tethersonde and we saw no evidence of a jet, we entered "Unk" in the column for Unknown. If the Tethersonde reached 600 m without showing a jet, we entered "No."

Direction This direction is the way the wind is coming from, with respect to true north. That is, we applied the magnetic declination (App. A) to the magnetic heading measured by the compass on the Tethersonde.

Table B2. Parameters of the low–level jets and inversions observed on *Akademik Fedorov* during the coordinated radiosounding program. Definitions are the same as in Table B1.

	Sounding	*Inversion?*	z_b *(m)*	z_t *(m)*	T_b *(°C)*	T_t *(°C)*	*Jet?*	z_j *(m)*	U_j *(m/s)*	*Direction at core (deg.)*
1	ZOND020	Yes	0	116	–25.3	–23.3	No			
2	ZOND021	Yes	432	654	–21.4	–15.6	No			
3	ZOND022	Yes	335	762	–20.6	–14.4	No			
4	ZOND023	Yes	383	687	–22.0	–16.0	No			
5	ZOND024	Yes	0	408	–26.5	–20.6	No			
6	ZOND025	Yes	0	1058	–30.4	–18.2	No			
7	ZOND026	Yes	0	474	–25.4	–19.2	No			
8	ZOND027	Yes	184	662	–23.2	–15.8	No			
9	ZOND028	Yes	172	696	–22.0	–16.3	No			
10	ZOND029	Yes	101	495	–20.8	–14.8	No			
11	ZOND030	Yes	0	555	–23.3	–15.7	No			
12	ZOND031	Yes	148	423	–19.4	–16.2	No			
13	ZOND032	Yes	132	546	–19.8	–17.1	No			
14	ZOND033	Yes	0	147	–18.2	–17.1	No			
15	ZOND034	Yes	143	261	–18.7	–18.3	No			
16	ZOND035	Yes	0	535	–21.9	–16.1	No			
17	ZOND036	Yes	0	448	–23.0	–15.9	No			
18	ZOND037	Yes	148	406	–20.4	–17.1	No			
19	ZOND038	Yes	476	939	–21.9	–16.6	No			
20	ZOND039	Yes	0	308	–24.0	–20.6	No			
21	ZOND040	Yes	811	1307	–23.4	–16.1	No			
22	ZOND041	Yes	0	179	–20.2	–19.6	No			
23	ZOND042	Yes	0	63	–20.0	–19.8	No			
24	ZOND043	Yes	381	1597	–23.7	–17.0	No			
25	ZOND044	Yes	0	836	–28.4	–17.7	No			
26	ZOND045	Yes	0	441	–28.9	–16.8	Yes	480	9.9	63
27	ZOND046	Yes	0	438	–28.7	–16.2	No			
28	ZOND047	Yes	0	460	–29.0	–16.0	No			
29	ZOND048	Yes	0	569	–29.5	–15.7	No			
30	ZOND049	Yes	0	729	–29.3	–13.4	No			
31	ZOND050	Yes	0	657	–29.4	–11.4	No			
32	ZOND051	Yes	0	869	–26.0	–9.9	No			
33	ZOND052	Yes	0	740	–29.5	–10.9	No			
34	ZOND053	Yes	0	959	–29.8	–12.7	No			
35	ZOND054	Yes	0	778	–28.1	–13.7	No			
36	ZOND055	Yes	0	809	–29.3	–13.5	No			
37	ZOND056	Yes	0	830	–32.8	–15.6	No			
38	ZOND057	Yes	0	1313	–31.9	–15.7	No			
39	ZOND058	Yes	0	1342	–32.7	–14.5	No			
40	ZOND059	Yes	0	1483	–31.6	–12.3	No			

APPENDIX C: PLOTS OF ICE STATION WEDDELL SOUNDINGS

Here we plot all the soundings listed in Table 2. Cross–reference the identification number on each plot with the corresponding number in Table 2 to see when and where the sounding was made and with which type of radiosonde. The plots show temperature and dew point and, for the Tethersonde ascents, wind speed.

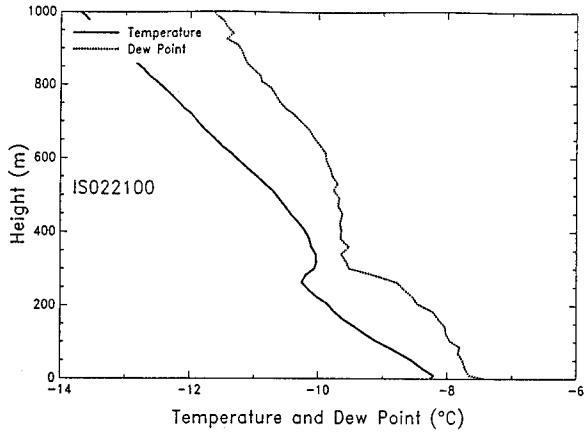

Figure C1.

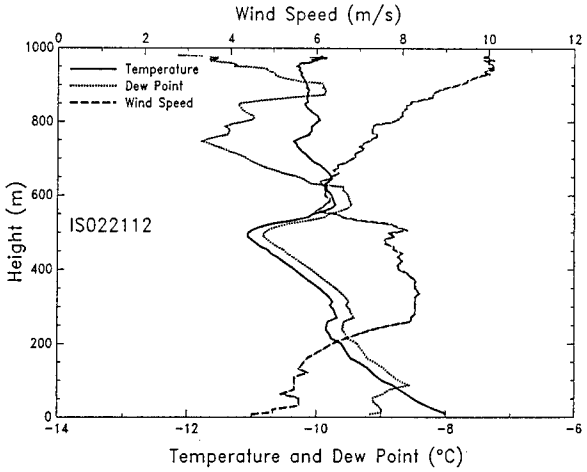

Figure C2.

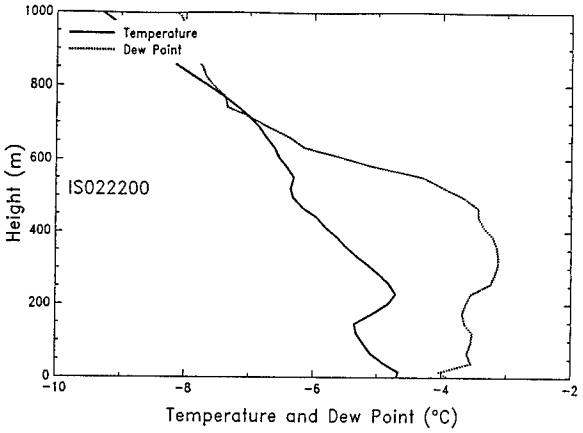

Figure C3.

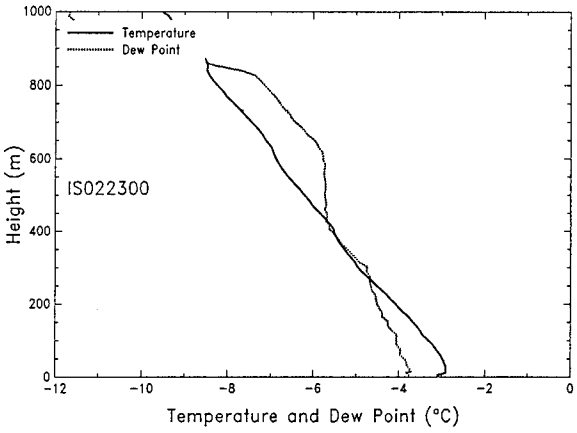

Figure C4.

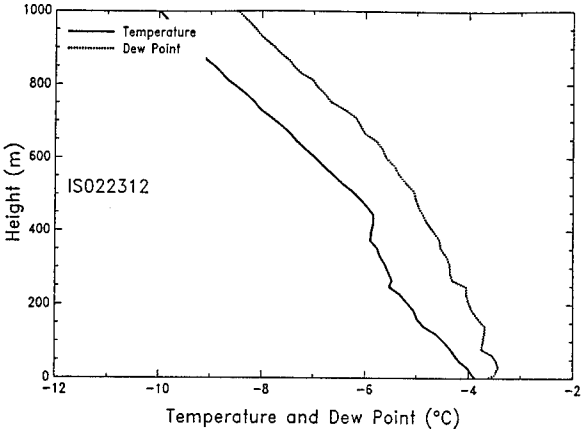

Figure C5.

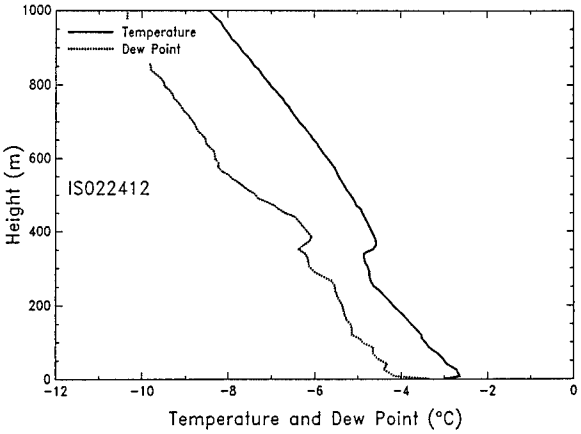

Figure C6.

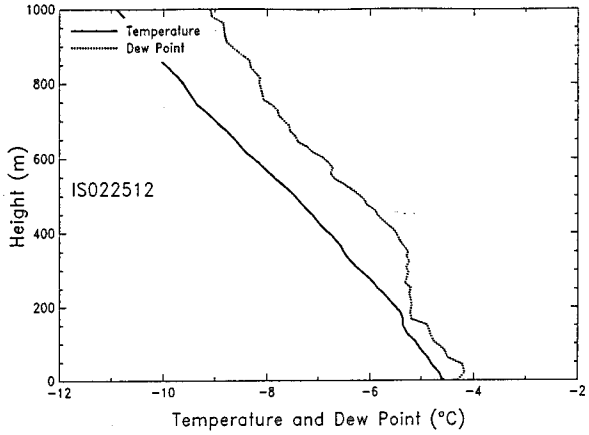

Figure C7.

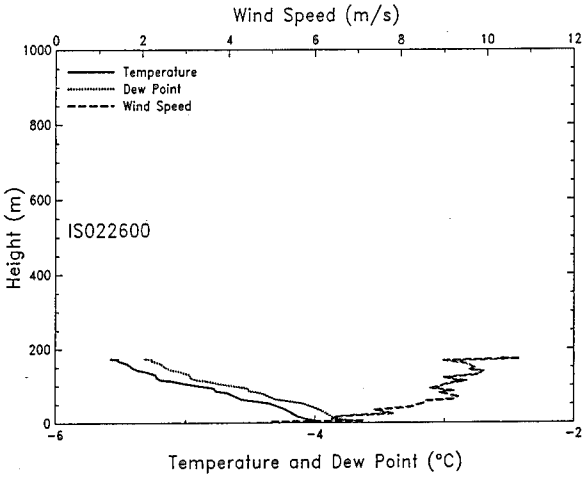

Figure C8.

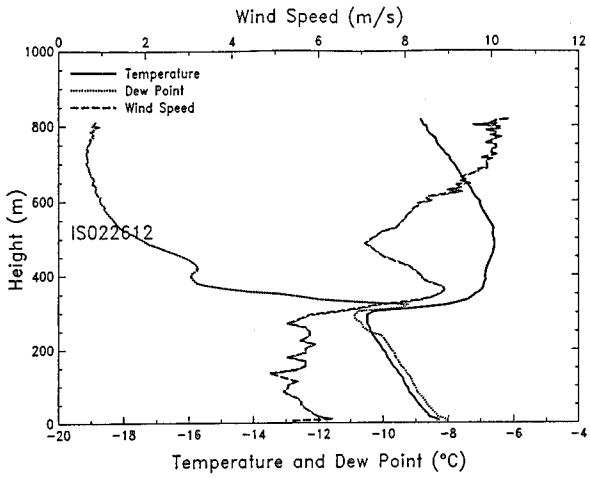

Figure C9.

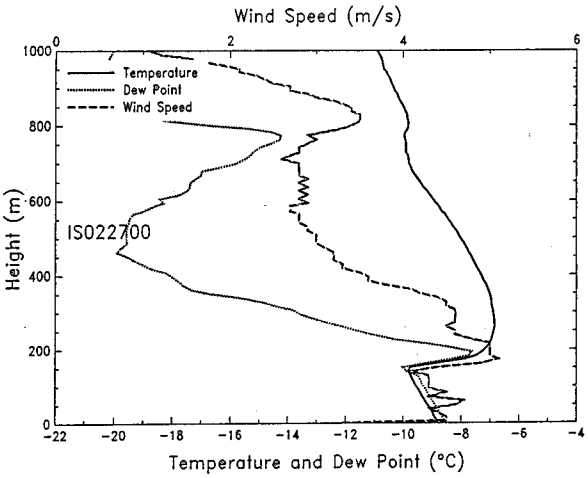

Figure C10.

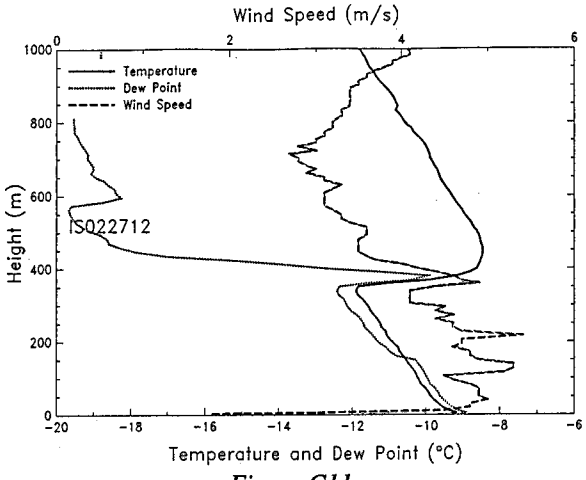

Figure C11.

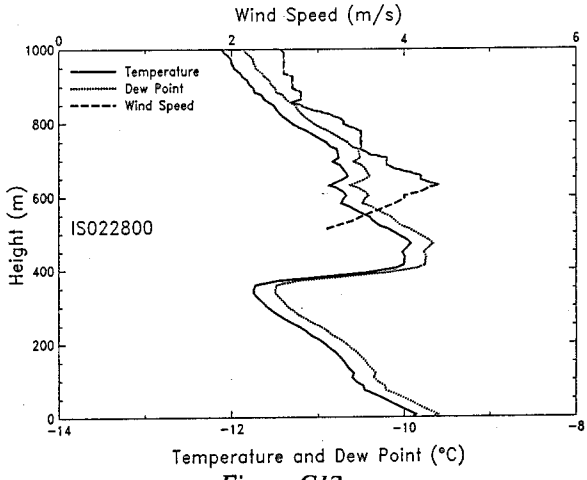

Figure C12.

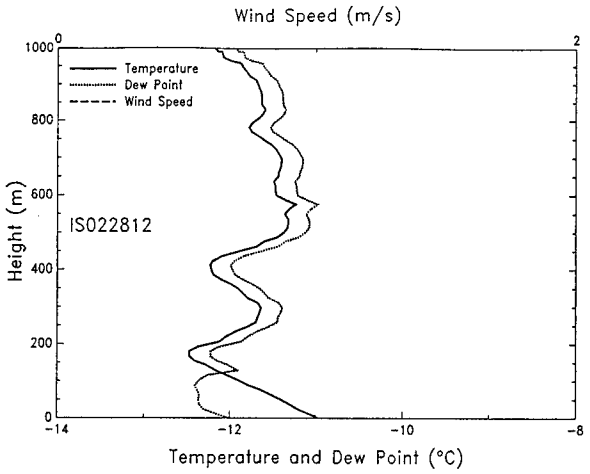

Figure C13.

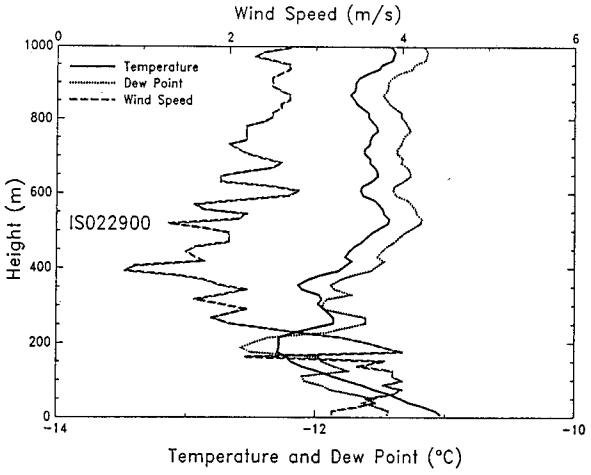

Figure C14.

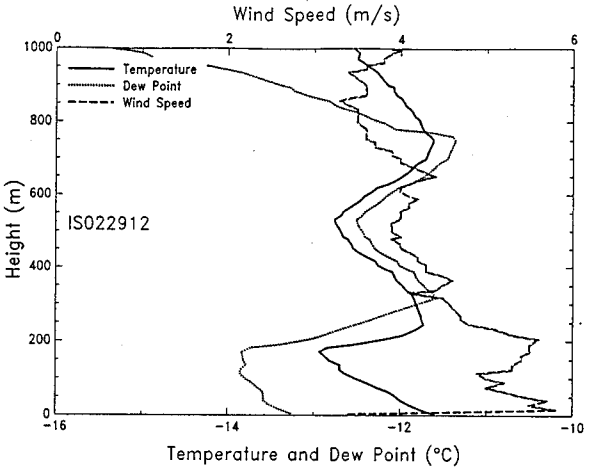

Figure C15.

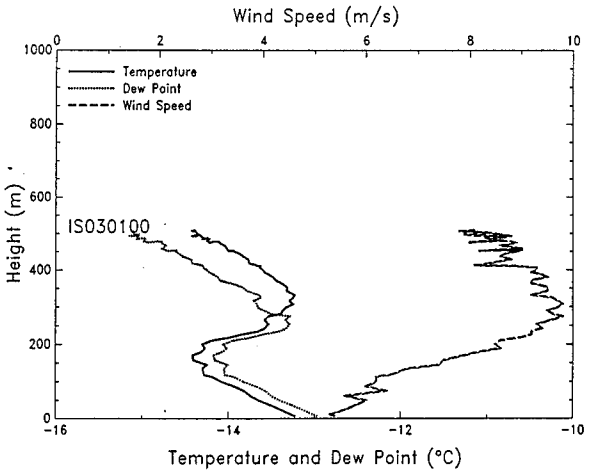

Figure C16.

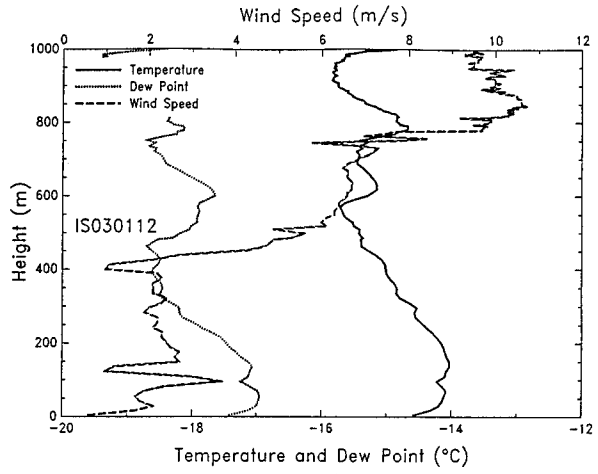

Figure C17.

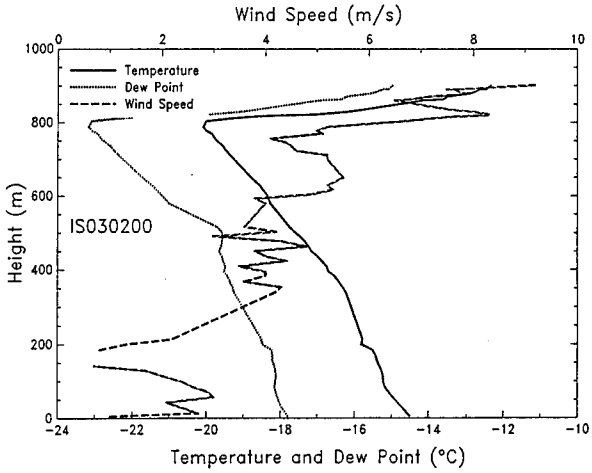

Figure C18.

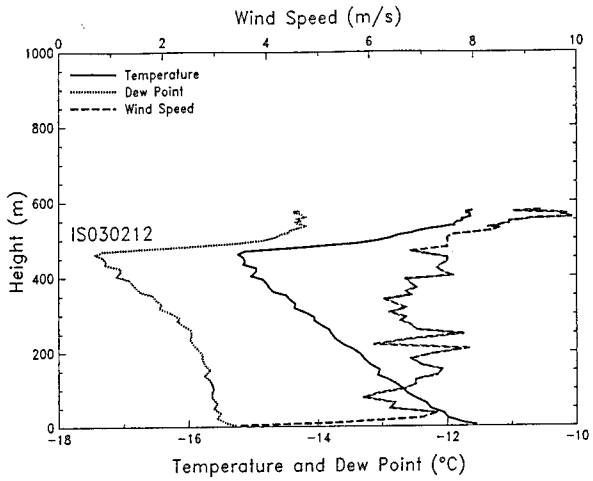

Figure C19.

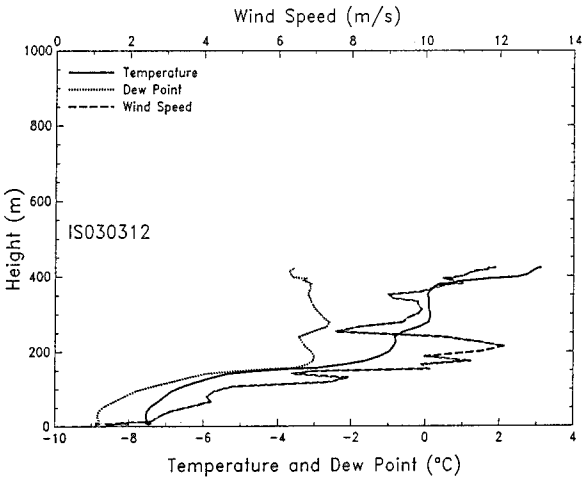

Figure C20.

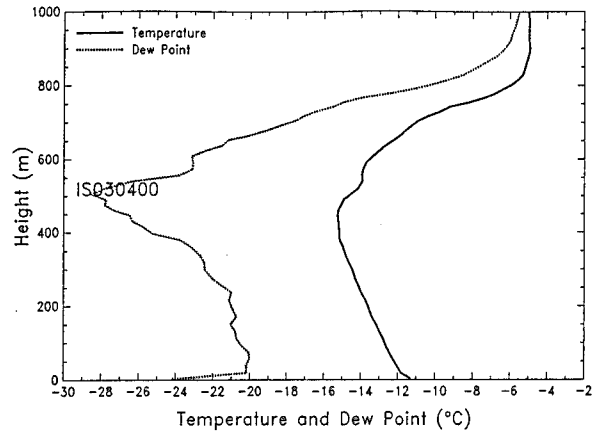

Figure C21.

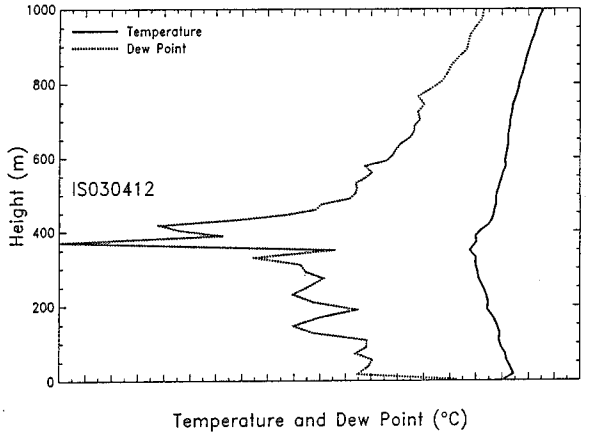

Figure C22.

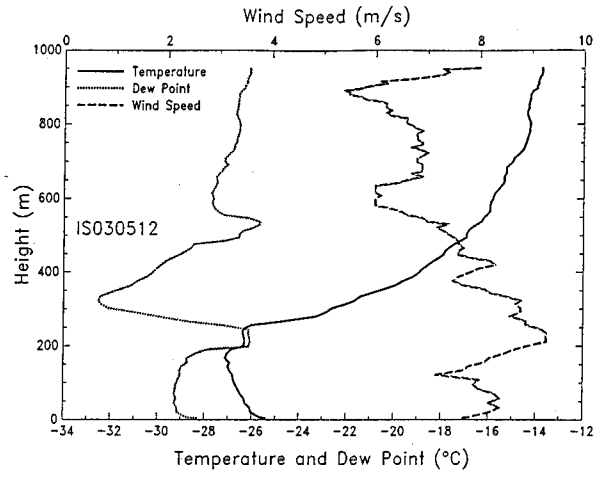

Figure C23.

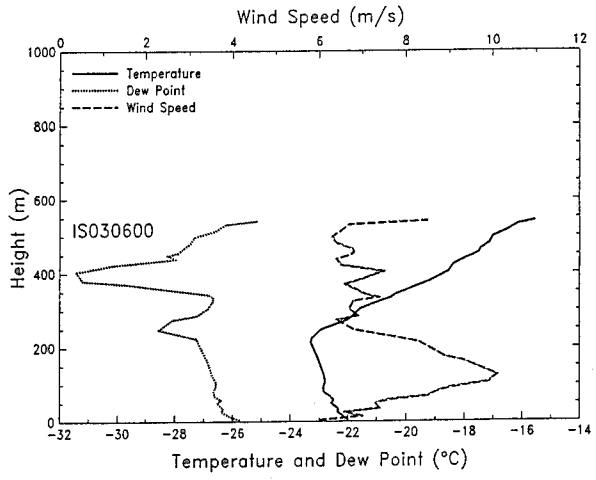

Figure C24.

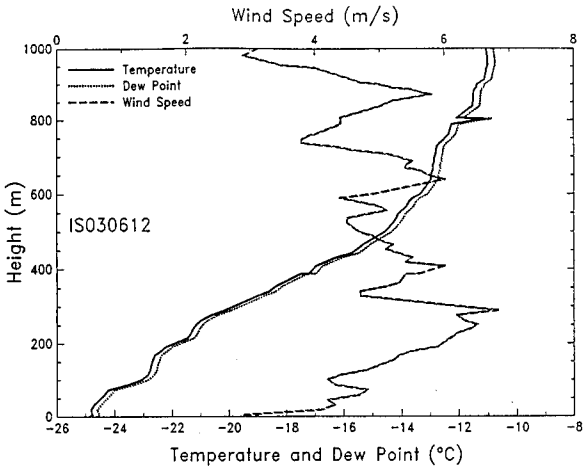

Figure C25.

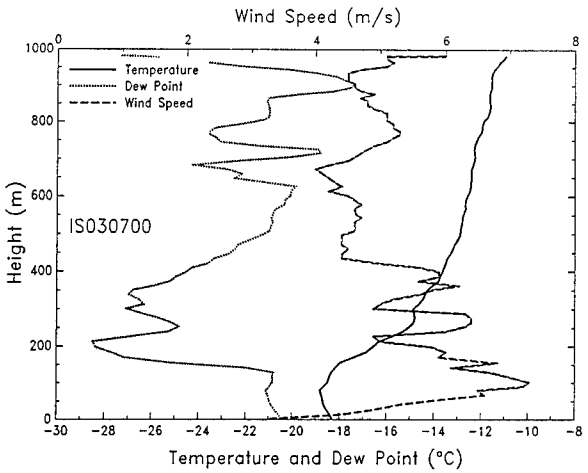

Figure C26.

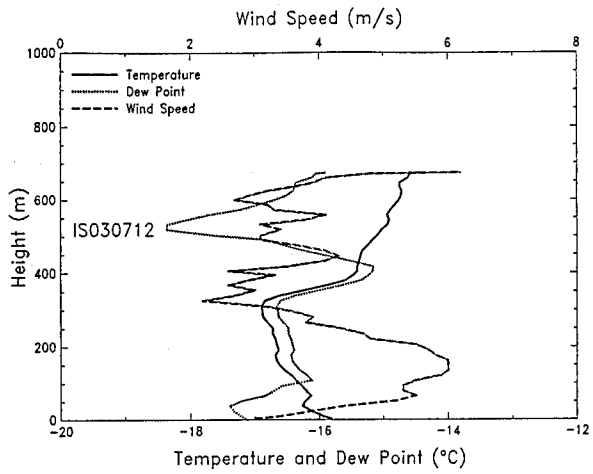

Figure C27.

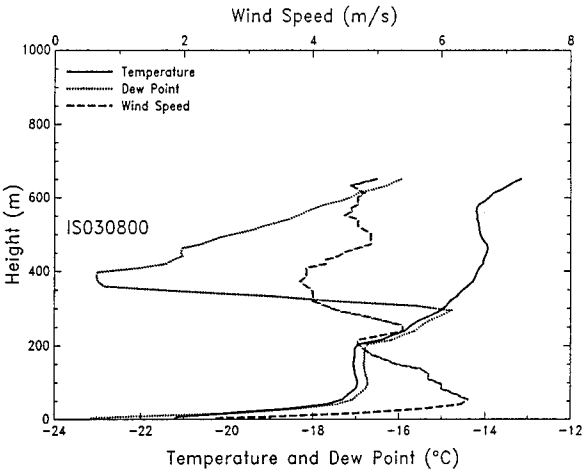

Figure C28.

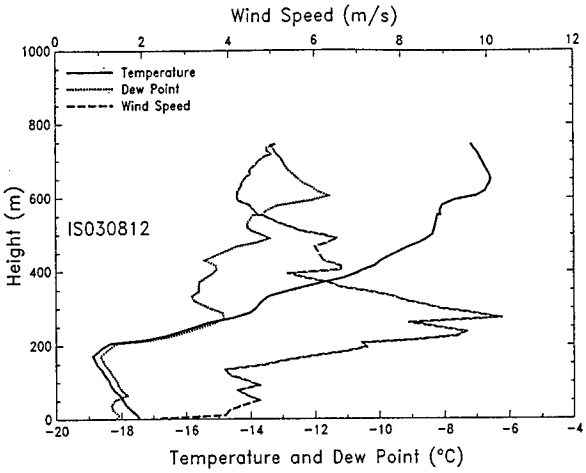

Figure C29.

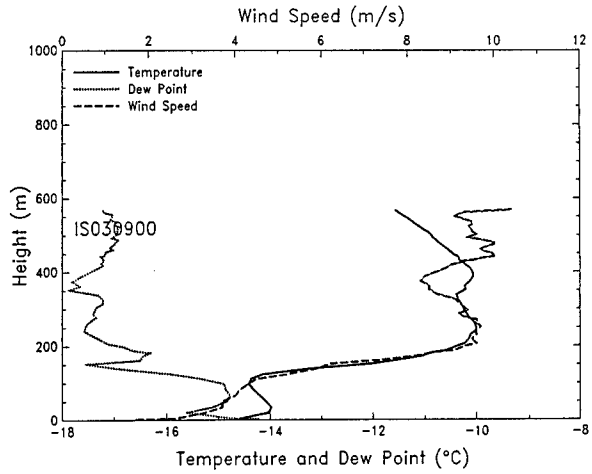

Figure C30.

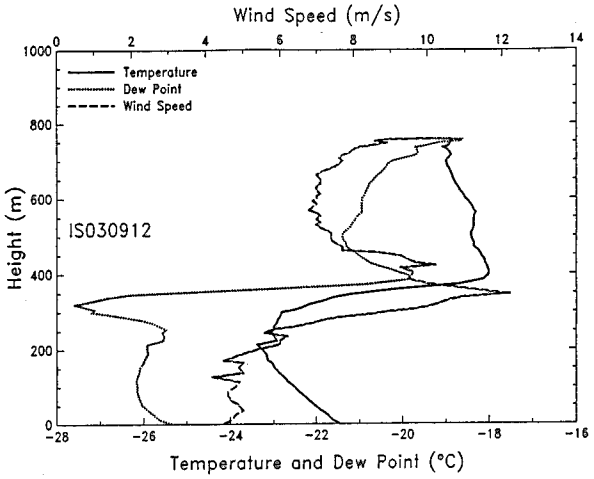

Figure C31.

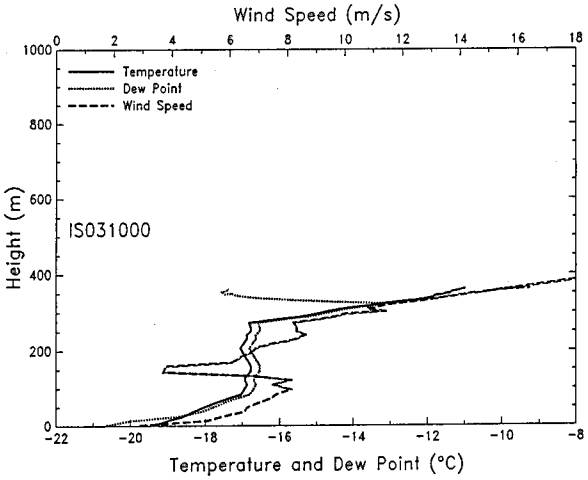

Figure C32.

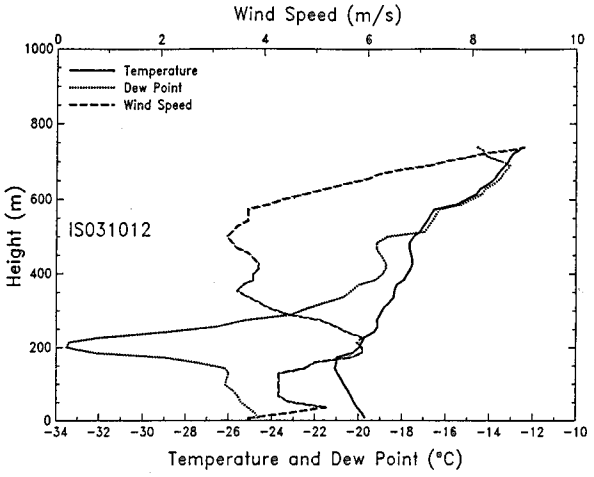

Figure C33.

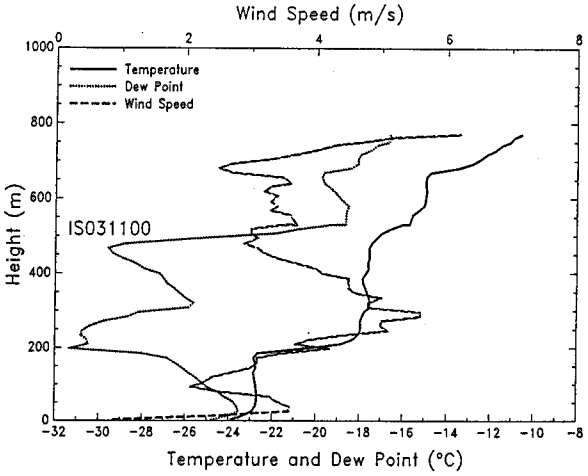

Figure C34.

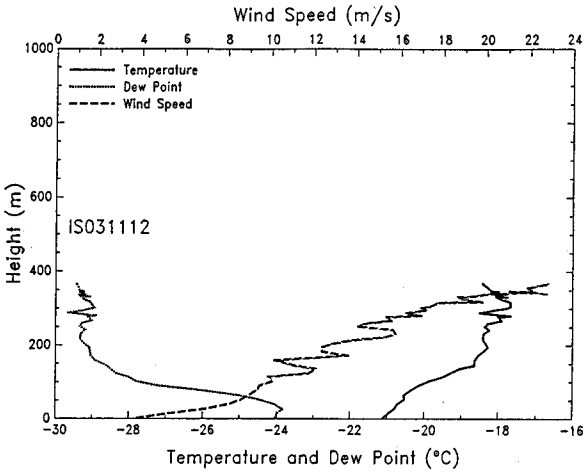

Figure C35.

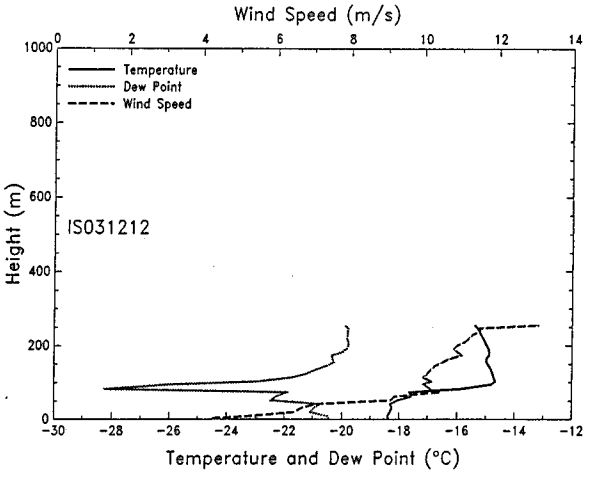

Figure C36.

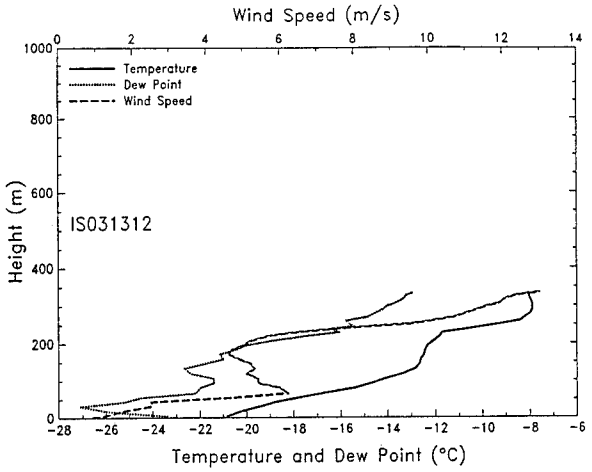

Figure C37.

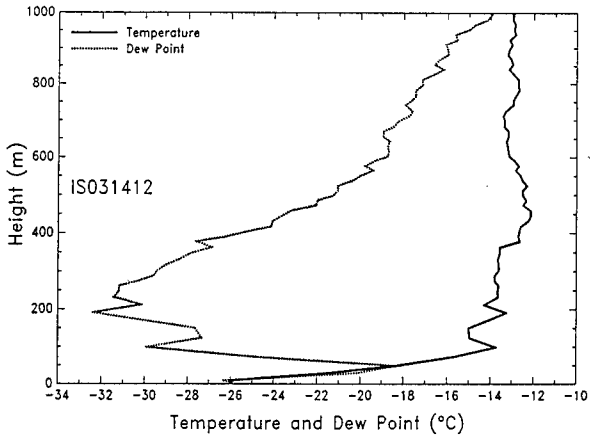

Figure C38.

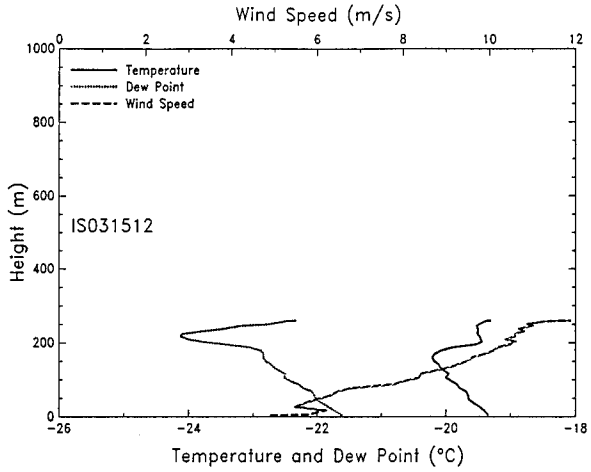

Figure C39.

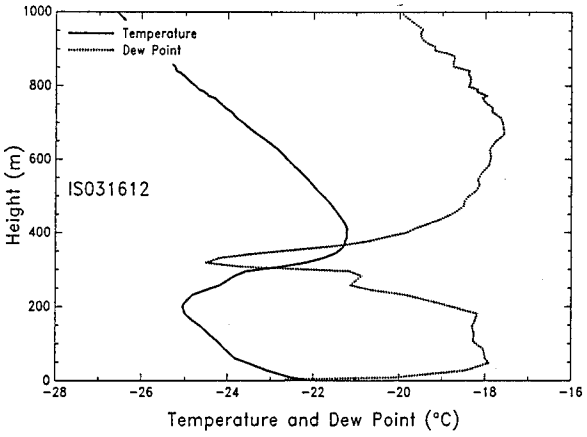

Figure C40.

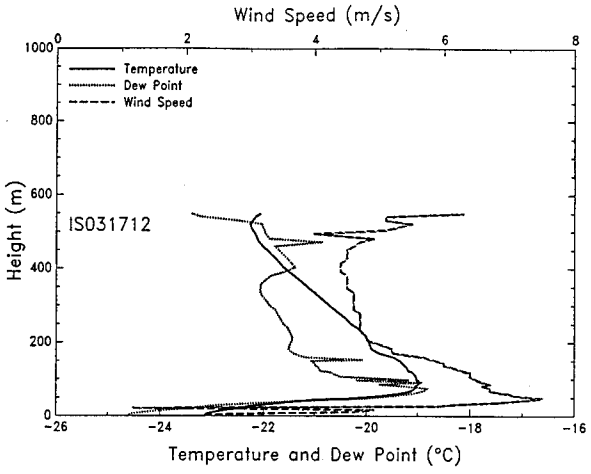

Figure C41.

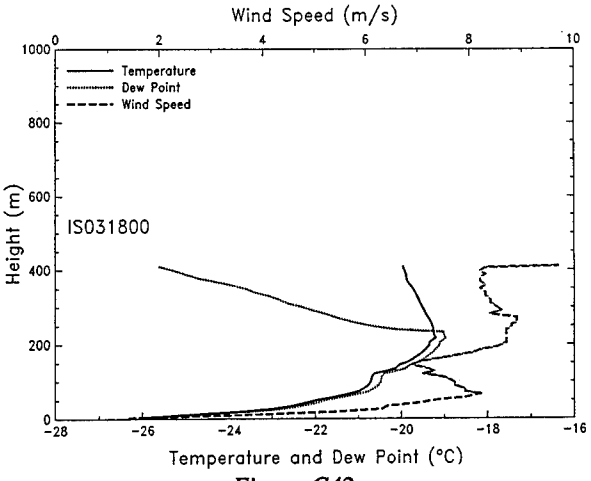

Figure C42.

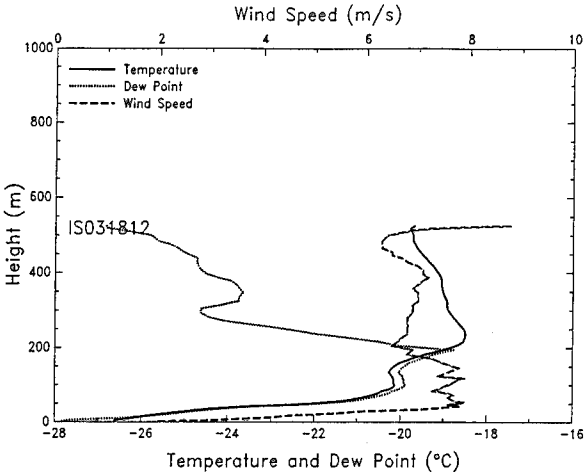

Figure C43.

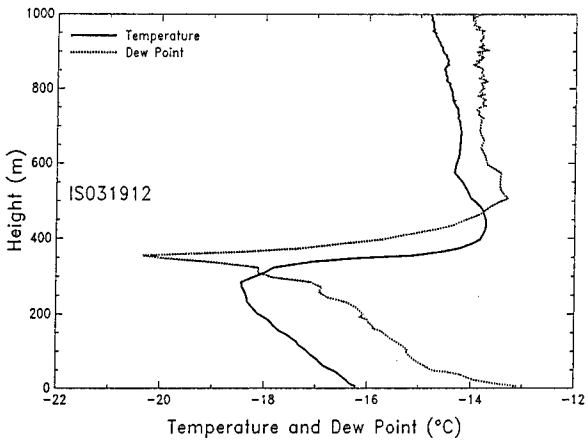

Figure C44.

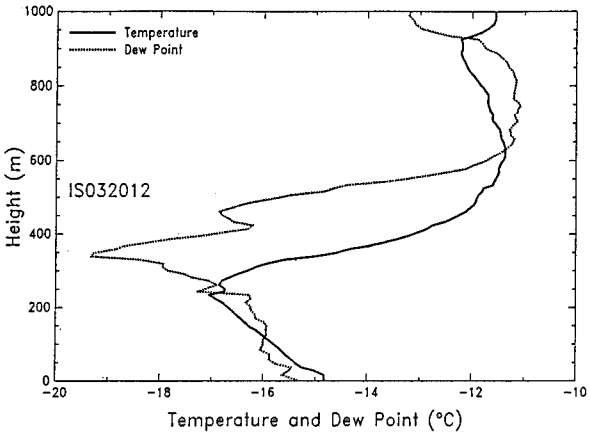

Figure C45.

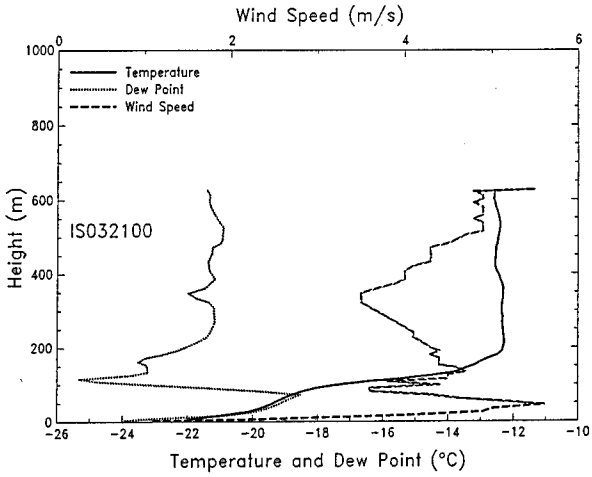

Figure C46.

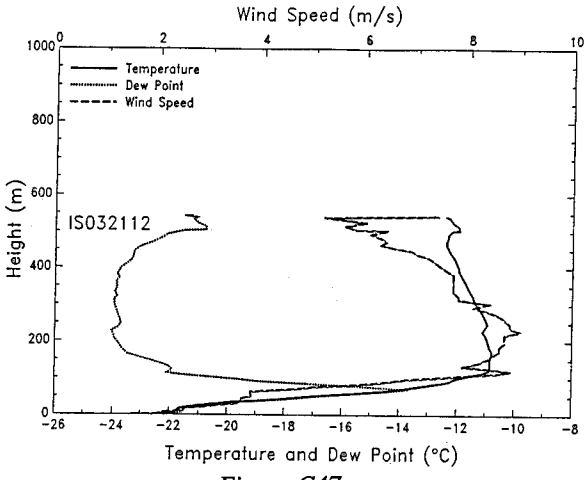

Figure C47.

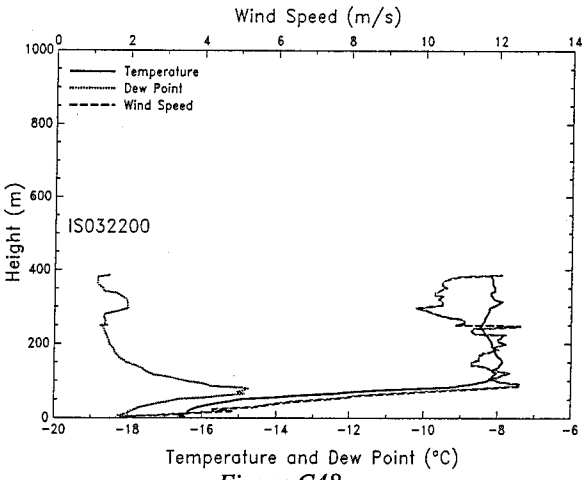

Figure C48.

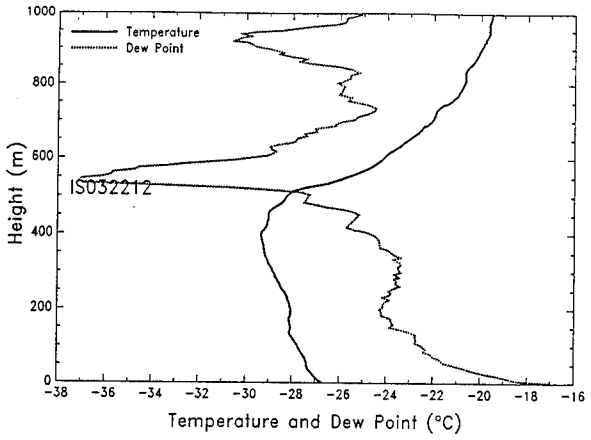

Figure C49.

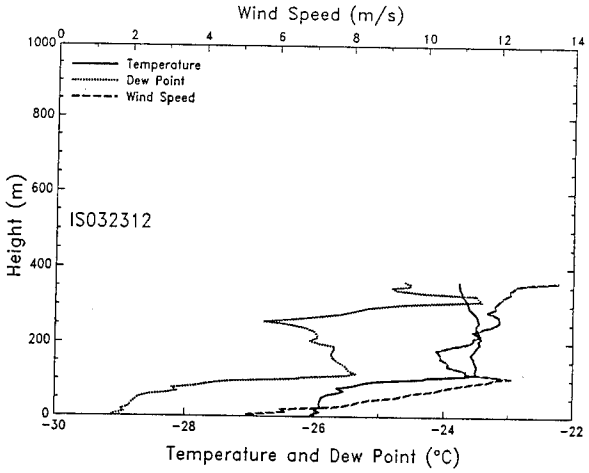

Figure C50.

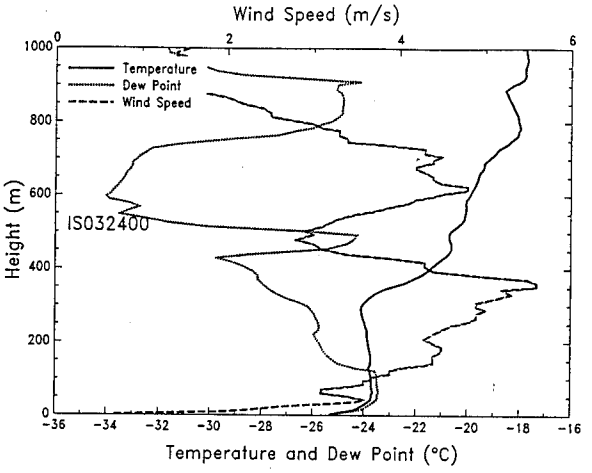

Figure C51.

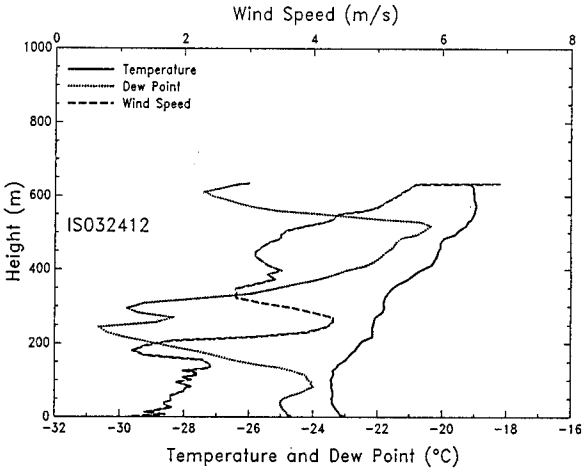

Figure C52.

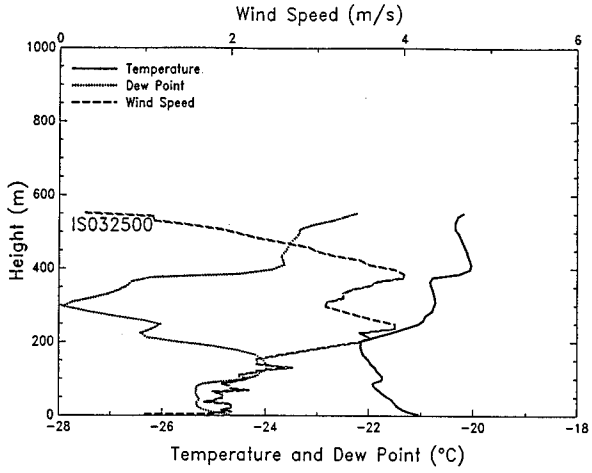

Figure C53.

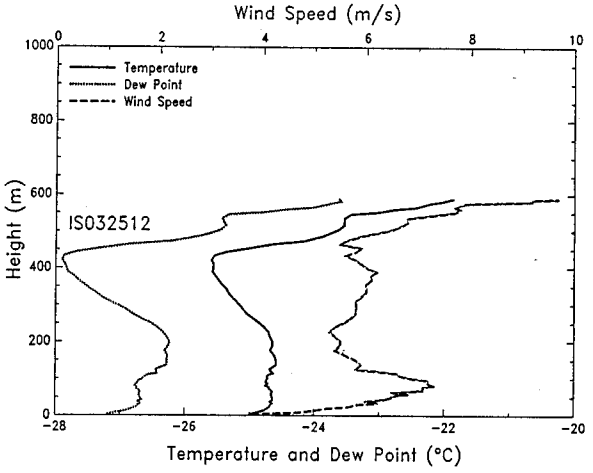

Figure C54.

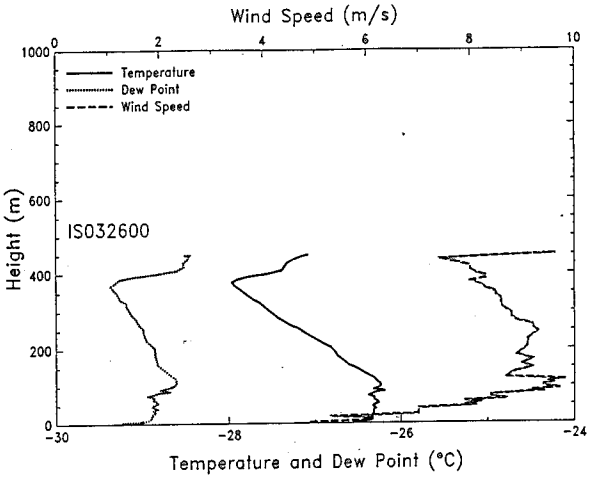

Figure C55.

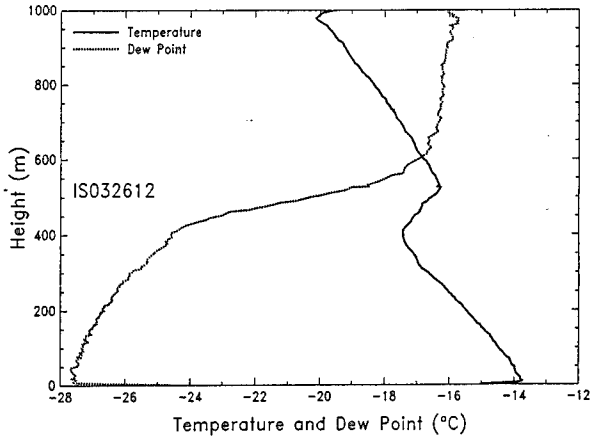

Figure C56.

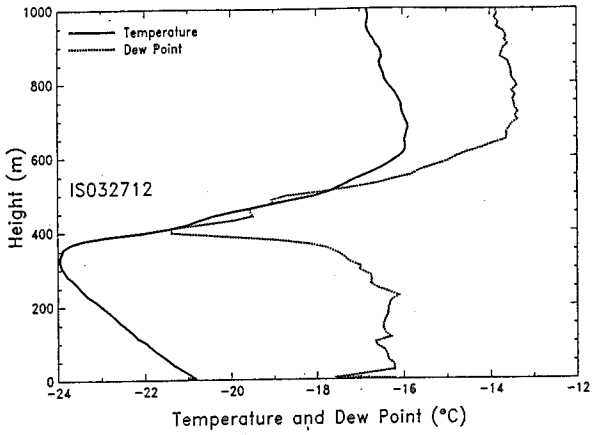

Figure C57.

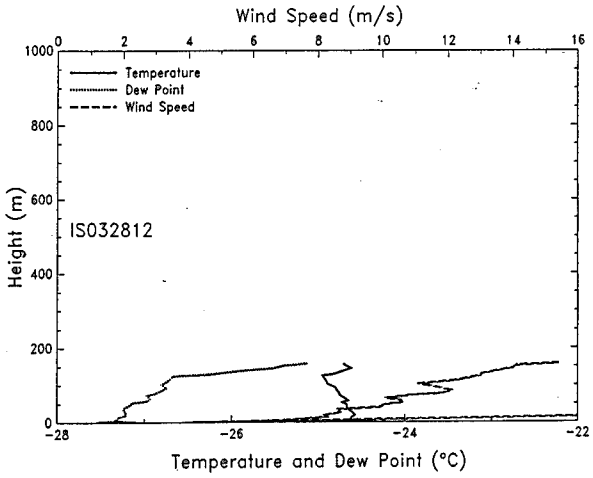

Figure C58.

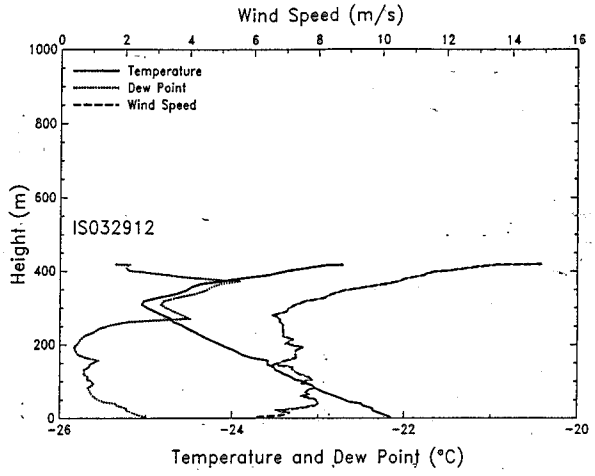

Figure C59.

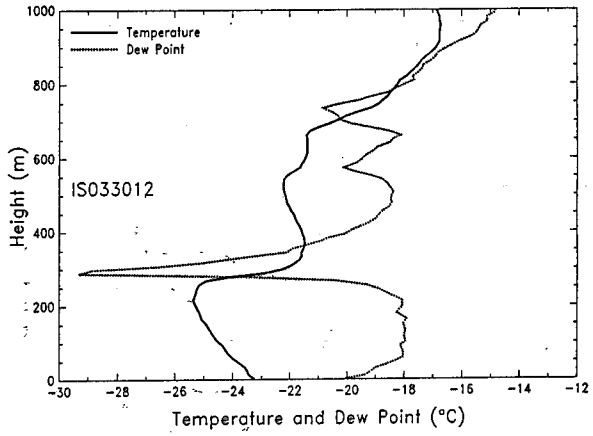

Figure C60.

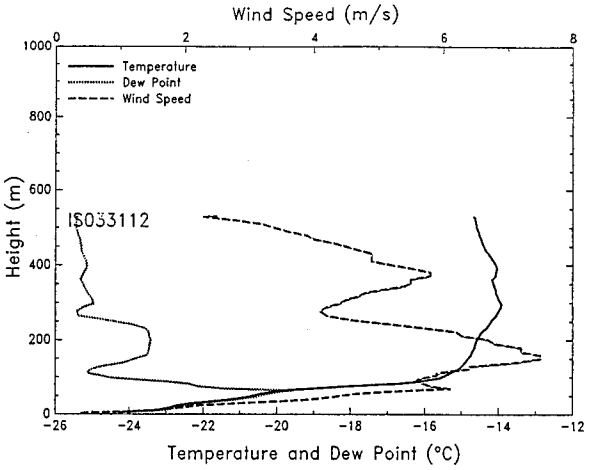

Figure C61.

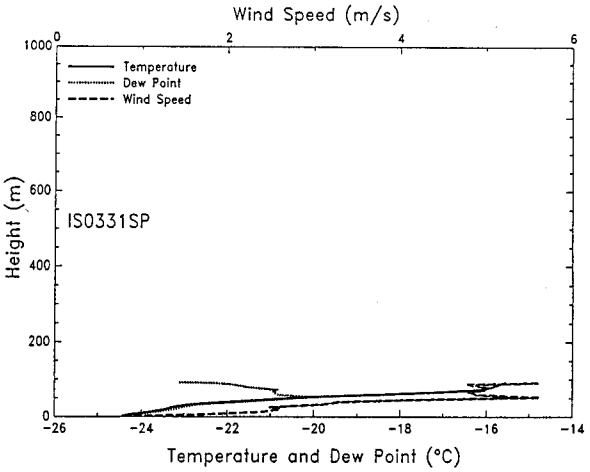

Figure C62.

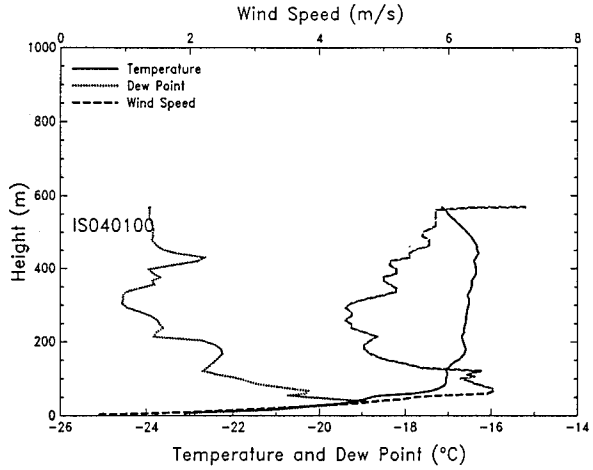

Figure C63.

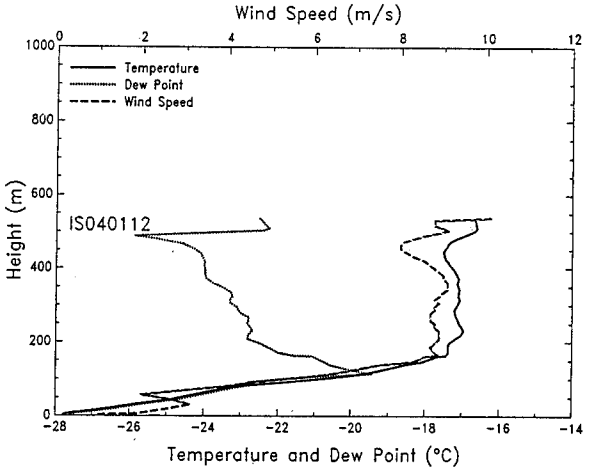

Figure C64.

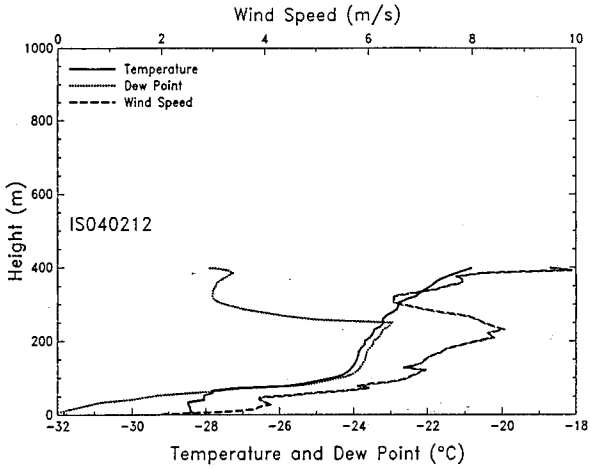

Figure C65.

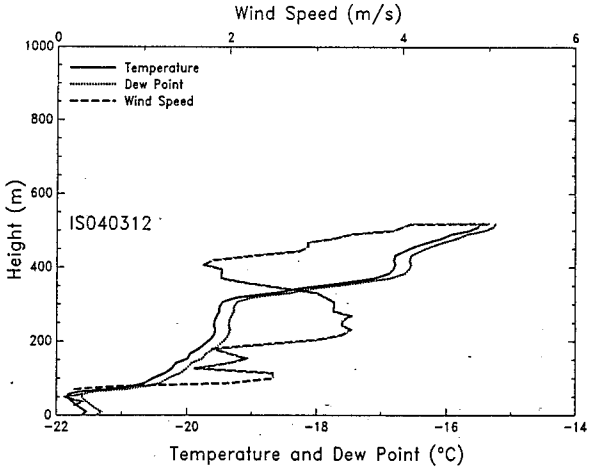

Figure C66.

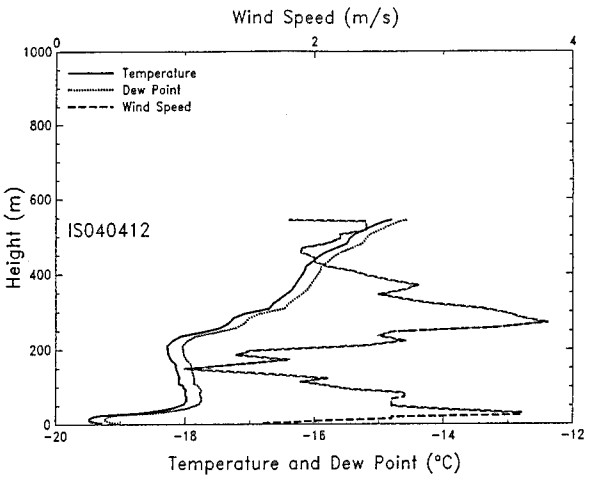

Figure C67.

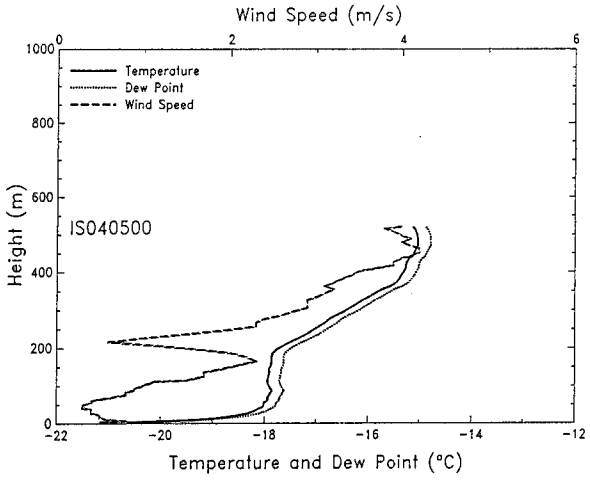

Figure C68.

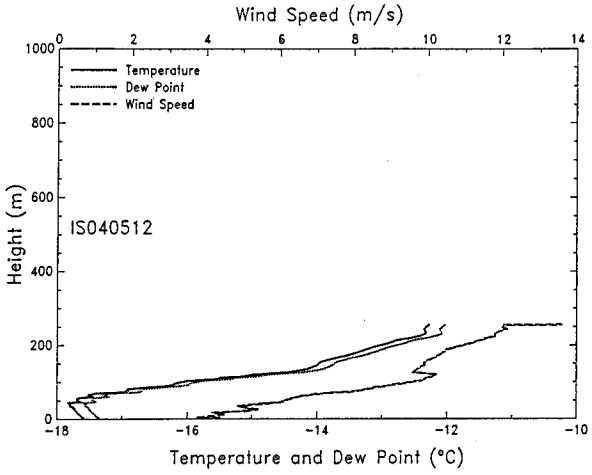

Figure C69.

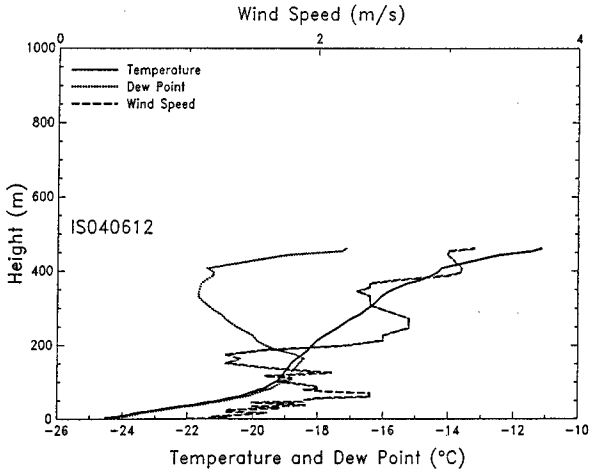

Figure C70.

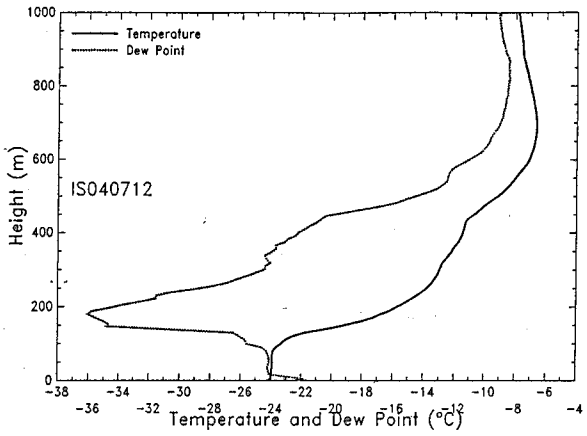

Figure C71.

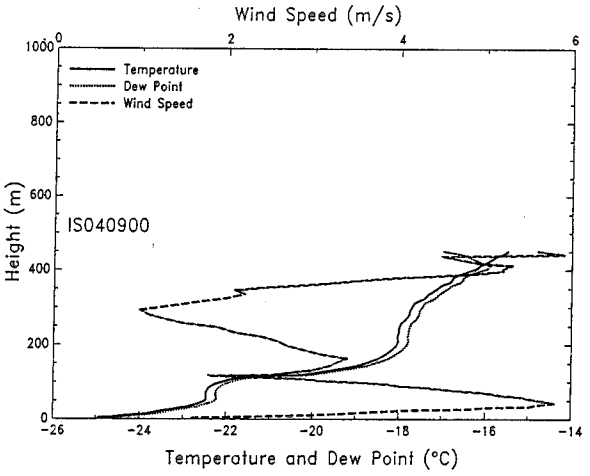

Figure C72.

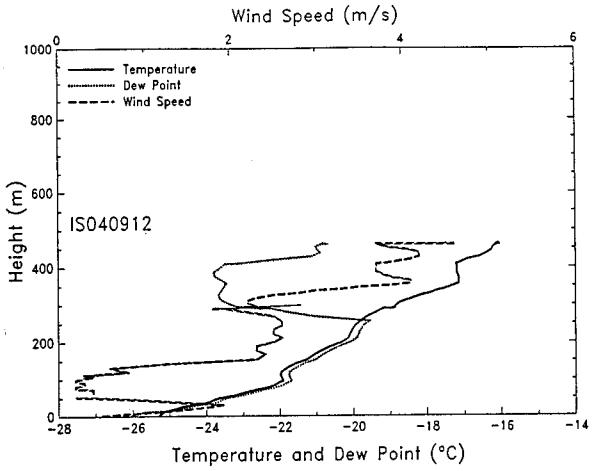

Figure C73.

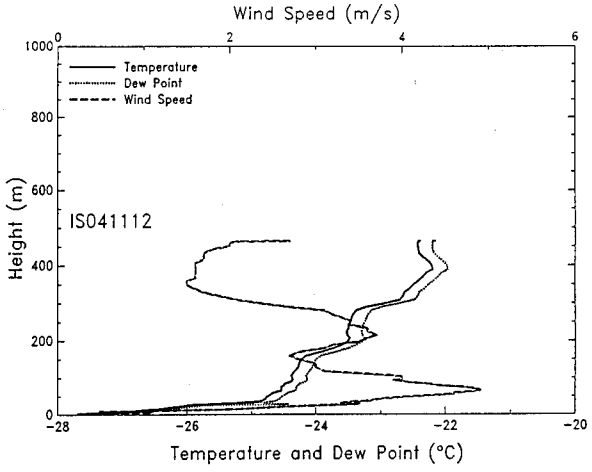

Figure C74.

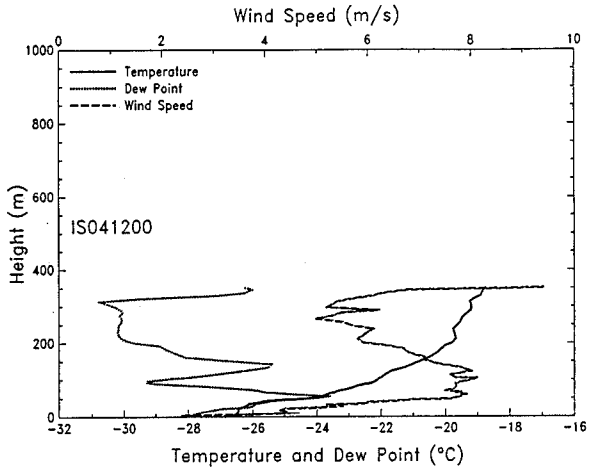

Figure C75.

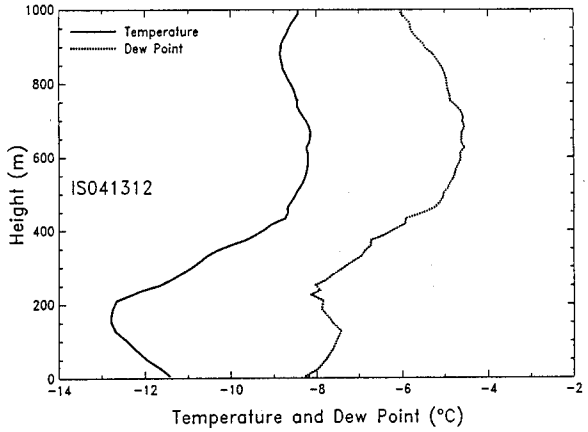

Figure C76.

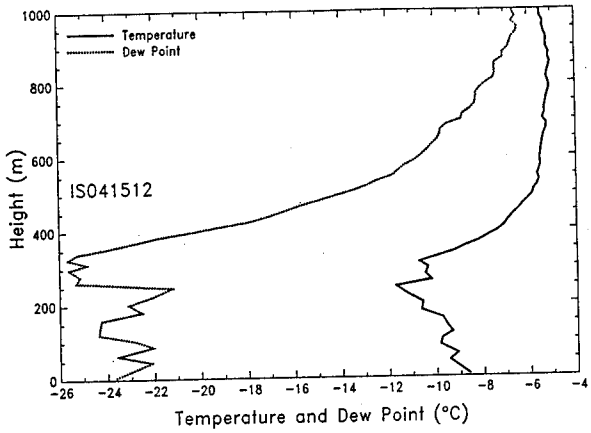

Figure C77.

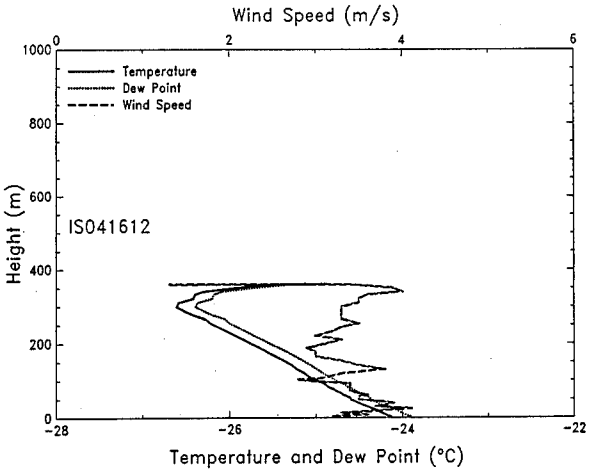

Figure C78.

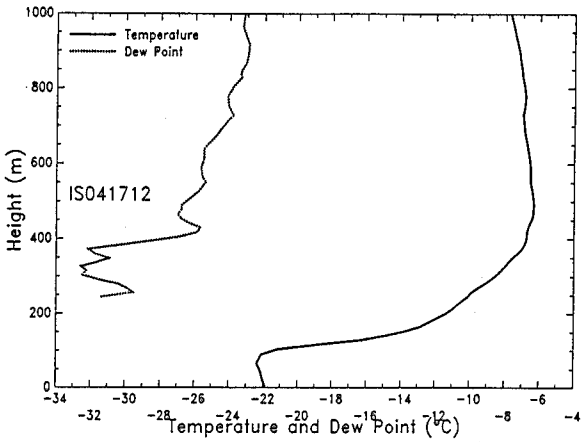

Figure C79.

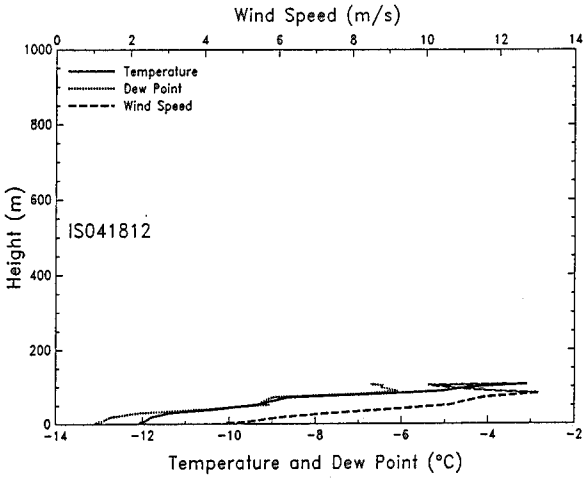

Figure C80.

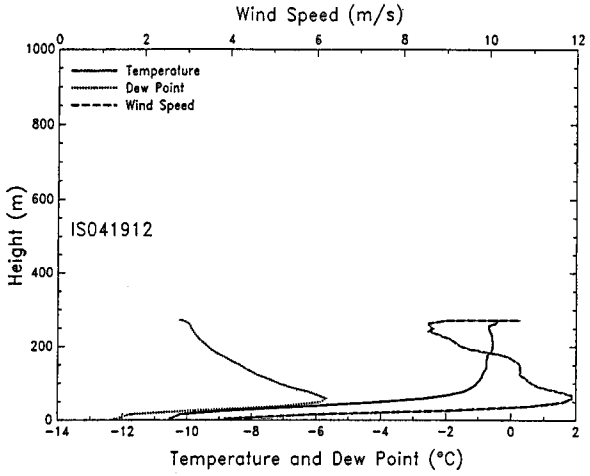

Figure C81.

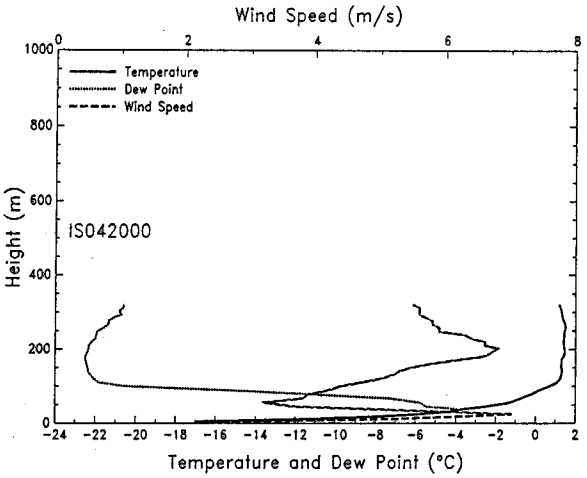

Figure C82.

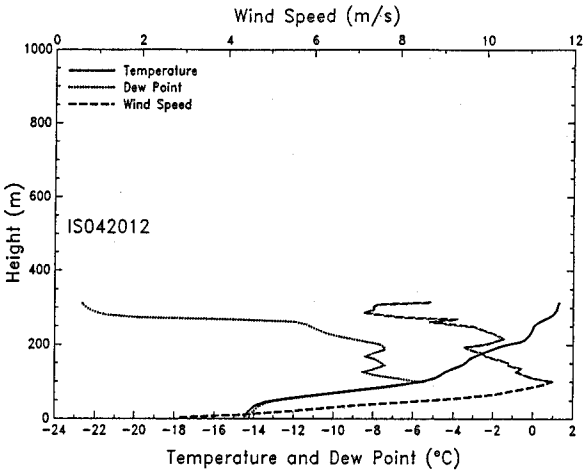

Figure C83.

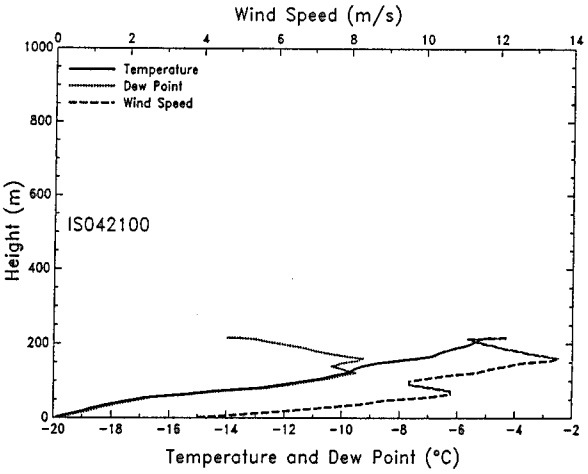

Figure C84.

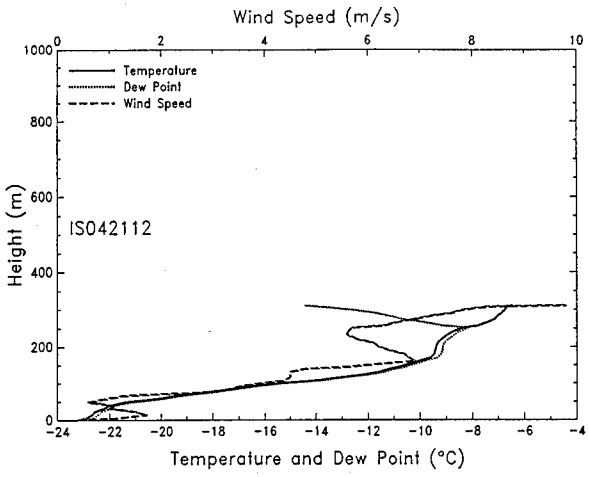

Figure C85.

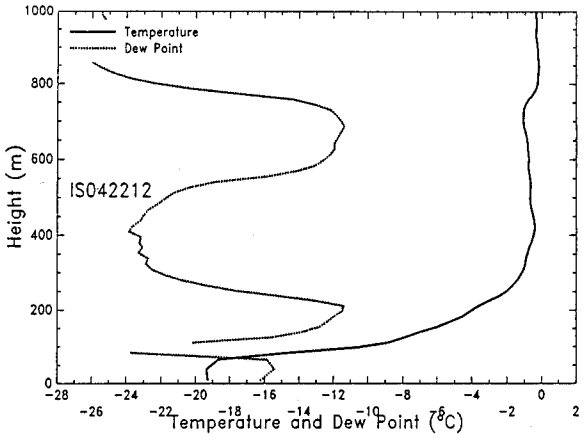

Figure C86.

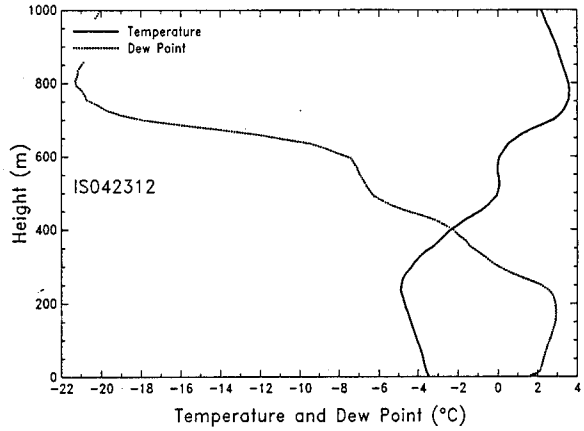

Figure C87.

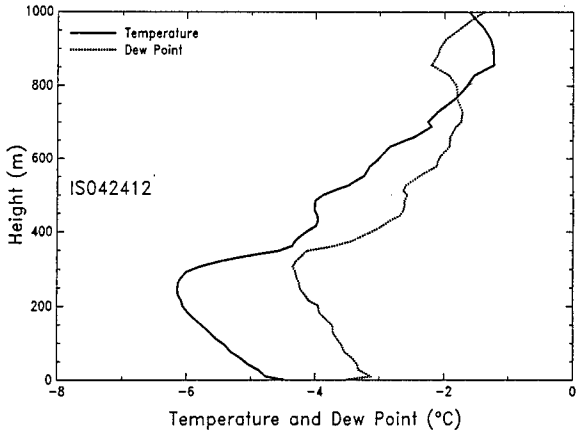

Figure C88.

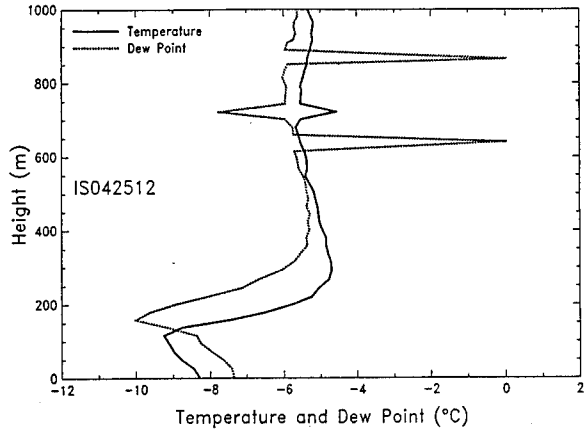

Figure C89.

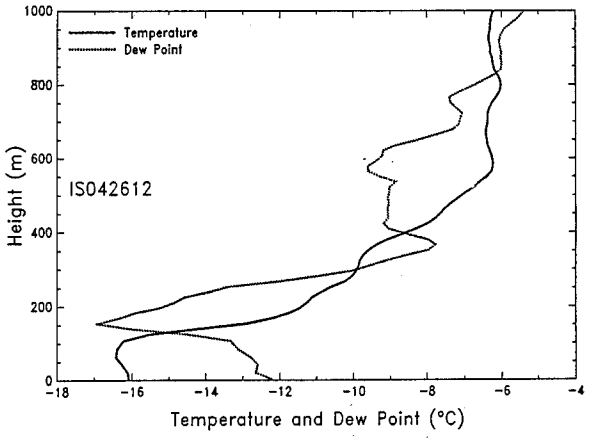

Figure C90.

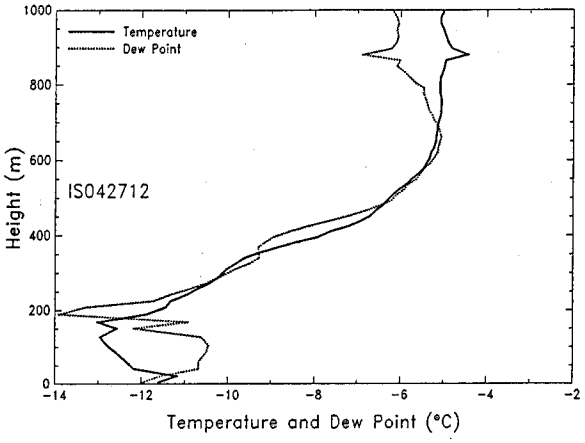

Figure C91.

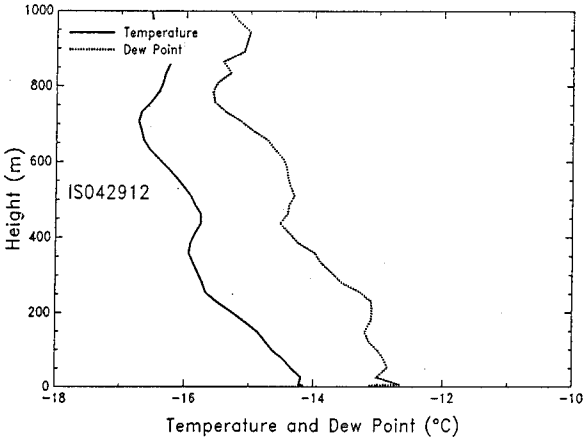

Figure C92.

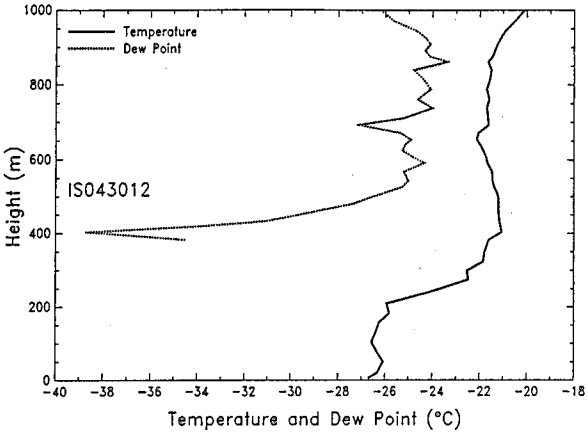

Figure C93.

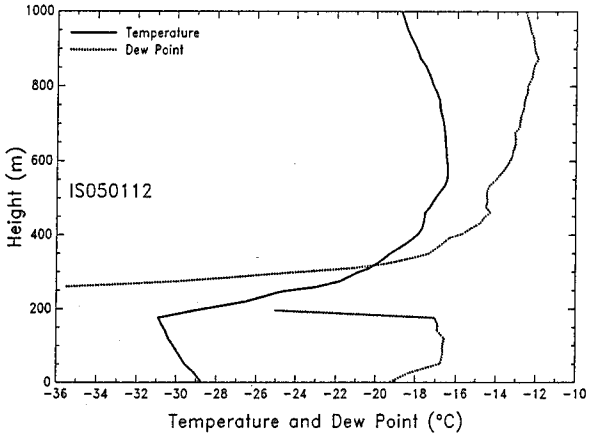

Figure C94.

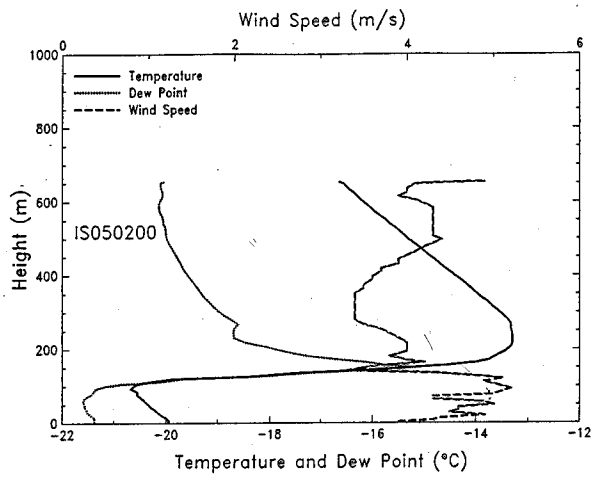

Figure C95.

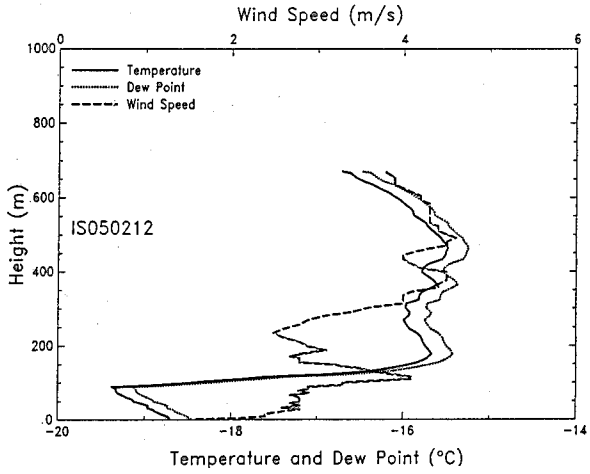

Figure C96.

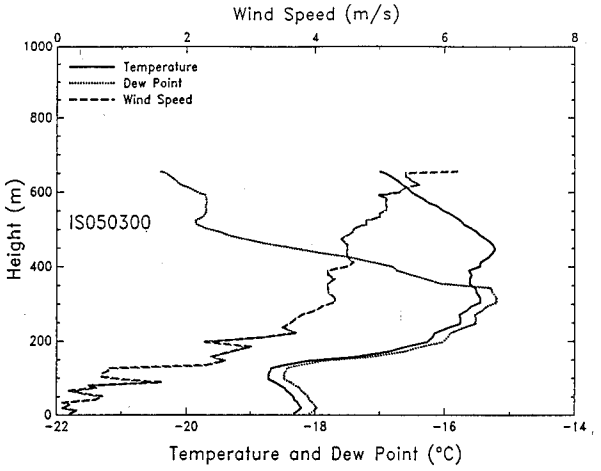

Figure C97.

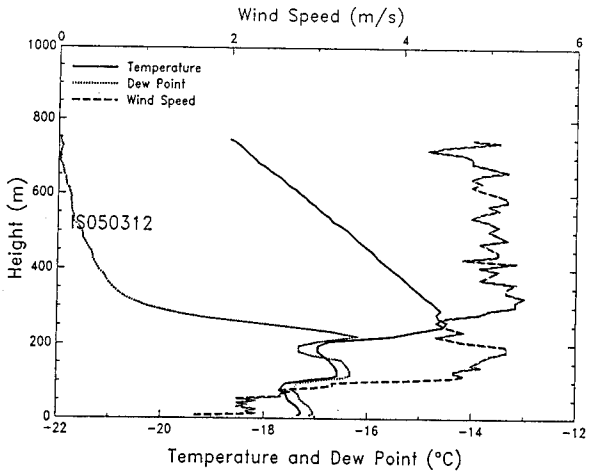

Figure C98.

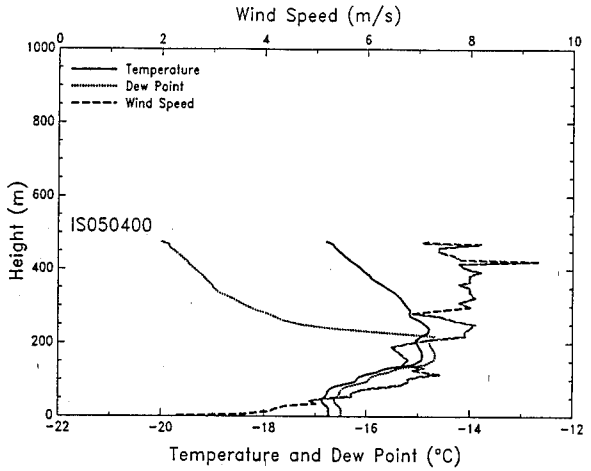

Figure C99.

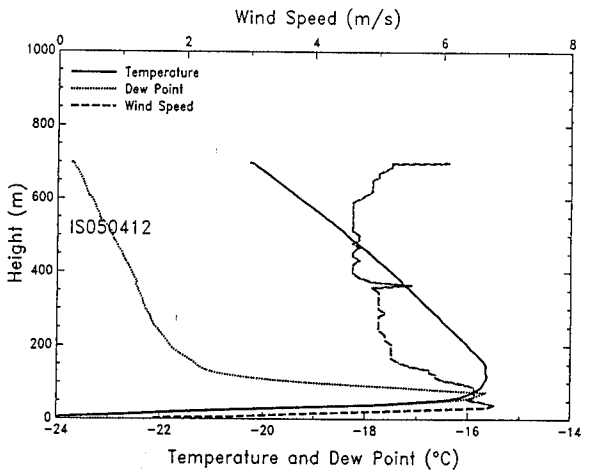

Figure C100.

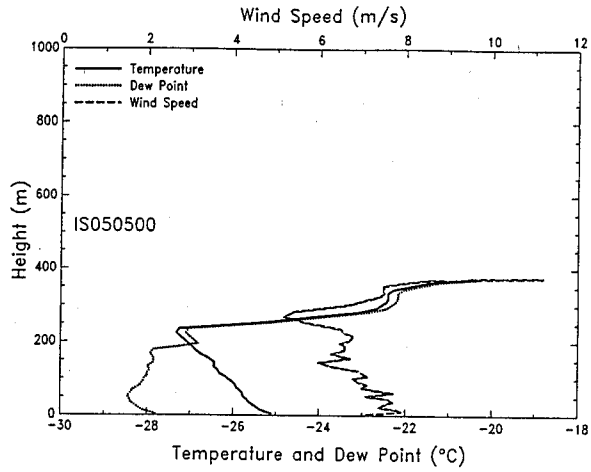

Figure C101.

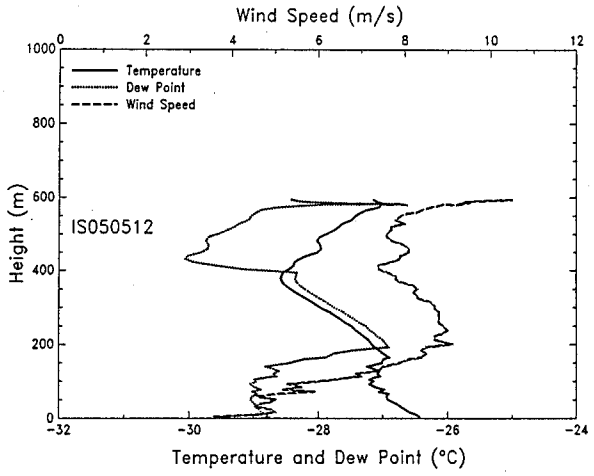

Figure C102.

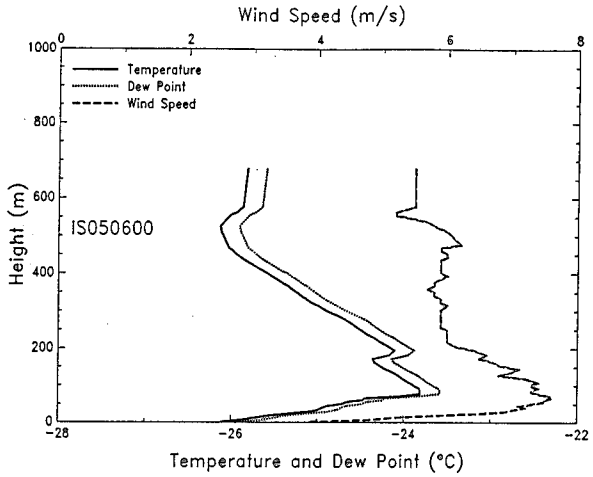

Figure C103.

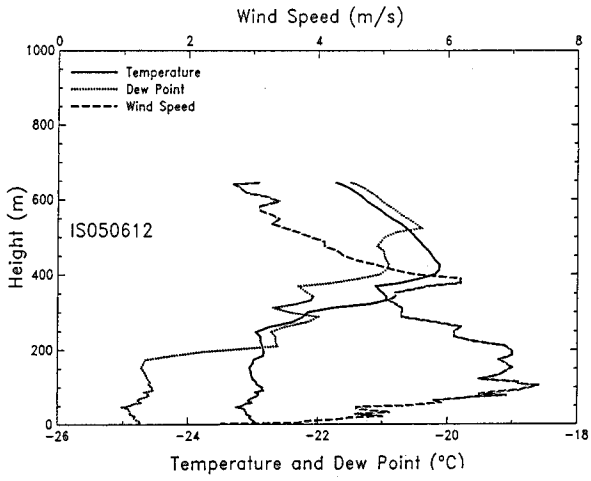

Figure C104.

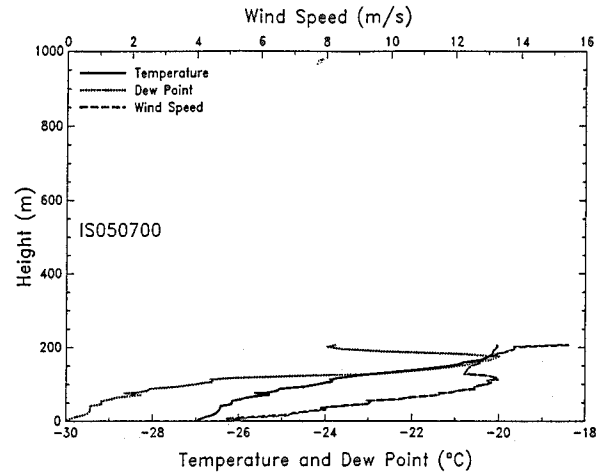

Figure C105.

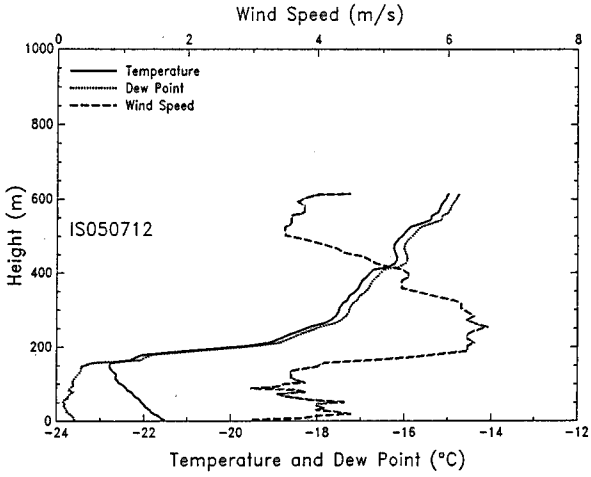

Figure C106.

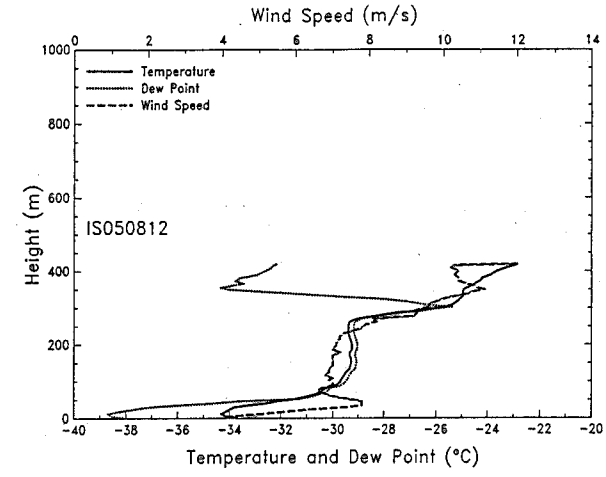

Figure C107.

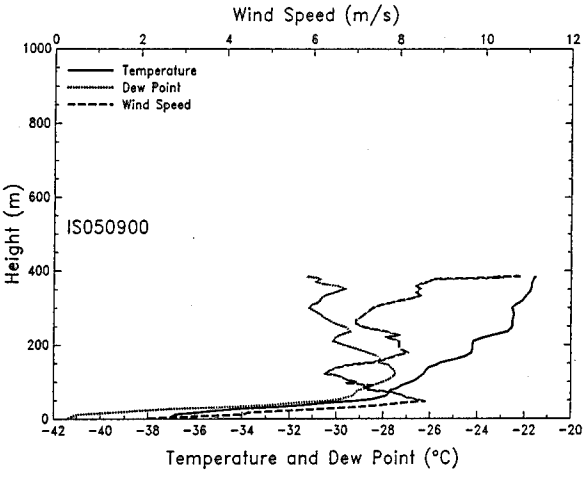

Figure C108.

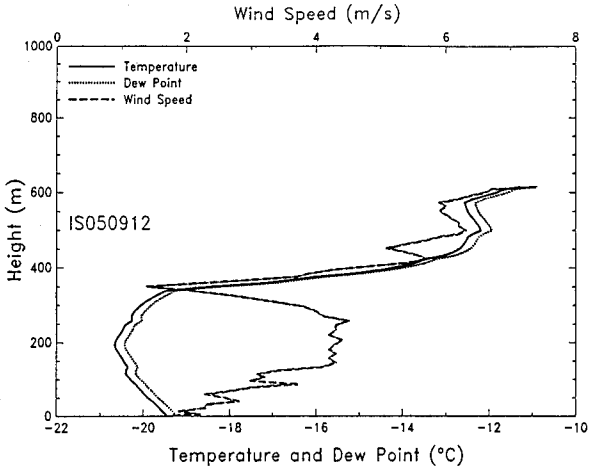

Figure C109.

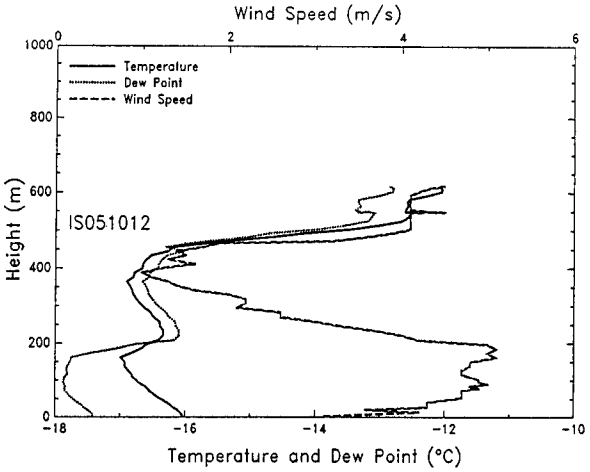

Figure C110.

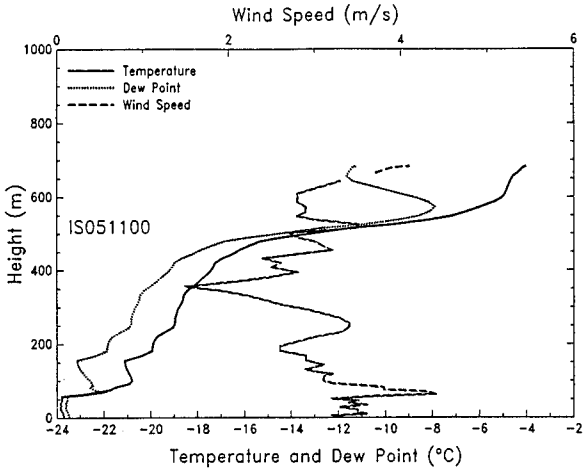

Figure C111.

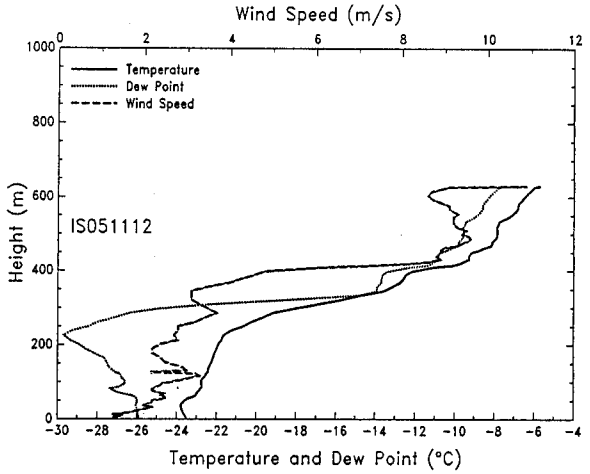

Figure C112.

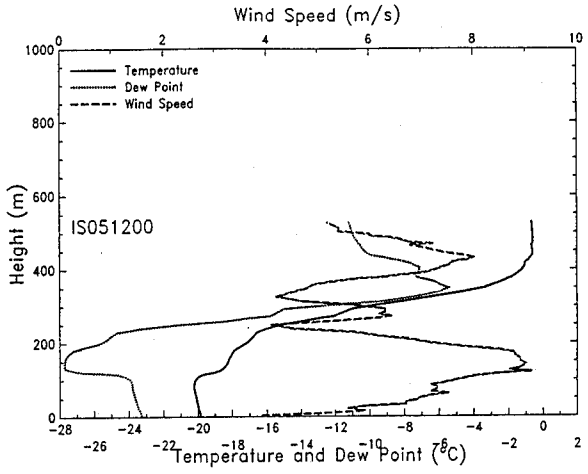

Figure C113.

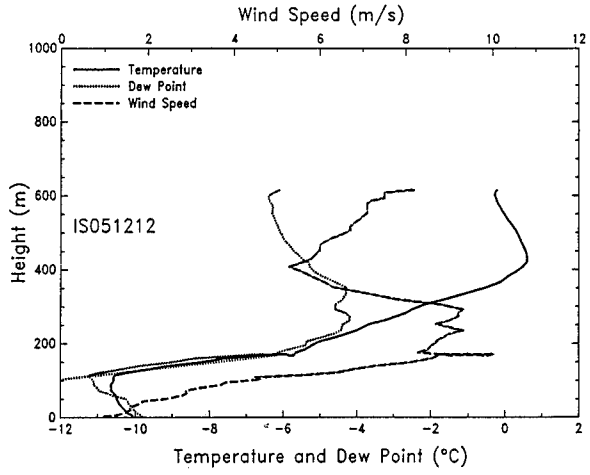

Figure C114.

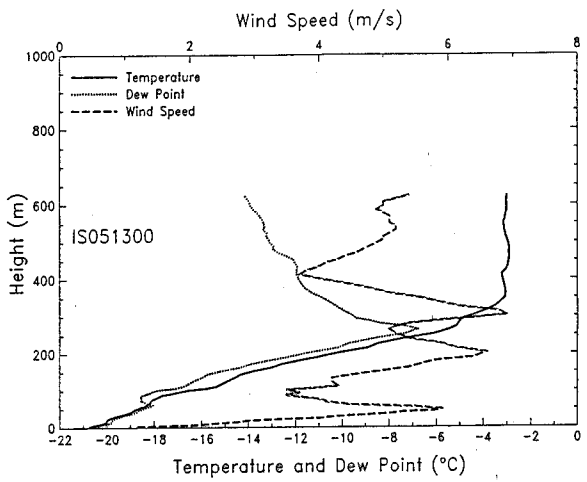

Figure C115.

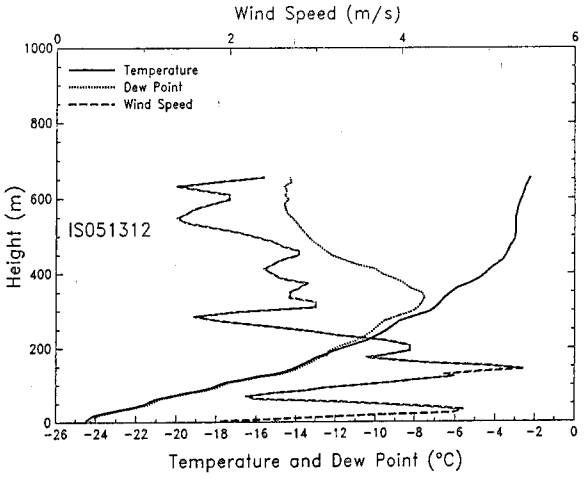

Figure C116.

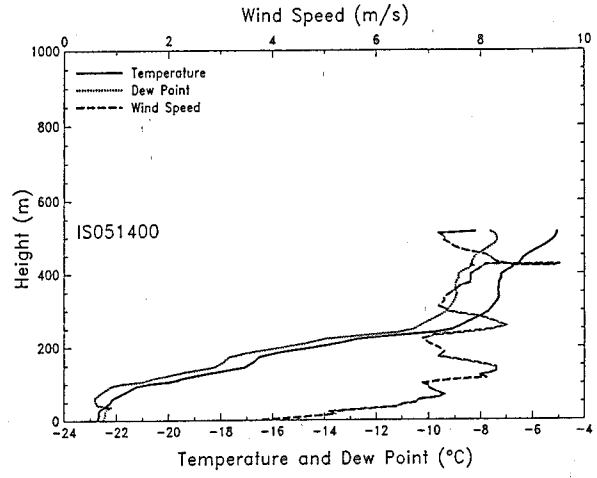

Figure C117.

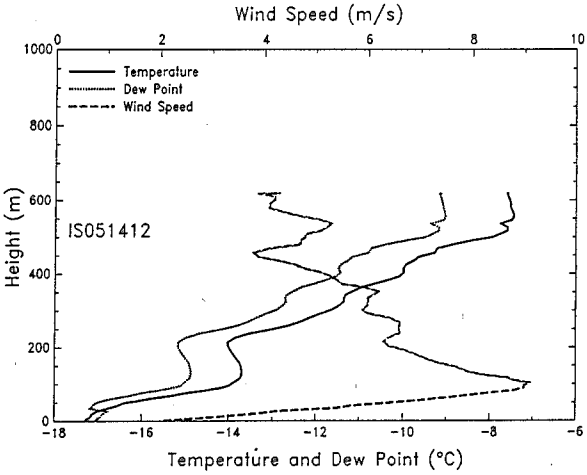

Figure C118.

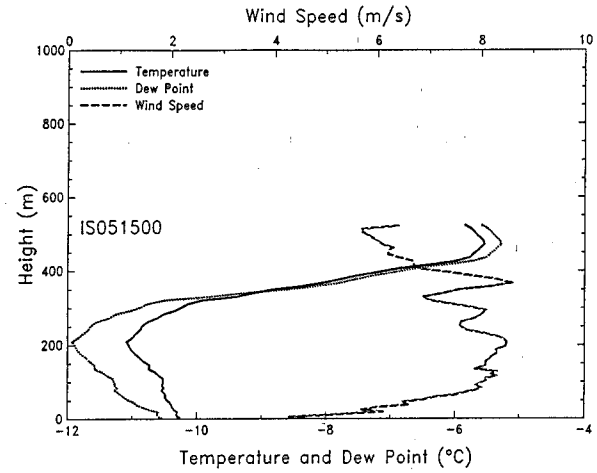

Figure C119.

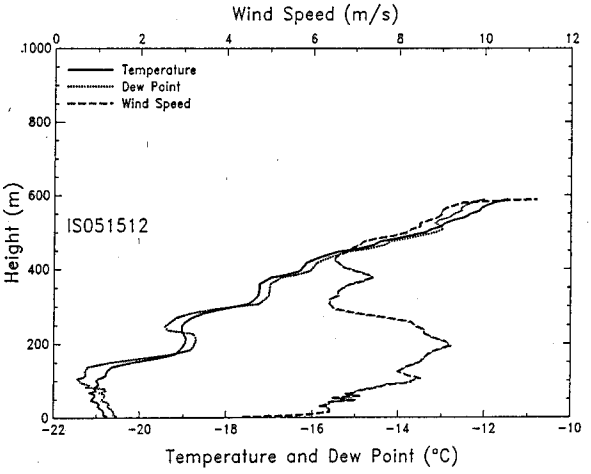

Figure C120.

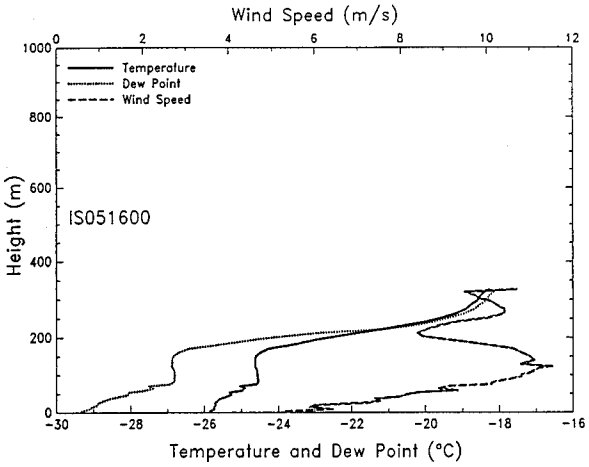

Figure C121.

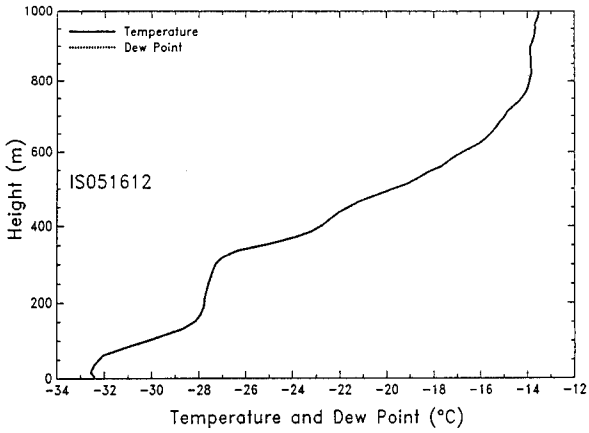

Figure C122.

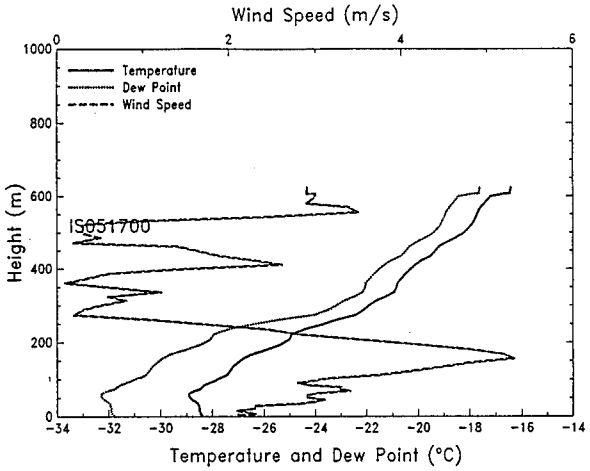

Figure C123.

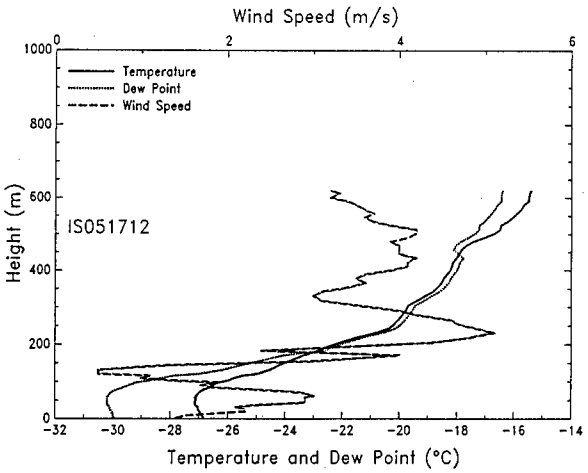

Figure C124.

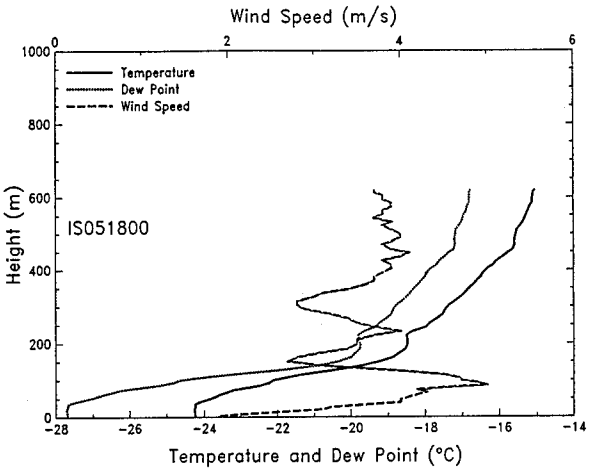

Figure C125.

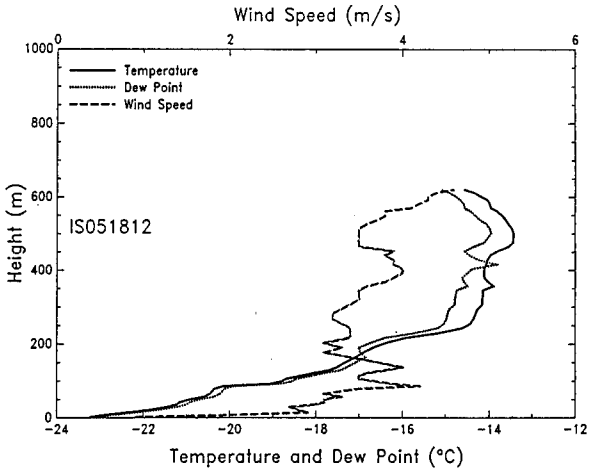

Figure C126.

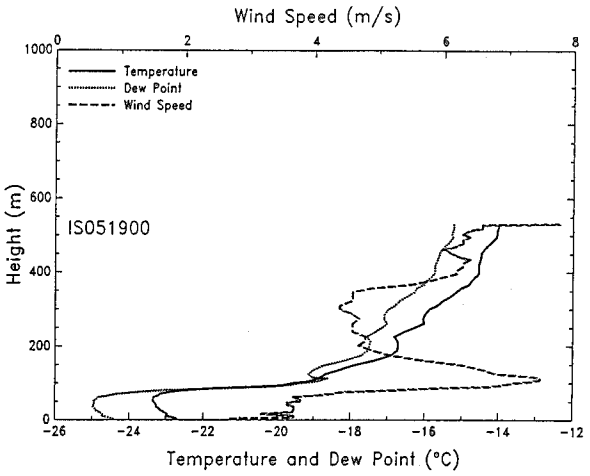

Figure C127.

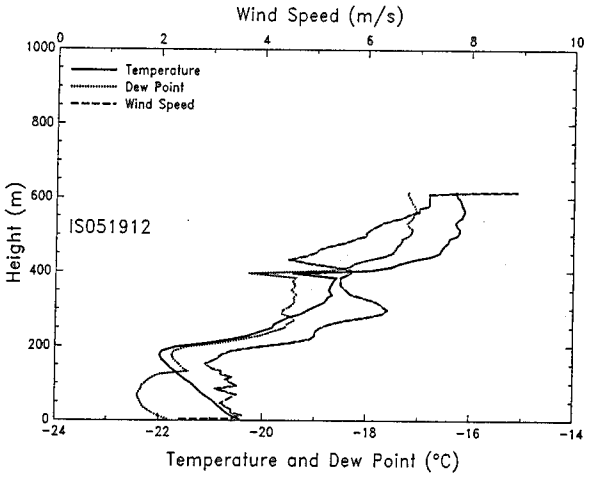

Figure C128.

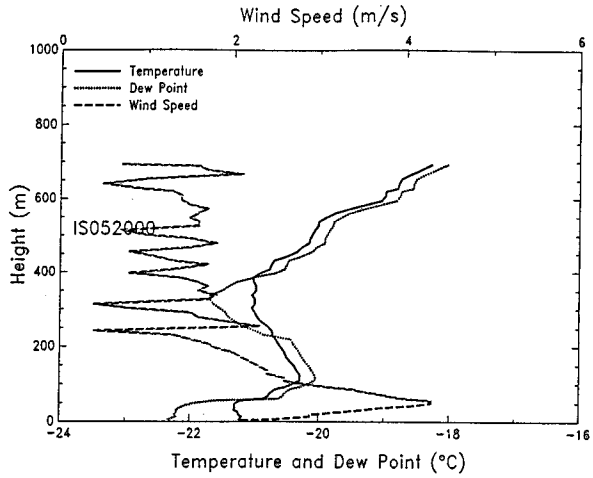

Figure C129.

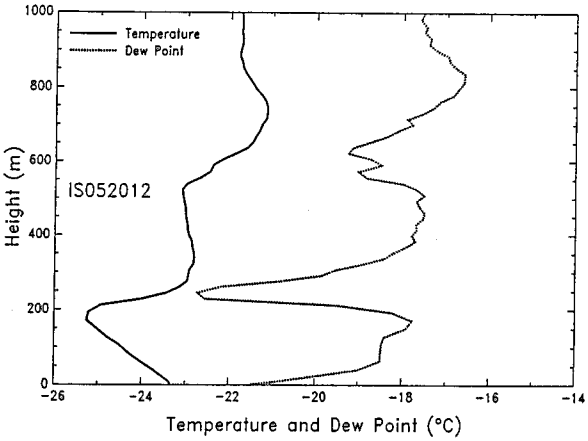

Figure C130.

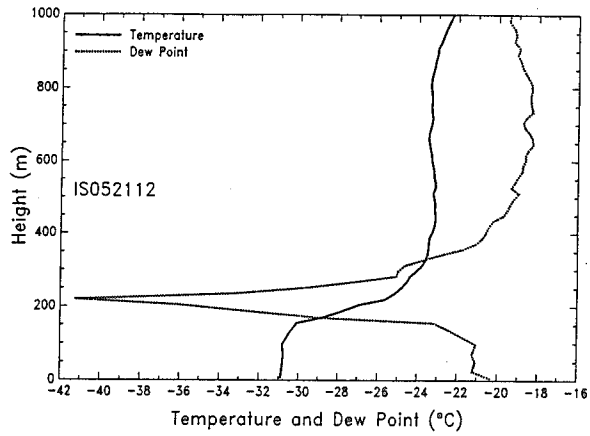

Figure C131.

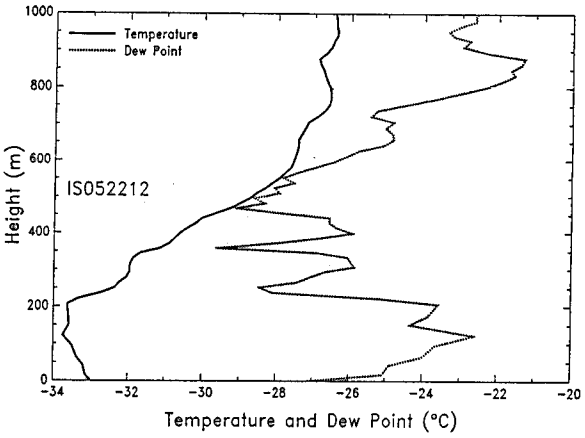

Figure C132.

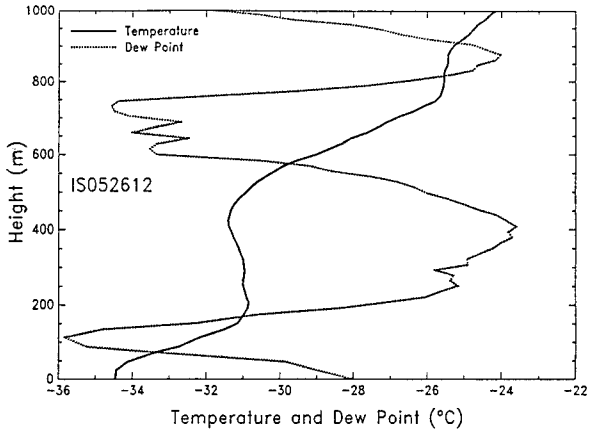

Figure C133.

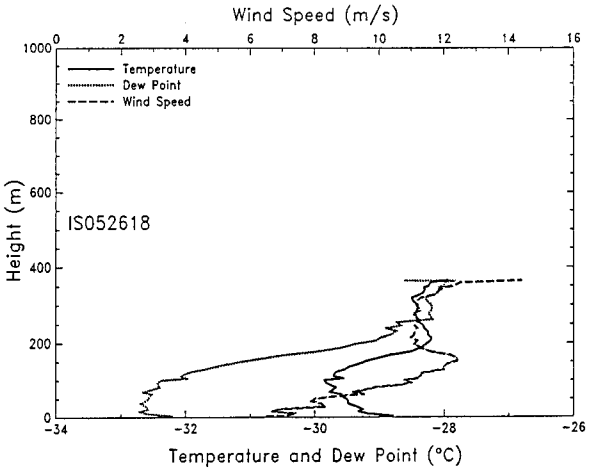

Figure C134.

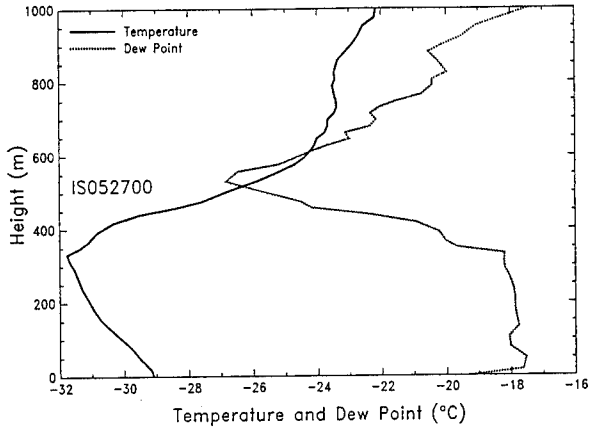

Figure C135.

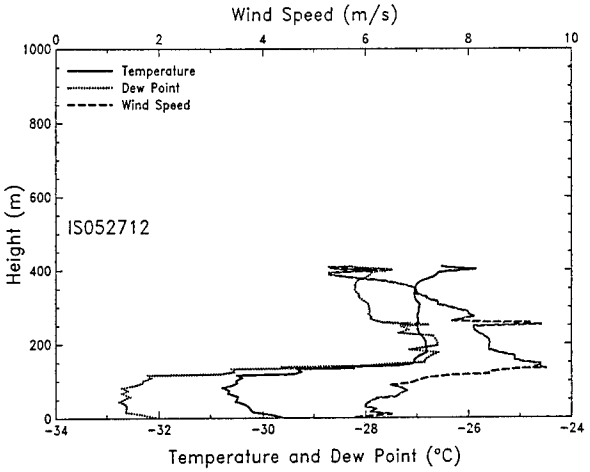

Figure C136.

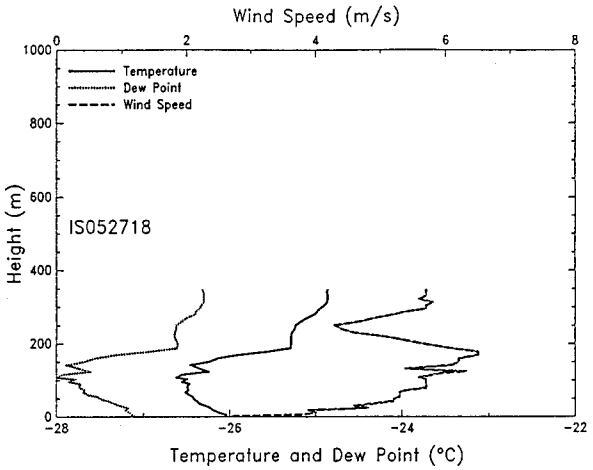

Figure C137.

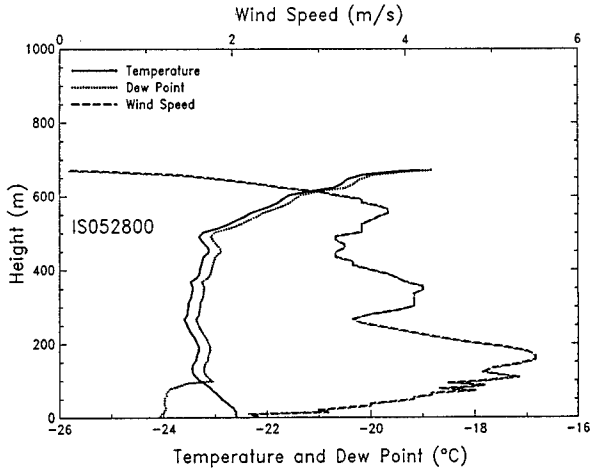

Figure C138.

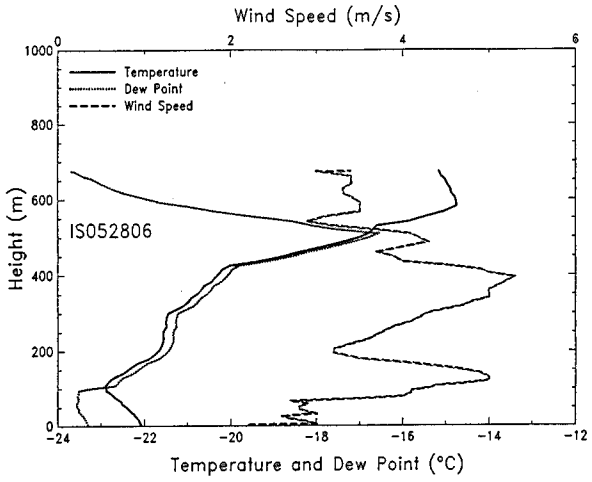

Figure C139.

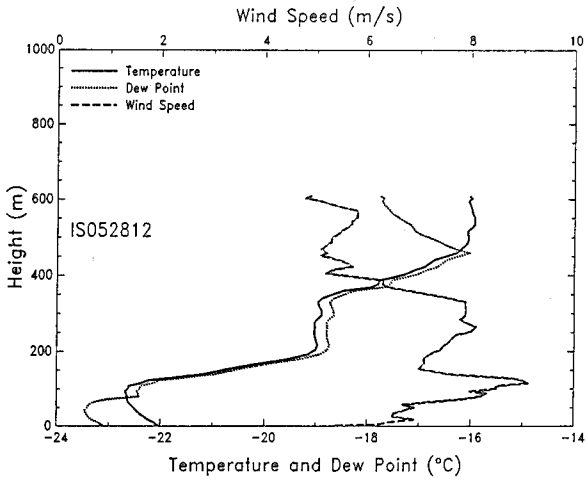

Figure C140.

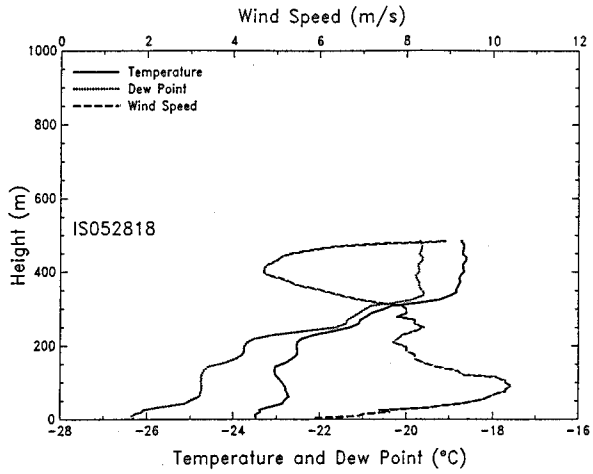

Figure C141.

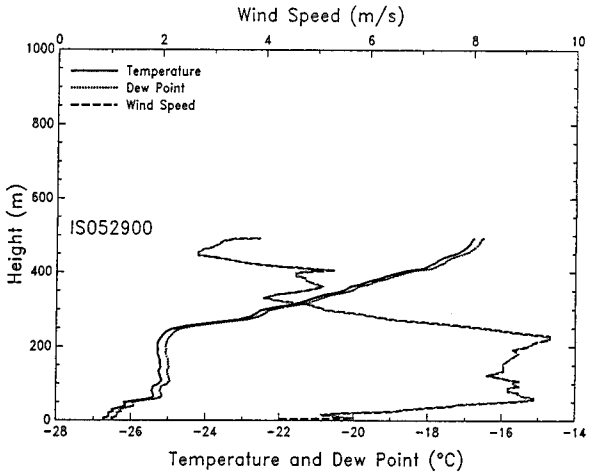

Figure C142.

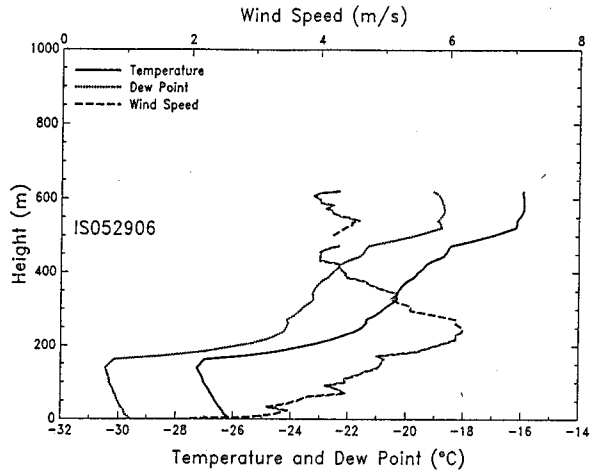

Figure C143.

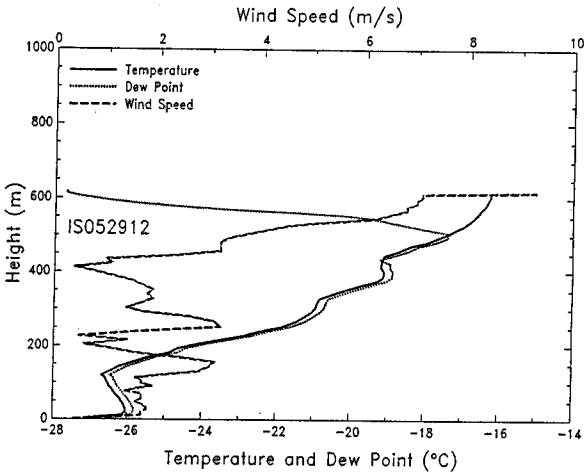

Figure C144.

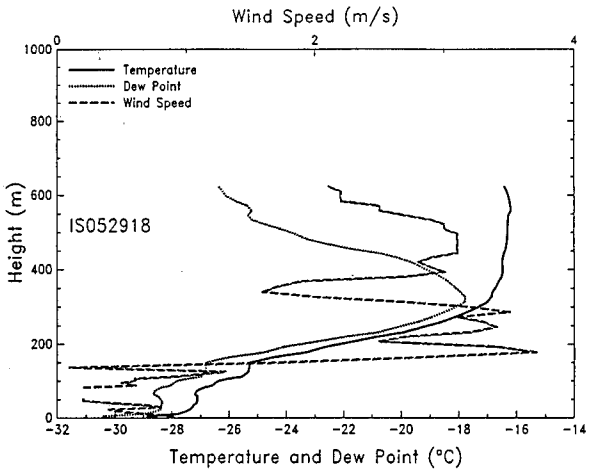

Figure C145.

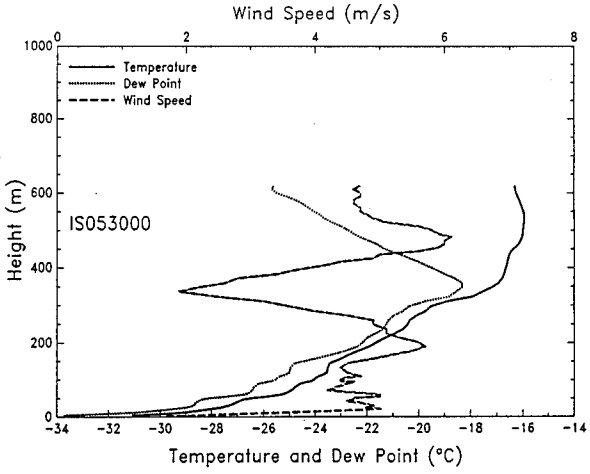

Figure C146.

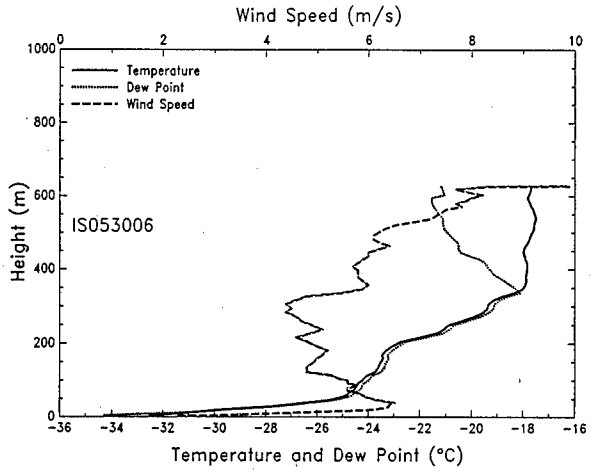

Figure C147.

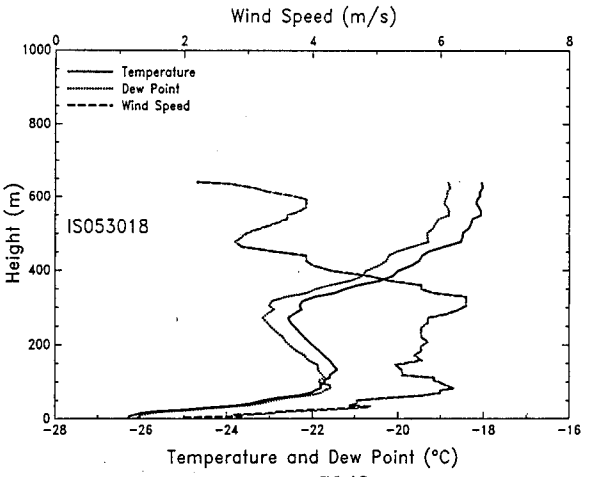

Figure C148.

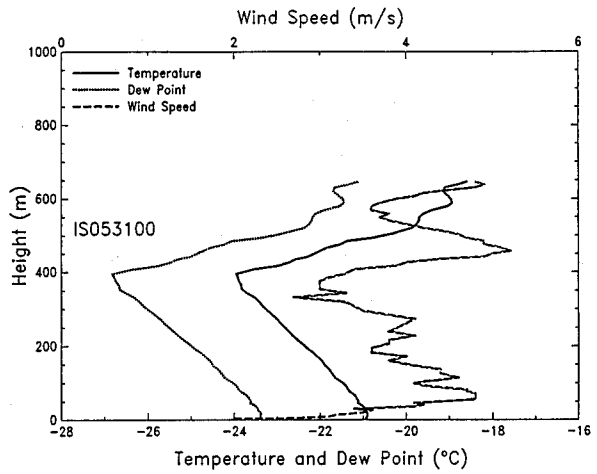

Figure C149.

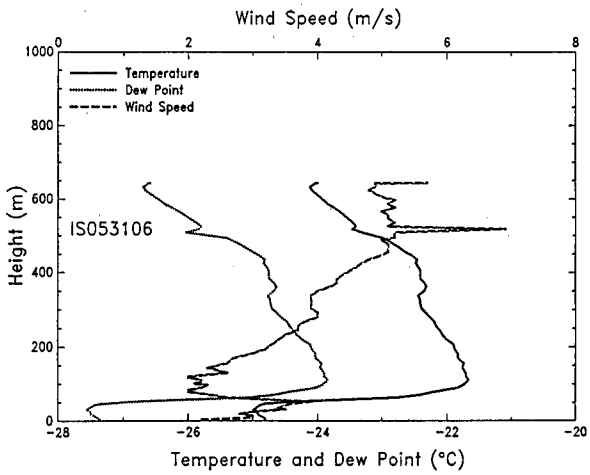

Figure C150.

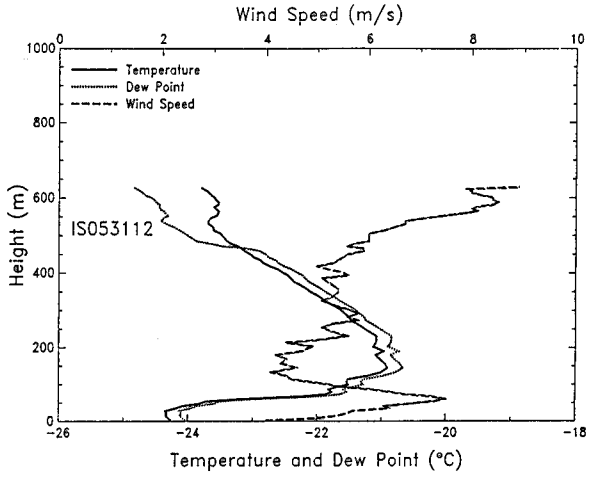

Figure C151.

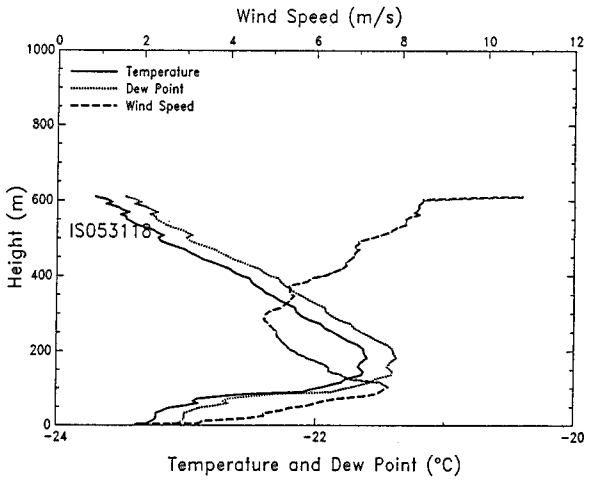

Figure C152.

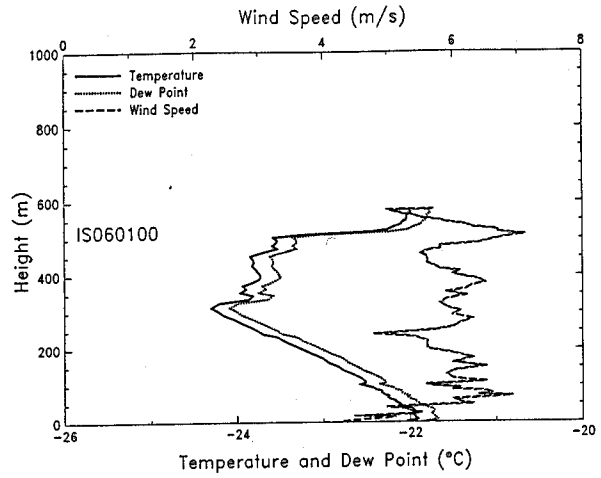

Figure C153.

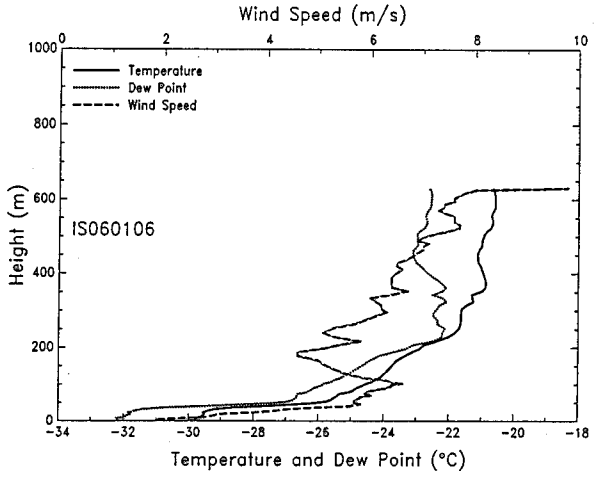

Figure C154.

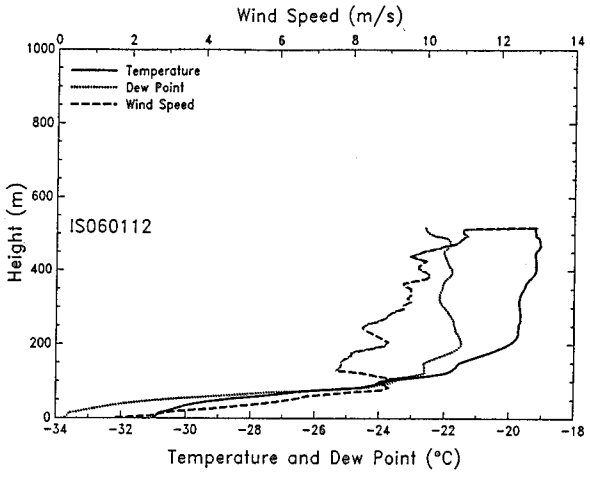

Figure C155.

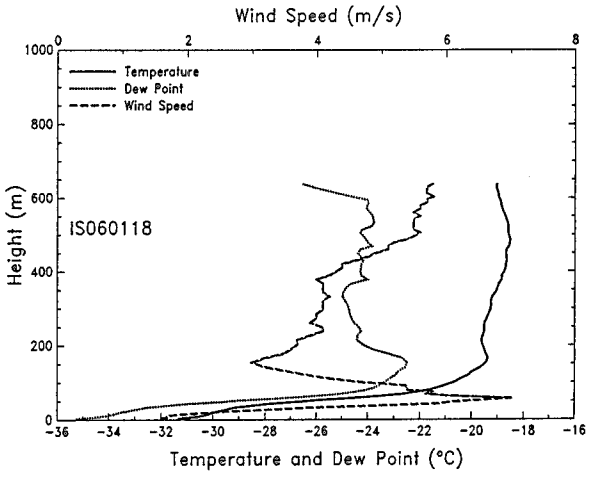

Figure C156.

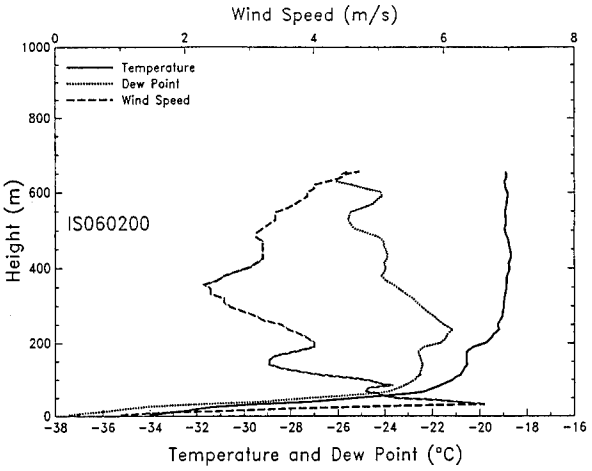

Figure C157.

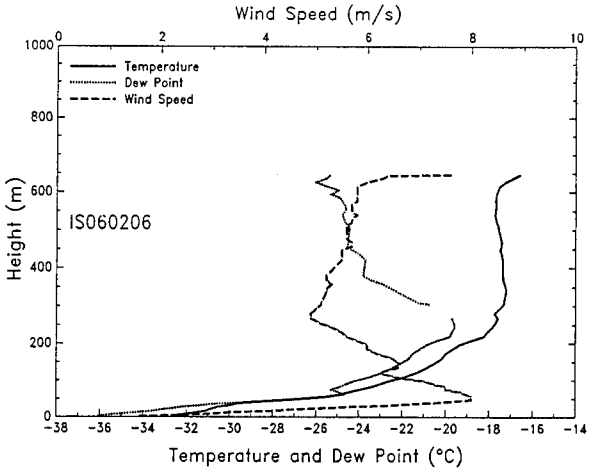

Figure C158.

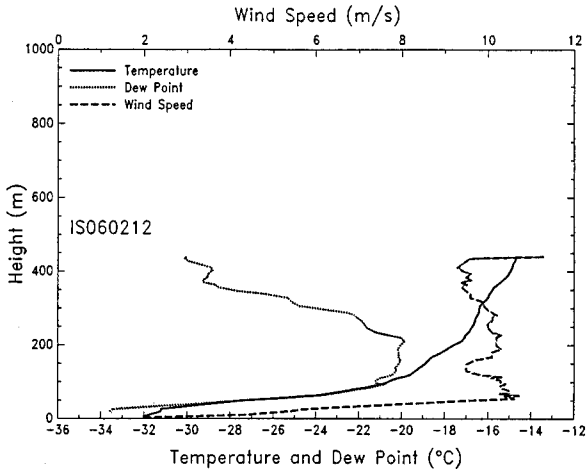

Figure C159.

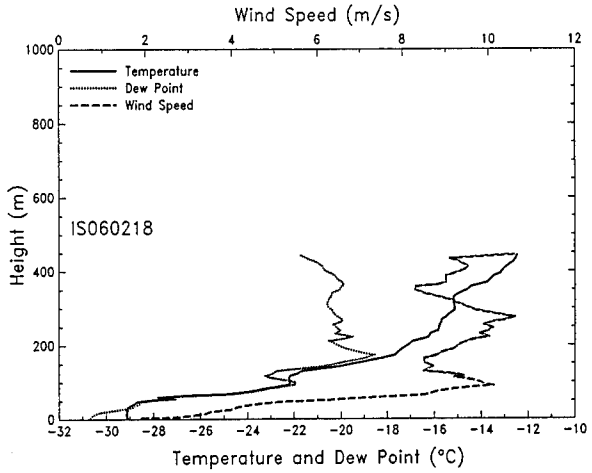

Figure C160.

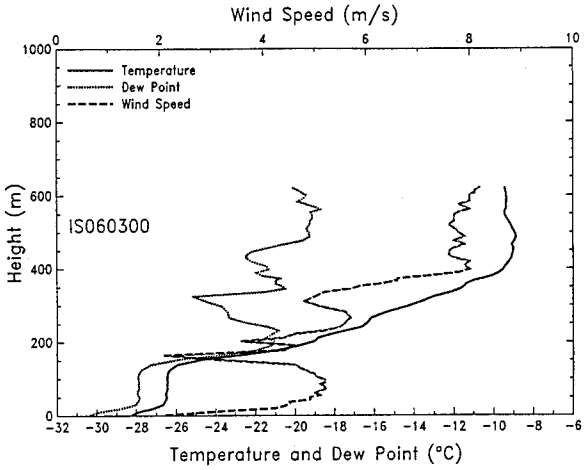

Figure C161.

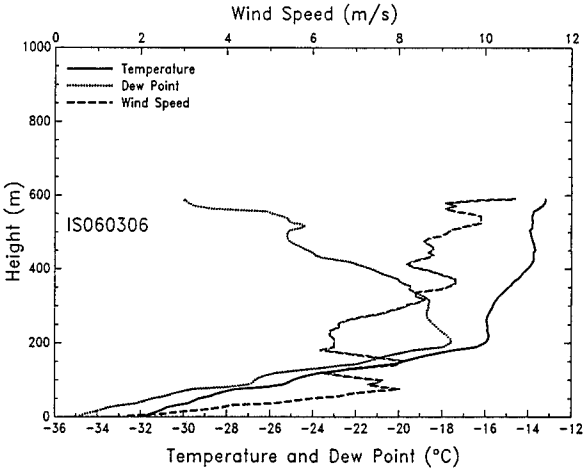

Figure C162.

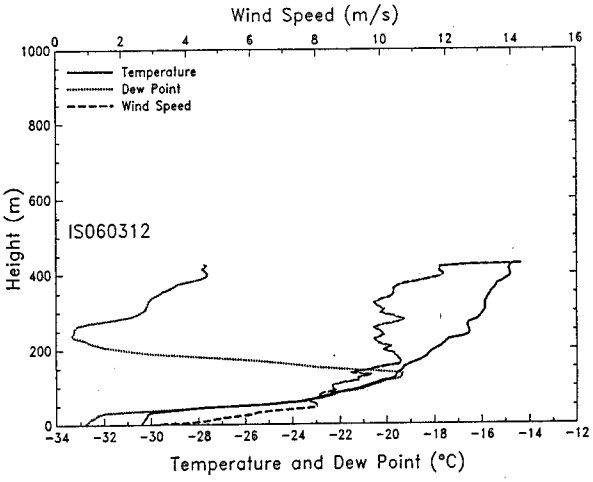

Figure C163.

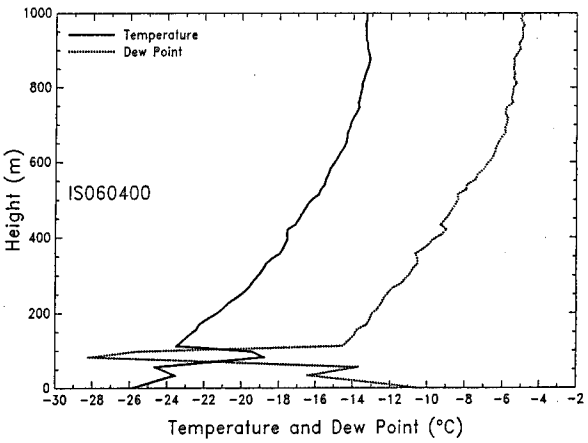

Figure C164.

APPENDIX D: PLOTS OF THE *AKADEMIK FEDOROV* SOUNDINGS

Here we plot all the soundings listed in Table 3. Cross–reference the identification number on each plot with the corresponding number in Table 3 to see when and where the sounding was made. Each plot shows temperature, dew point, and wind speed.

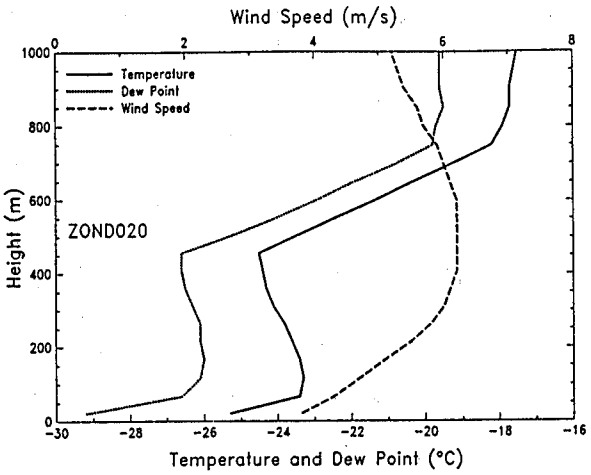

Figure D1.

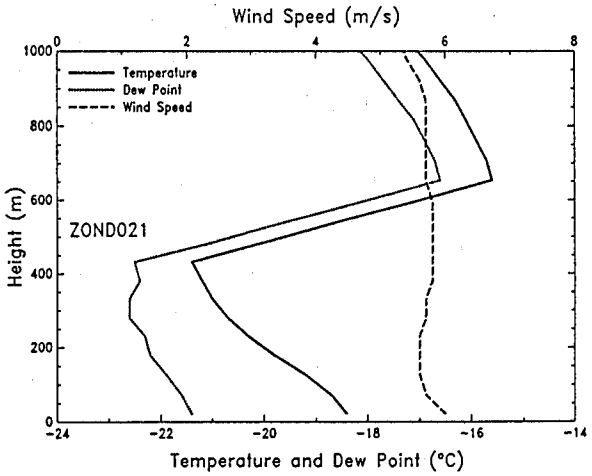

Figure D2.

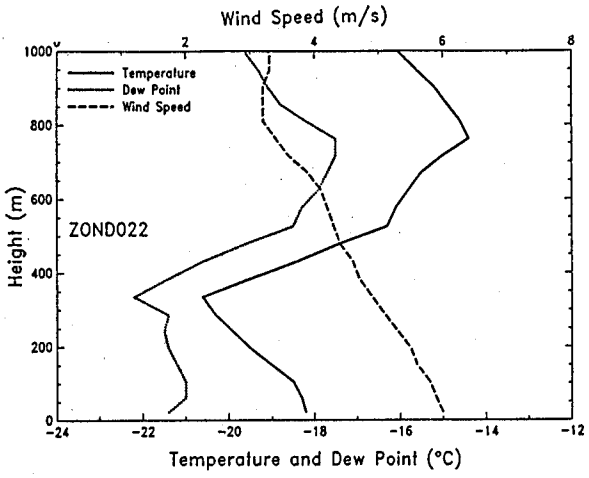

Figure D3.

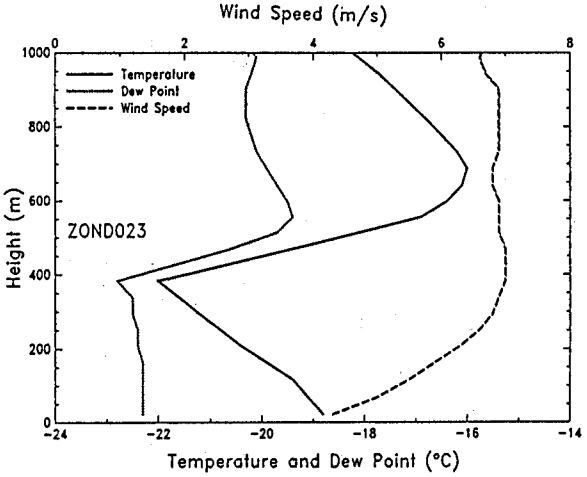

Figure D4.

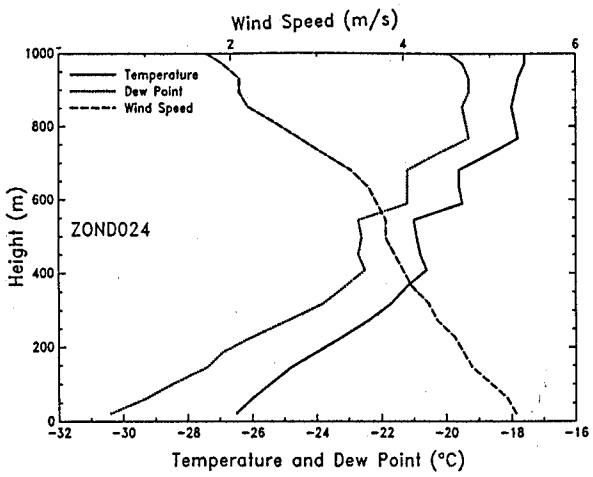

Figure D5.

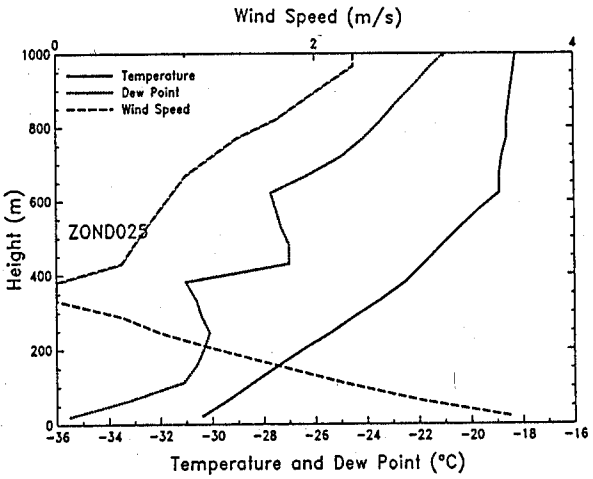

Figure D6.

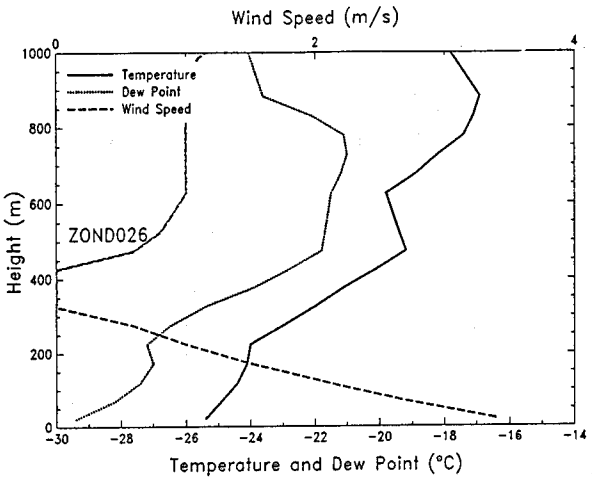

Figure D7.

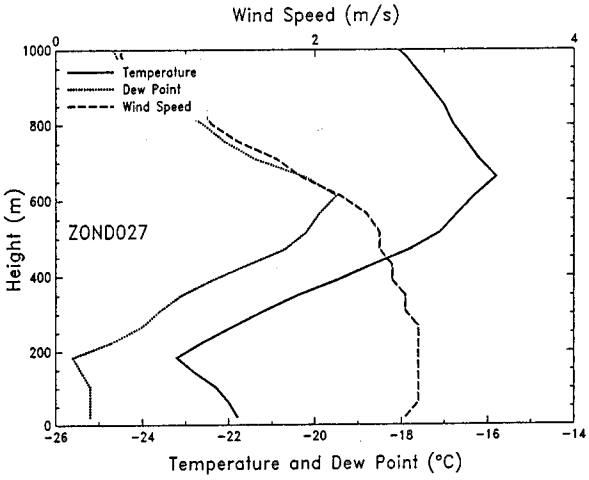

Figure D8.

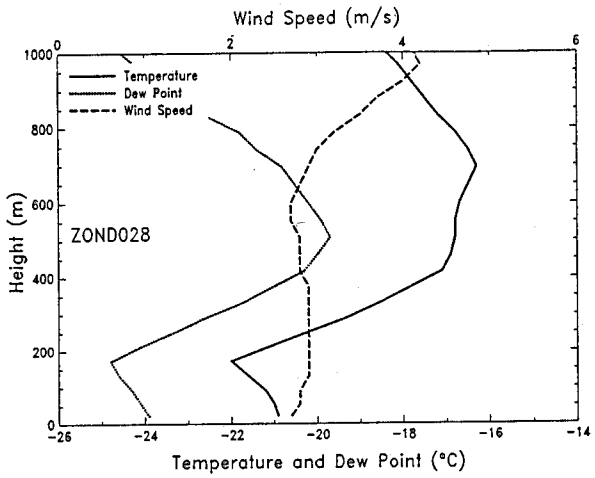

Figure D9.

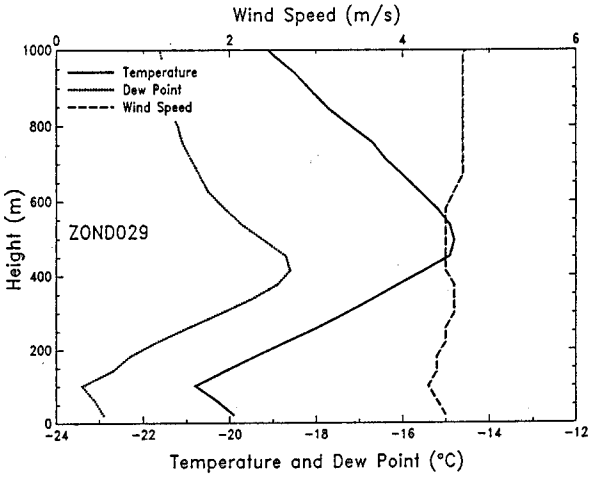

Figure D10.

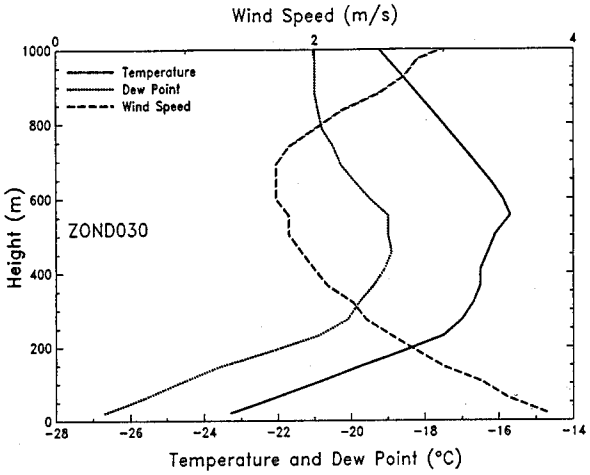

Figure D11.

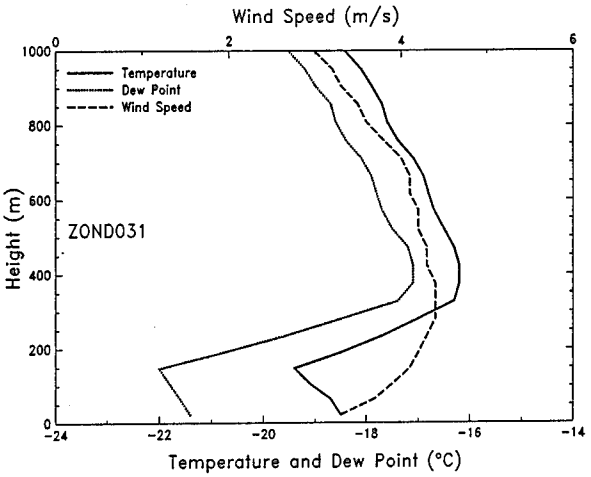

Figure D12.

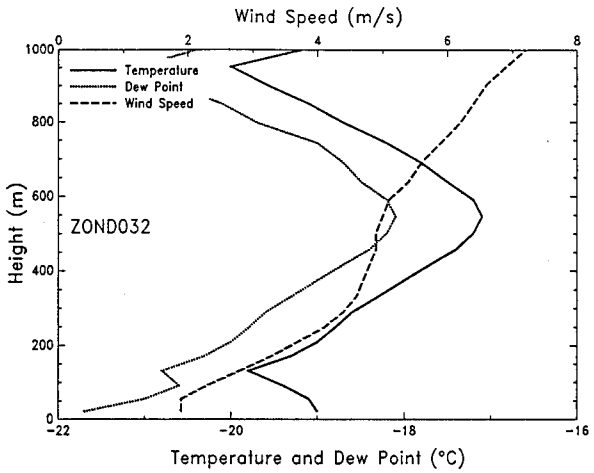

Figure D13.

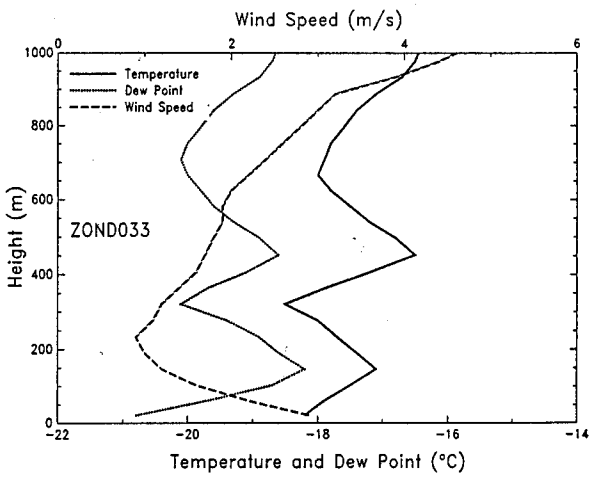

Figure D14.

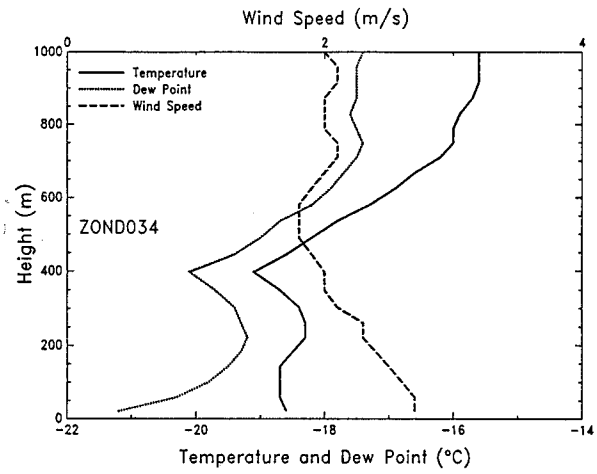

Figure D15.

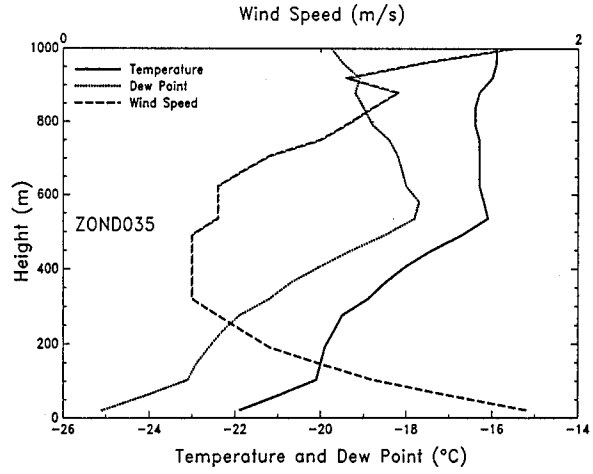

Figure D16.

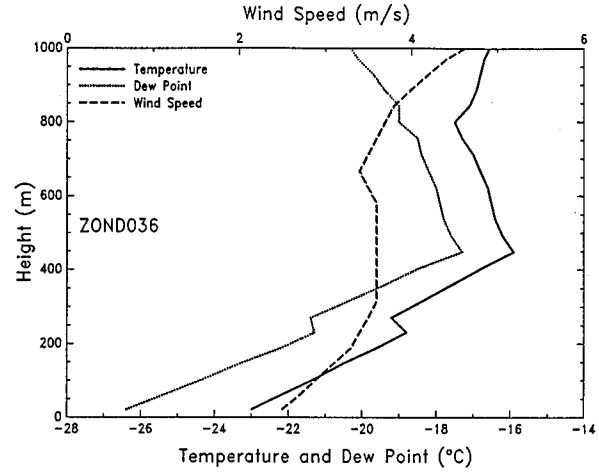

Figure D17.

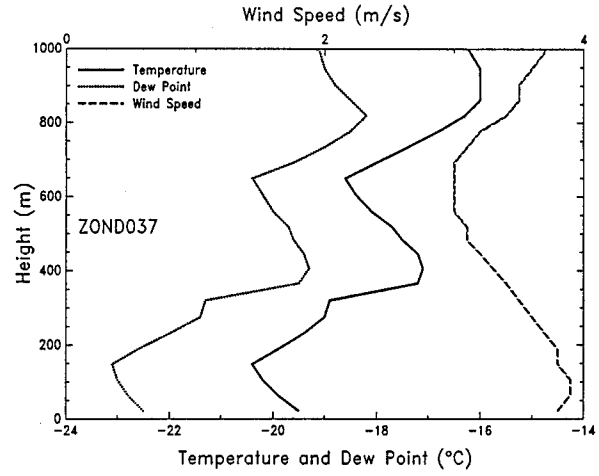

Figure D18.

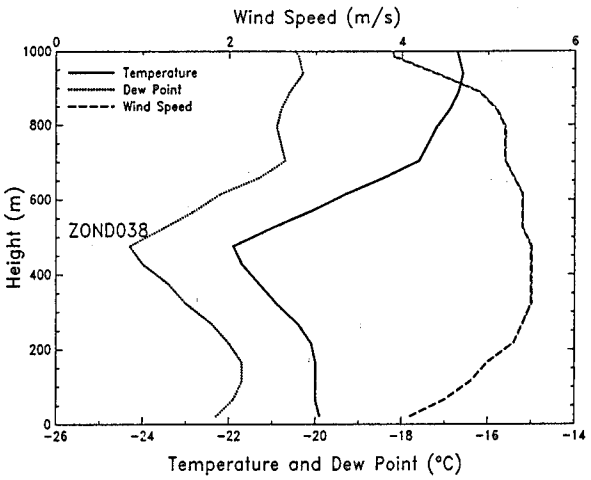

Figure D19.

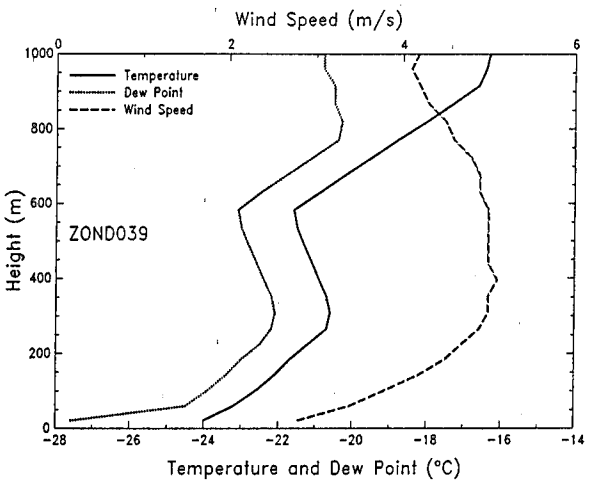

Figure D20.

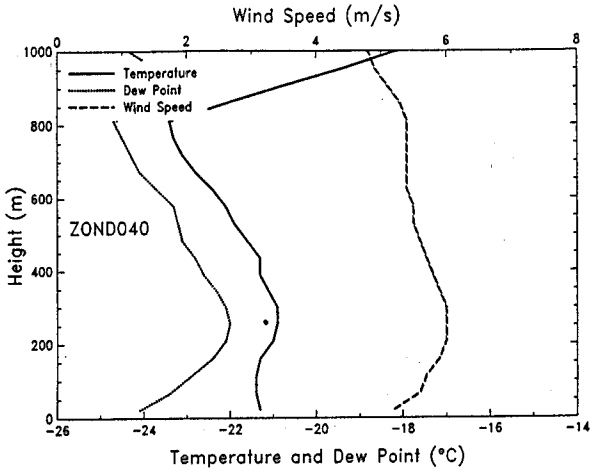

Figure D21.

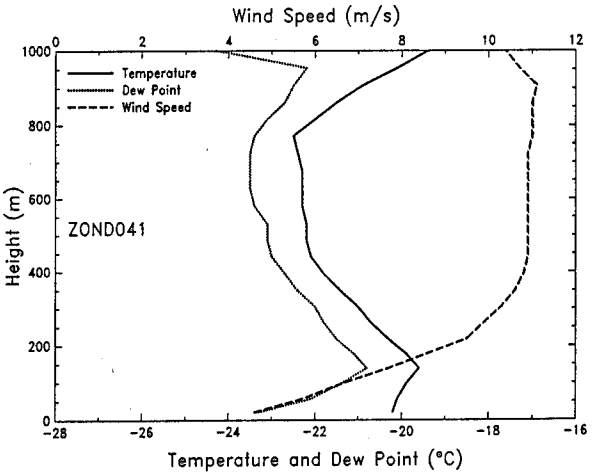

Figure D22.

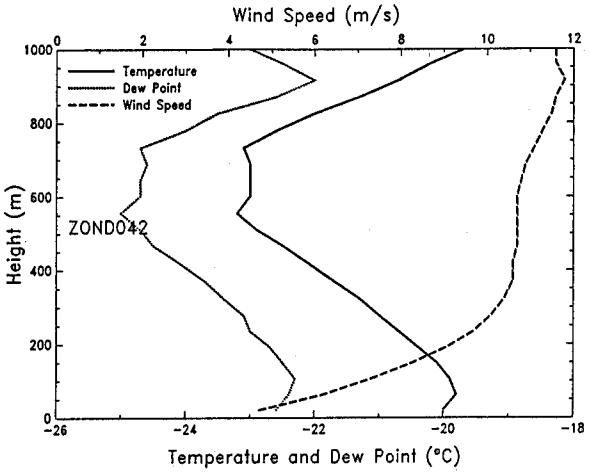

Figure D23.

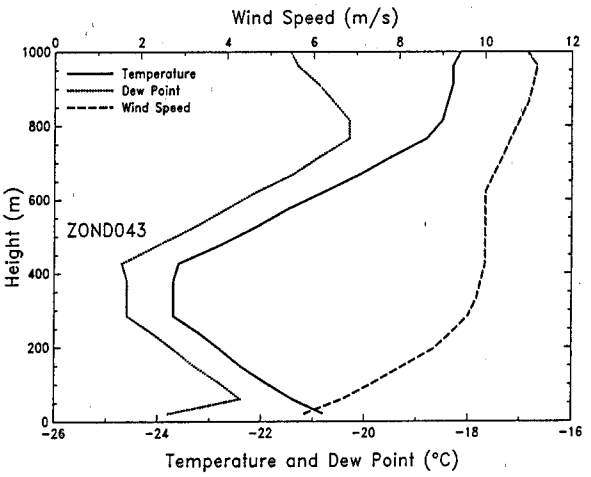

Figure D24.

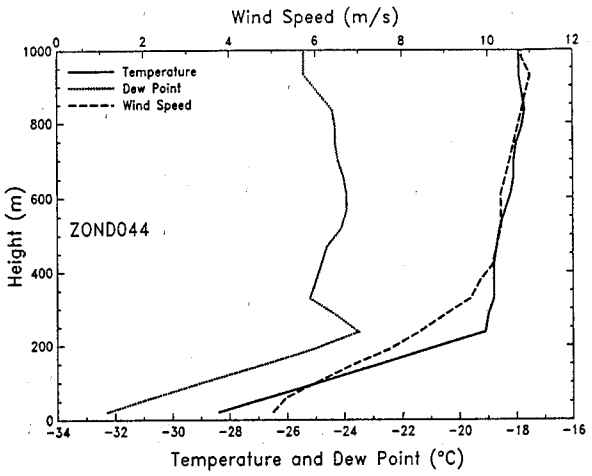

Figure D25.

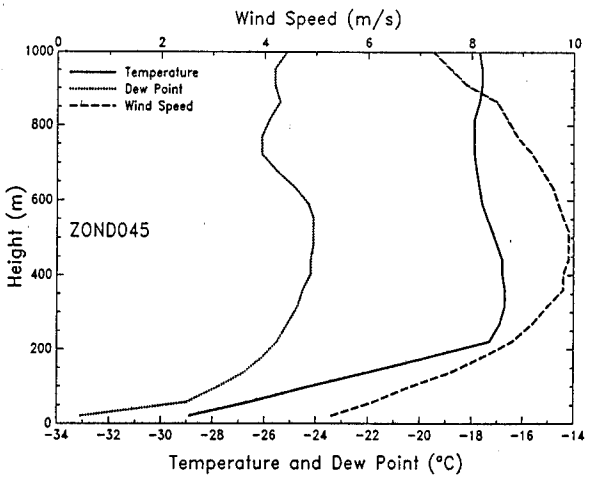

Figure D26.

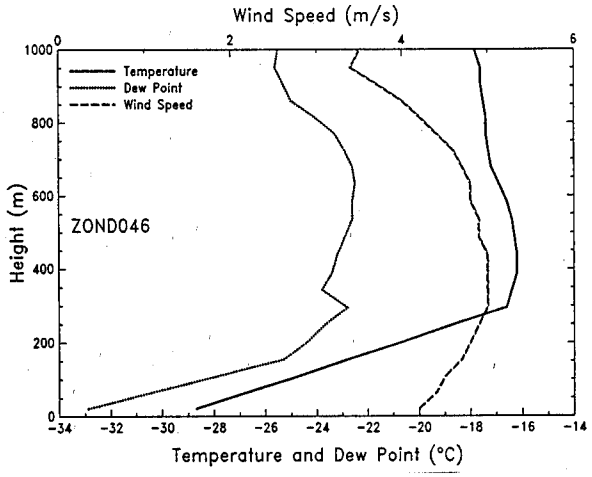

Figure D27.

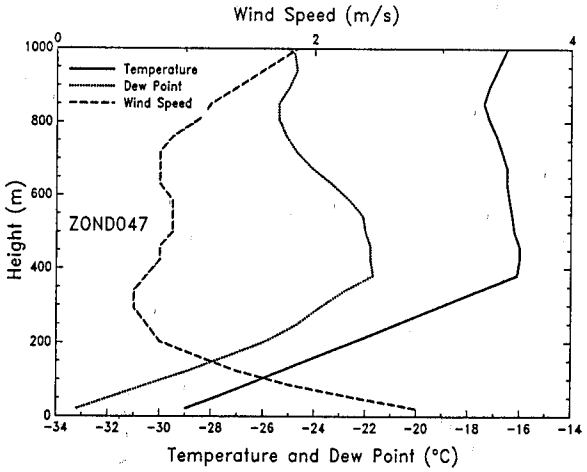

Figure D28.

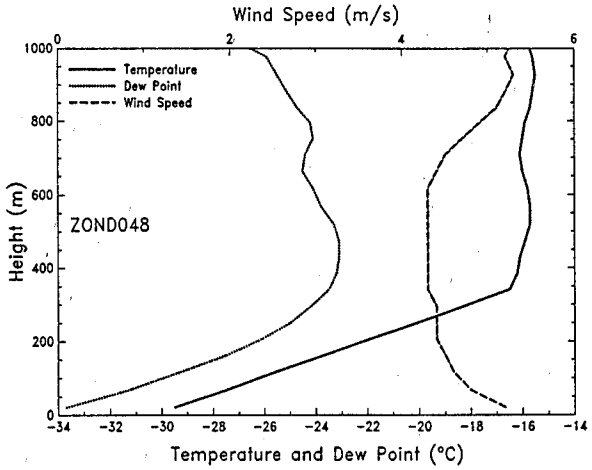

Figure D29.

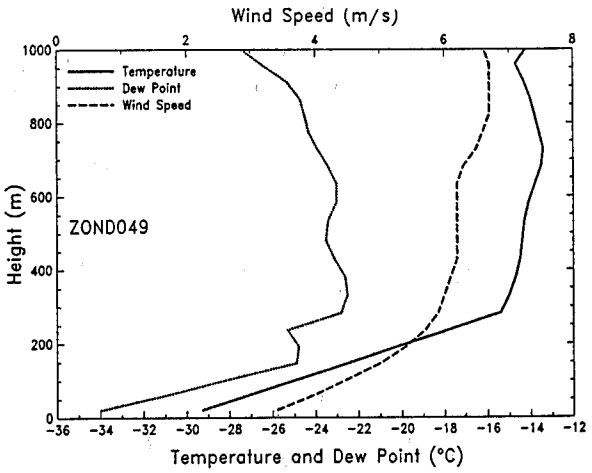

Figure D30.

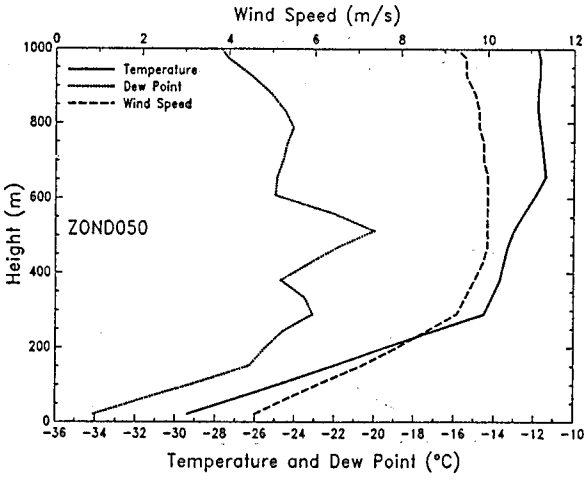

Figure D31.

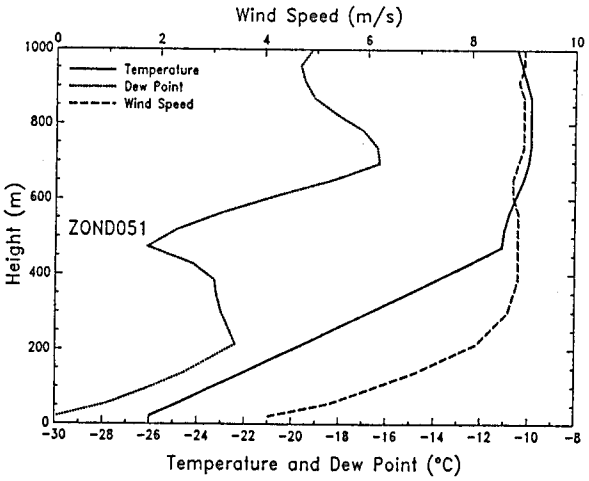

Figure D32.

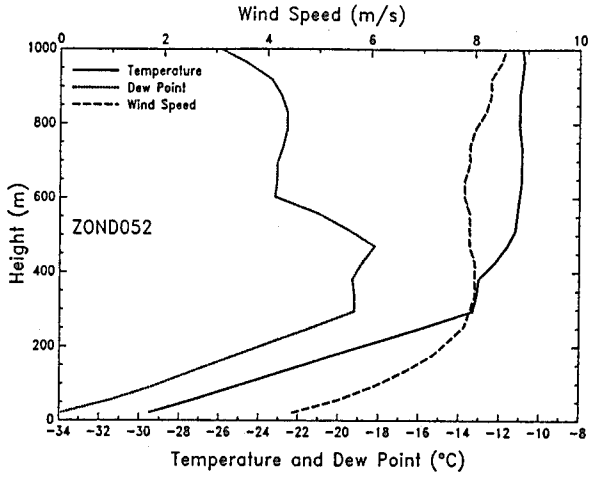

Figure D33.

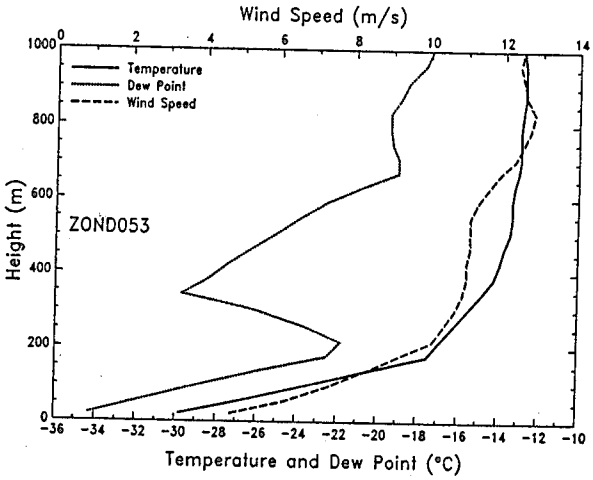

Figure D34.

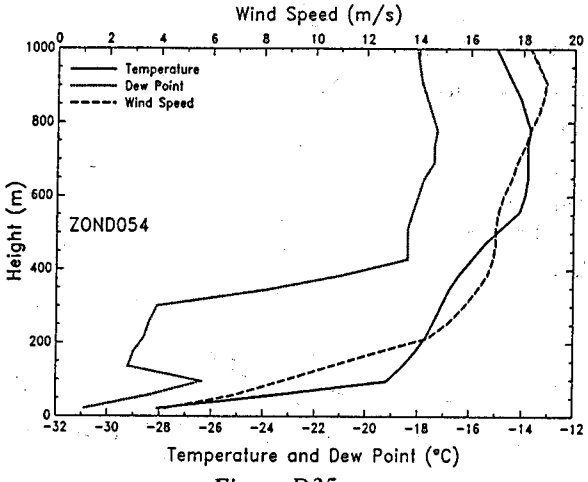

Figure D35.

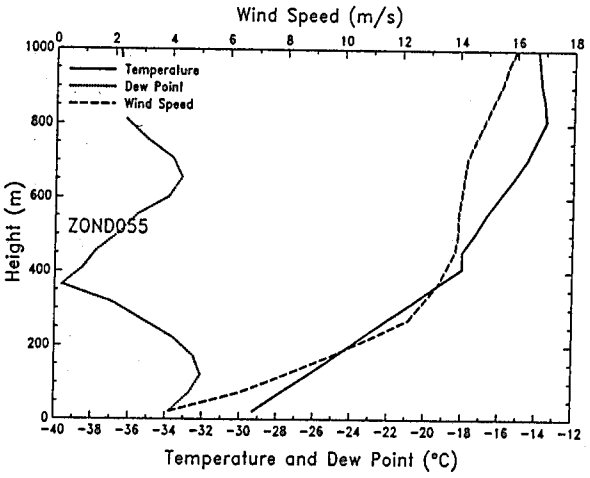

Figure D36.

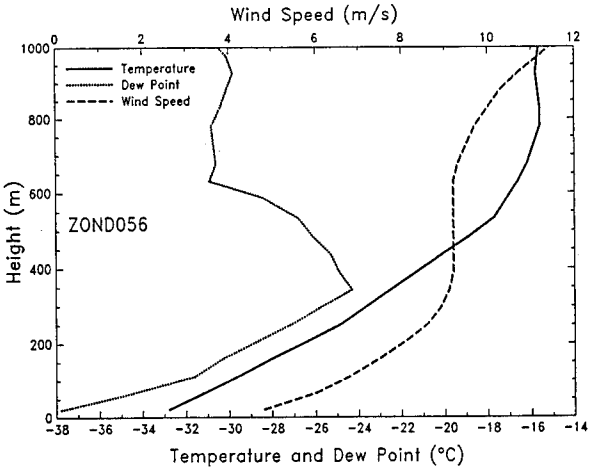

Figure D37.

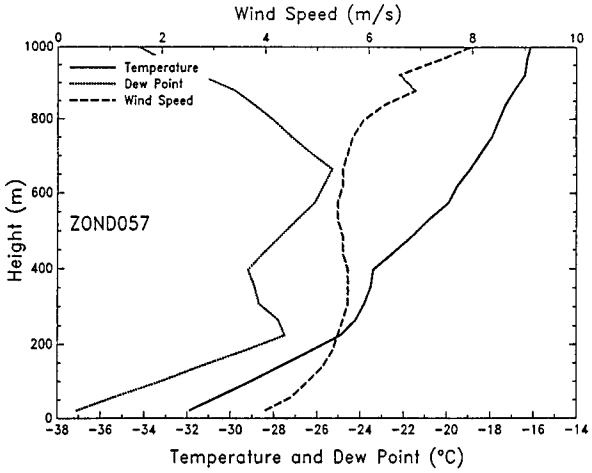

Figure D38.

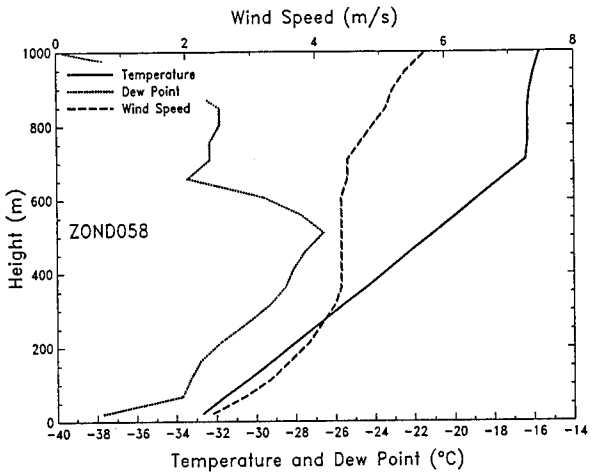

Figure D39.

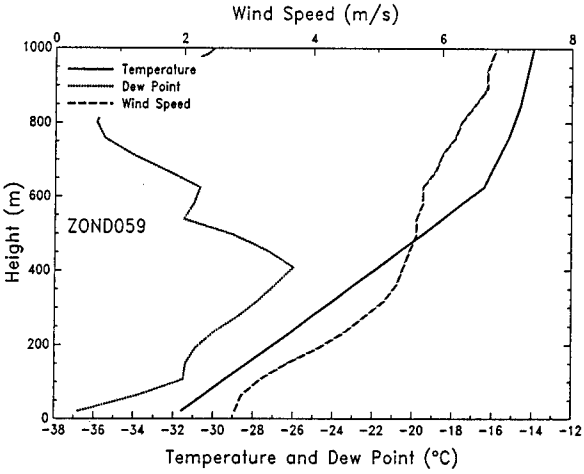

Figure D40.

REPORT DOCUMENTATION PAGE

Form Approved
OMB No. 0704-0188

1. AGENCY USE ONLY (Leave blank)	2. REPORT DATE	3. REPORT TYPE AND DATES COVERED
	August 1994	

4. TITLE AND SUBTITLE

Upper-Air Data Collected on
Ice Station Weddell

5. FUNDING NUMBERS

Grant OPP-9024544

6. AUTHORS

Kerry J. Claffey, Edgar L Andreas and Aleksandr P. Makshtas

7. PERFORMING ORGANIZATION NAME(S) AND ADDRESS(ES)

U.S. Army Cold Regions Research and Engineering Laboratory, Hanover, New Hampshire 03755-1290
and
Arctic and Antarctic Research Institute, St. Petersburg, Russia

8. PERFORMING ORGANIZATION REPORT NUMBER

Special Report 94-25

9. SPONSORING/MONITORING AGENCY NAME(S) AND ADDRESS(ES)

Office of Polar Programs
National Science Foundation
Arlington, Virginia 22230

10. SPONSORING/MONITORING AGENCY REPORT NUMBER

11. SUPPLEMENTARY NOTES

12a. DISTRIBUTION/AVAILABILITY STATEMENT

Approved for public release; distribution is unlimited.

Available from NTIS, Springfield, Virginia 22161.

12b. DISTRIBUTION CODE

13. ABSTRACT (*Maximum 200 words*)

From February to June 1992, as Ice Station Weddell (ISW) drifted through the uncharted western Weddell Sea, we launched radiosondes, typically twice a day, to study the structure of the lower atmosphere. Here, we describe the ISW radiosounding program, report on the availability of the data, and offer preliminary analyses of some of the atmospheric features we observed. For 10 days in late May and early June, as the Russian icebreaker *Akademik Fedorov* approached ISW from the northeast to help remove the ice camp, we made simultaneous soundings four times a day from ISW and from the *Fedorov*. We, therefore, also describe here the radiosounding system on the *Fedorov*, report on the availability of these data, and present preliminary comparisons of the simultaneous ISW and *Fedorov* soundings. Our soundings showed that temperature inversions were very common in this part of the Weddell Sea in fall and winter. Over 95% of the ISW soundings and 100% of the *Fedorov* soundings showed low-level temperature inversions. Of these, over 40% of the ISW soundings and over 67% of the *Fedorov* soundings were surface-based. A low-level jet in the wind speed profile was also common. We found such a jet in almost 80% of the ISW soundings for which we had wind information. The jet core was usually between 25 and 175 m above the surface, and speeds in the core were commonly between 4 and 10 m/s.

14. SUBJECT TERMS

Air–sea–ice interaction	Atmospheric temperature inversion	Radiosounding
Antarctica	Boundary-layer meteorology	Weddell Sea
Atmospheric structure	Low-level atmospheric jet	Wind speed

15. NUMBER OF PAGES
68

16. PRICE CODE

17. SECURITY CLASSIFICATION OF REPORT	18. SECURITY CLASSIFICATION OF THIS PAGE	19. SECURITY CLASSIFICATION OF ABSTRACT	20. LIMITATION OF ABSTRACT
UNCLASSIFIED	UNCLASSIFIED	UNCLASSIFIED	UL